PREDICTION OF HEAT TRANSFER COEFFICIENTS IN DRAG REDUCING TURBULENT PIPE FLOWS

By

AFSHIN JAHANSHAHI GHAJAR

Bachelor of Science

Oklahoma State University

Stillwater, Oklahoma

1974

Submitted to the Faculty of the Graduate College
of the Oklahoma State University
in partial fulfillment of the requirements
for the Degree of
MASTER OF SCIENCE
December, 1975

PREDICTION OF HEAT TRANSFER COEFFICIENTS

IN DRAG REDUCING TURBULENT

PIPE FLOWS

Thesis Approved:

W. J. Iederman, Jr.
Thesis Adviser

Jerald D. Parker

Del M. Moore

N. N. Durham
Dean of the Graduate College

TABLE OF CONTENTS

LIST OF TABLES

LIST OF FIGURES

Figure Page

NOMENCLATURE

English Letter Symbols

A	- universal temperature profile constant, slope
A^+	- constant that characterizes thickness of wall layer
a	- coefficient of power law viscosity relation
B	- law of the wall constant, intercept
c	- specific heat
C	- a concentration dependent parameter
C_M	- McNally correction factor, $C_M = 2.76$
D	- diameter of pipe
E	- non-dimensional eddy diffusivity, $E = \varepsilon/\nu$
F	- Fanning friction factor, $F = 2\tau_w/\rho U_m^2$
f	- Moody friction factor, $f = 8\tau_w/\rho U_m^2$
h	- heat transfer coefficient
j	- Colburn j factor, $j = St\ Pr^{2/3}$
K	- von Karman constant
k	- thermal conductivity
Nu	- Nusselt number, $Nu = (2r_o)h/k$

n - exponent of power-law viscosity relation

P - instantaneous pressure

$\overline{P^*}$ - mean pressure

$\overline{P}$ - non-dimensional mean pressure, $\overline{P} = \overline{P^*}/\rho U_m^2$

p - fluctuating pressure component

Pr - Prandtl number, $Pr = \nu/\alpha = \mu c/k$

$\dot{q}_o''$ - heat flux (heat transfer rate per unit of area) at surface

Re - Reynolds number, $Re = (2r_o)U_m/\nu$

R - Reynolds number based on pipe radius, $R = r_o U_m/\nu$

r_o - radius of pipe

r_o^+ - non-dimensional pipe radius, $r_o^+ = r_o U_\tau/\nu$

r - radial coordinate direction

$\overline{r}$ - non-dimensional radial coordinate, $\overline{r} = r/r_o$

St - Stanton number, $St = h/\rho c U_m$

T - instantaneous temperature

$\overline{T^*}$ - mean temperature

T_m - mixed mean temperature, defined by Equation (3.4)

T_o - fluid temperature at surface

T^+ - non-dimensional temperature, $T^+ = (T_o - \overline{T^*})U_\tau \rho c/\dot{q}_o''$

t - fluctuating temperature component

t_1 - polymer relaxation time

U - instantaneous streamwise velocity

$\overline{U^*}$ - streamwise mean velocity

$\overline{U}$ - non-dimensional streamwise mean velocity, $\overline{U} = \overline{U^*}/U_m$

U_m - mass average velocity, defined by Equation (2.11)

U^+ - non-dimensional velocity, $U^+ = \overline{U^*}/U_\tau$

U_τ - shear velocity, $U_\tau = (\tau_w/\rho)^{1/2}$

U_τ^* - critical or onset wall shear velocity

u - streamwise fluctuating velocity component

V_r - instantaneous radial velocity

$\overline{V}_r$ - radial mean velocity

v_r - radial fluctuating velocity component

$\overline{uv}_r$ - Reynolds stress

x - streamwise coordinate direction

$\overline{x}$ - non-dimensional streamwise coordinate direction, $\overline{x} = x/r_o$

y - coordinate direction normal to wall

$\overline{y}$ - non-dimensional direction normal to wall, $\overline{y} = y/r_o$

y^+ - non-dimensional distance normal to wall, $y^+ = yU_\tau/\nu$

y_1^+ - edge of viscous sublayer

y_2^+ - edge of buffer zone

y_j^+ - intersection of Equation (2.22) with the viscous sublayer equation

Greek Letter Symbols

ΔU^+	- upward shift in the logarithmic velocity profile
ν	- kinematic viscosity, $\nu = \mu/\rho$
μ	- absolute viscosity
ρ	- fluid density
ε	- turbulent eddy diffusivity
τ_w	- wall shear stress
α	- molecular thermal diffusivity, $k/\rho c$
β	- drag reduction parameter, defined by Equation (3.43) or (3.44)
θ	- non-dimensional fluid temperature, $\theta = (\overline{T^*} - T_o)/(T_m - T_o)$

Subscripts

w,o	- refers to value of variable at wall
r	- refers to radial direction
m	- mass average; also evaluated at mixed mean state
M	- momentum
H	- heat
f	- evaluated at film temperature
1	- evaluated at the edge of the viscous sublayer

Abbreviations

ppm	- parts per million
Corr.	- correction
Poly.	- polymer
in.	- inch
I.D.	- inside diameter

CHAPTER I

INTRODUCTION

Many investigators have shown that the frictional loss in turbulent pipe flow of a solvent can be reduced by adding certain high molecular weight additives to it. The phenomenon is referred to as drag reduction. With these polymeric solutions, a lower pressure gradient is needed to maintain the same flow rate, or a higher flow rate can be obtained for the same pressure gradient. Parallel to drag reduction there is a reduction of the heat transfer coefficient. This is to be expected because the same mechanism is involved in the turbulent transport of both momentum and heat.

There are several engineering applications where knowledge of the heat transfer in drag reducing flows is needed. For example, in a heat exchange process, either the cooling water or the process water could have polymer added to it for the purpose of reducing the drag. As a second example, a liquid with drag reducing characteristics may naturally occur in the production of paper and in food processing, or may constitute one of the components in a chemical process. Therefore, it is important to examine the effect of polymeric solutions on heat transfer characteristics of turbulent flow.

The objectives of this study are:

1) To extend the prediction scheme of Cess (1) and Reischman (2) for the turbulent transport of momentum and consequently predict the

mean velocity profile in drag reducing turbulent pipe flows.

2) To check the validity of the prediction scheme with experimental velocity profiles.

3) To develop a simple heat transfer prediction model for drag reducing turbulent pipe flows for the case of constant heat rate, from a knowledge of the average flow rate and pressure drop in the pipe.

4) To check the validity of the prediction method with the available experimental results, theoretical models, and correlations.

Previous investigators have remarked that the effects of drag reducing additives on turbulent wall flows can be regarded as making the quantity B, which appears in the universal logarithmic law of the wall, depend upon the shear stress and the additive properties. The law of the wall can be expressed as:

$$U^+ = \frac{1}{K} \ln y^+ + B \qquad (1.1)$$

For a Newtonian fluid B is constant. However, for polymeric solutions the value of B is not constant, and Meyer (3) has shown that values three to four times greater than the Newtonian value of B are encountered with these solutions. The value of B increases both with the concentration of additive and with the shear stress. The problem is to specify or to predict this increase in the value of B, which is directly related to the thickness of the near-wall region (viscous sublayer and buffer region).

Several investigators have used different methods to account for this thickening of the near-wall region in their velocity profile calculations. Poreh and Paz (4) have changed the limits of the three regions of the flow such that their velocity profile would fit the

measurements of Elata, et al. (5) in pipe flow of dilute polymer. In the calculation procedure outlined by Wells (6), the wall layer thickness was obtained semiempirically using Meyer's (3) equation and relating this quantity to friction factor data. Howard (7) calculates the thickness of the near-wall region by matching the Van Driest (8) velocity distribution to the experimentally determined distribution of velocity profile. The suggested model of this study predicts mean velocity profiles using the proposed eddy diffusivity model of Cess (1). In this model the thickness of the wall layer is calculated in a very logical manner and does not require fitting of the velocity profile to experimental measurements or the use of some correlation. In the present model the damping factor A^+, the constant that characterizes the thickness of the wall layer, is determined directly from the information about the general flow parameters. In contrast to the models of Wells (6), and Poreh and Paz (4), this model does not require information on polymer properties.

The velocity profile and heat transfer prediction scheme is based on knowledge of the average velocity, geometry of the flow duct, kinematic viscosity of the solution, wall shear stress, thermal conductivity, and Prandtl number. The first four inputs would fix the velocity profile, and the two additional inputs are necessary for the heat transfer calculations. Similar to models of Wells (6) and Poreh and Paz (4), the integral expression for heat transfer was developed for the case of constant heat rate with the assumption that the eddy diffusivities of heat and momentum are equal (Reynolds analogy).

The velocity profile prediction scheme is outlined in Chapter II where it is also compared to the experimental results of Virk (9). The

development of the heat transfer model is outlined in Chapter III. The heat transfer prediction scheme is compared with theoretical models of Poreh and Paz (4), Wells (6), correlation of Smith, et al. (10), and the results of seven drag reducing heat transfer experiments. The scope of the experimental heat transfer data in drag reducing fluids used in the present study is shown in Table II, Appendix A.

CHAPTER II

VELOCITY PROFILE

Calculation of heat transfer coefficients which will be introduced in Chapter III requires an expression for the velocity profile. In this chapter an expression for the velocity profile will be obtained from the equations of motion. Integration of these equations is possible after the non-linear Reynolds stress term in these equations has been replaced by an expression for the eddy diffusivity. The eddy diffusivity model proposed by Cess (1) for turbulent pipe flow was used in this study. In the latter part of this chapter calculation procedures will be outlined and the results will be compared and discussed with the data available in the literature.

Integral Expression for Velocity Profile

The analysis begins with the Navier-Stokes equation in the x-direction for an axisymmetric flow in a circular tube written in terms of mean velocities and fluctuations from the mean. After averaging with respect to time, this equation becomes

$$\frac{1}{r}\frac{\partial}{\partial r}\left[r\left(\nu\frac{\partial \overline{U}^{*}}{\partial r} - \overline{uv}_{r}\right)\right] = \frac{1}{\rho}\frac{\partial \overline{P}^{*}}{\partial x} \qquad (2.1)$$

A schematic diagram showing the coordinate system is given in Figure 1.

In writing Equation (2.1), the following assumptions were made:

a) The flow is fully developed.

b) The fluid properties are constant.

c) The flow is axisymmetric and two dimensional.

d) The flow is steady.

In conjunction with assumption a) recall that in a fully developed trubulent pipe flow the conditions are

a) $\overline{V}_r = 0$

b) The velocity field is independent of the coordinate x

In Equation (2.1) the velocity and pressure perturbations are

$$U = \overline{U^*} + u$$

$$V_r = v_r \qquad (2.2)$$

$$P = \overline{P^*} + p$$

In order to obtain a velocity profile $\overline{U^*}$, the equation of motion should be integrated. Integration is possible only after the Reynolds stress term $(-\rho\overline{uv}_r)$ has been specified. The eddy diffusivity models provide such an expression. Consequently, the eddy diffusivity of momentum is defined as,

$$\varepsilon_M = \frac{-\overline{uv}_r}{\frac{d\overline{U^*}}{dr}} \qquad (2.3)$$

Replacing the Reynolds stress term in Equation (2.1) by Equation (2.3), Equation (2.1) becomes

$$\frac{1}{r}\frac{\partial}{\partial r}\left[r(\nu + \varepsilon_M)\frac{d\overline{U^*}}{dr}\right] = \frac{1}{\rho}\frac{\partial \overline{P^*}}{\partial x} \qquad (2.4)$$

Before integrating Equation (2.4), first non-dimensionalize such that

$$\bar{U} = \frac{\overline{U^*}}{U_m} , \quad \bar{P} = \frac{\overline{P^*}}{\rho U_m^2}$$

$$E = \frac{\epsilon_M}{\nu} , \quad \bar{x} = \frac{x}{r_o} , \quad \bar{r} = \frac{r}{r_o} \tag{2.5}$$

Thus Equation (2.4) becomes

$$\frac{1}{\bar{r}} \frac{\partial}{\partial \bar{r}} \left[\bar{r}(1+E) \frac{d\bar{U}}{d\bar{r}}\right] = RF \tag{2.6}$$

where

$$R = \frac{r_o U_m}{\nu} \quad \text{and} \quad F = \frac{d\bar{P}}{d\bar{x}} \tag{2.7}$$

Notice that in the equation for the non-dimensional pressure drop (2.7) the partial derivatives have been replaced by total derivatives. From the time-averaged momentum equation in the r-direction and the assumption that at the wall $\bar{v}_r^2=0$, it can be easily shown that the pressure is a function of $\bar{x}$ only.

Equation (2.6) may be integrated twice with the aid of the boundary conditions

$$\frac{d\bar{U}}{d\bar{r}} = 0 \qquad \text{at} \qquad \bar{r} = 0$$

and (2.8)

$$\bar{U} = 0 \qquad \text{at} \qquad \bar{r} = 1$$

The result of integration is

$$\bar{U}(\bar{r}) = \frac{RF}{2} \int_{1}^{\bar{r}} \frac{r_1}{1+E(r_1)} \, dr_1 \tag{2.9}$$

If the eddy diffusivity distribution is known, the velocity profile may be calculated from Equation (2.9); however, the choice of an eddy diffusivity expression is not totally free.

Normalization of Equation (2.9) requires that,

$$1 = RF \int_{0}^{1} \int_{1}^{\bar{r}} \left[\frac{r_1}{1+E(r_1)} \, dr_1\right] \bar{r} \, d\bar{r} \tag{2.10}$$

The eddy diffusivity expression in Equation (2.10) must be chosen so that this equation is satisfied. Consequently the eddy diffusivity must be determined such that the product of RF determined from Equation (2.10) agrees with the experimental condition. In deriving Equation (2.10) the defining equation for U_m was used

$$U_m = \frac{2}{r_o^2} \int_{0}^{r_o} \overline{U^*} \, r \, dr \tag{2.11}$$

When non-dimensionalized, Equation (2.11) becomes

$$1 = 2 \int_{0}^{1} \bar{U} \, \bar{r} \, d\bar{r} \tag{2.12}$$

Simple substitution of Equation (2.9) for $\bar{U}(\bar{r})$ in Equation (2.12), would yield Equation (2.10).

Before going any further it is necessary to derive a relationship between F and the wall shear stress or alternately the shear velocity.

The need for this relationship would become evident later. By definition

$$\tau_w = \mu \left(\frac{d\overline{U^*}}{dr}\right)_w \tag{2.13}$$

After non-dimensionalization Equation (2.13) becomes

$$\tau_w = \frac{\mu U_m}{r_o} \left(\frac{d\bar{U}}{d\bar{r}}\right)_w \tag{2.14}$$

The assumption of a linear velocity profile throughout the viscous layer leads to the conclusion that E = 0 in that region. At the wall where $\bar{r} = 1$ and E = 0 Equation (2.9) shows that

$$\left(\frac{d\bar{U}}{d\bar{r}}\right)_w = \frac{1}{2} RF \tag{2.15}$$

Thus

$$F = \frac{2\tau_w}{\rho U_m^2} = \frac{2U_\tau^2}{U_m^2} \tag{2.16}$$

where

$$U_\tau = \left(\frac{\tau_w}{\rho}\right)^{1/2} \tag{2.17}$$

The value of F obtained from Equation (2.16) is solely dependent on experimental values. Equation (2.16) also shows that F is the Fanning friction factor but here it is calculated using pressure-drop and flow rate data. Therefore, it will be referred to as the experimental value of F.

Eddy Diffusivity

In order to calculate the velocity profile, there is a need for an integrable expression for eddy diffusivity; this is shown by the velocity profile expression, Equation (2.9).

In this study the eddy diffusivity model suggested by R. D. Cess (1) for turbulent pipe flows was employed. The Cess model is a continuous function and does not go to zero at the pipe center line. This expression for the eddy diffusivity of momentum is a combination of Van Driest's (8) sublayer equation and Reichardt's (11) middle law expression. Cess combines these two expressions to yield (see Tiederman and Reynolds (12)),

$$E = \frac{1}{2}\left\{1 + \frac{K^2 r_o^{+2}}{9}\left[1 - \left(\frac{r}{r_o}\right)^2\right]^2\left[1 + 2\left(\frac{r}{r_o}\right)^2\right]^2\left[1 - \exp\left(\frac{-(1-r/r_o)}{A^+/r_o^+}\right)\right]^2\right\}^{1/2} - 1/2 \qquad (2.18)$$

where

$$r_o^+ = \frac{r_o U_\tau}{\nu} \qquad (2.19)$$

In Equation (2.18), K and A^+ are free constants. K is called the von Karman constant and 1/K is proportional to the slope of the log portion of the universal law of the wall. A^+ is a constant that characterizes the thickness of the wall layer flow, in wall coordinates.

After determining the two parameters A^+ and K involved in the expression for eddy diffusivity it is possible to calculate the distribution of the eddy diffusivity. Consequently after the Reynolds

number has been specified, the velocity profile can be calculated from a simple integration of Equation (2.9).

Calculation Procedures

The procedure to be outlined in this section was first adopted by M. M. Reischman (2) for drag reducing flows in a two-dimensional channel.

The basic idea is that F, R, and K are specified in the Cess model and A^+ is determined by iteration such that Equation (2.10) will be satisfied. This differs from the normal solvent-flow procedure where the value of A^+ is a constant bounded by

$$20 \leq A^+ \leq 30 \tag{2.20}$$

In drag reducing flows this is not the case because the thickness of the near-wall region (viscous sublayer and buffer region) increases as the amount of drag reduction increases. Therefore, it is not possible to make a reasonable apriori estimate of A^+ and it must be calculated by an iterative scheme.

The inputs to the iterative computer scheme are the values of R, F, K, and initial value of A^+. The values of R and F are fixed by the experimental conditions. The final value of A^+ is determined by the normalization condition Equation (2.10) and iteration. The initial value of A^+ is iterated in order to get a convergence between the experimental value of F and the value of F obtained from Equation (2.10). For each calculation the value of the von Karman constant K was set at a fixed value. This was possible because it has been established that in a drag reducing flow the slope of the log portion

is the same as the solvent slope, where 1/K is proportional to the slope of the log portion of the universal law of the wall.

Distribution of $E(\overline{r})$ and $\overline{U}(\overline{r})$ are computed within the iterative program from Equations (2.18) and (2.9) respectively. The experimental value of F obtained from Equation (2.16) is compared to the value of F from normalization condition Equation (2.10). If the error is large, the value of A^+ is changed and the process is repeated. The iteration for a final value of A^+ and a final mean velocity profile is stopped when a sufficiently small error of about 0.1% exists between the two compared F values. The numerical integrations were performed using a 1/3 Simpson's Rule with 400 equally spaced integrational increments. See Appendix C for the computer flow chart.

Results and Discussion

In order to verify the computational scheme, this velocity profile prediction technique was implemented for solvent flows.

Figure 2 shows the comparison between the solvent data of Virk (9) and the calculated mean velocity profiles in non-dimensional wall layer coordinates using the Cess model and K = 0.4. The agreement is excellent at both Reynolds numbers.

Figure 3 demonstrates the change in the dimensionless velocity profiles at two different Reynolds numbers. The calculated profiles are compared to the data of Nikuradse (13) for smooth pipes. The agreement is good at both Reynolds numbers. Consequently the Cess model provides a meaningful family of velocity profiles.

Mean velocity proviles predicted for drag reducing flows are compared with the experimental data of Virk (9) in Figure 4. Virk's

measurements were made with a Pitot tube in the center portion of a 32.1 mm. pipe in which a 1000 ppm solution of polyethylene oxide, Polyox N3000, was flowing. The agreement is good at both Reynolds numbers.

Figure 5 compares the present prediction technique with the prediction of Debrule (14). His prediction method uses Deisseler's diffusivity equation for the near-wall region and is only valid close to the wall. The two prediction methods are in excellent agreement for the near-wall region for all Reynolds numbers. The predicted velocity profiles of the present model have been presented in form of a continuous curve. Debrule presents his predictions in form of two "patched" equations for the near-wall and turbulent core region and the differences in Figure 5 is due to this "patching" of equations.

Figure 6 compares the predicted mean velocity profiles for both solvent and drag reducing flows. The locus of solvent velocity data for the near-wall region is shown by $U^+ = y^+$ and for the turbulent core by the following expression

$$U^+ = 1/K \ln y^+ + B \qquad (2.21)$$

where $1/K = 2.50$ and $B = 3.5$, $U^+ = \overline{U^*}/U_\tau$ and $y^+ = yU_\tau/\nu$. K and B are the two constants that define the universal velocity profile $U^+ = F(y^+)$ for Newtonian fluids and are thus independent of the Reynolds number. The log protion of the velocity profile appears to be identical to that of the solvent except for a vertical shift. This part of the mean velocity profile can be described in the form of the law of the wall by

$$U^+ = 1/K \ln y^+ + B + \Delta U^+ \qquad (2.22)$$

The term ΔU^+ denotes the upward shift of the logarithmic profile with respect to the universal logarithmic profile for solvent flow which was expressed by Equation (2.21) when $\Delta U^+ = 0$. The shift ΔU^+ in the profile depends on the flow conditions, as well as the nature and concentration of the polymer. The region between the viscous sublayer $U^+ = y^+$ and the turbulent core is called the buffer region. Figure 7 shows the three regions that exist in a drag-reducing turbulent boundary layer as proposed by Reischman (2).

The change in the velocity profiles of solvent and drag reducing flows may be described by saying that the viscous sublayer and the buffer region extend further from the wall in drag reducing flows than in solvent flows. This is in agreement with the thickening of "viscous sublayer" proposed in many papers.

The eddy diffusivity distributions for solvent and drag reducing flows are compared in Figure 8 at comparable Reynolds numbers. Note that Figure 8 indicates a dip in the eddy diffusivity in the central region, but it does not go to zero at the center line of the pipe. Also, from Figure 8 it can be noted that the eddy diffusivity distributions for solvent and drag reducing flows basically show the same trends. The solvent eddy diffusivities have higher values than the polymer solutions at the same Reynolds number. Thus the Cess model predicts that the addition of polymer in water drastically reduces the eddy diffusivity near the wall.

CHAPTER III

HEAT TRANSFER

In this chapter an expression for the heat transfer coefficient will be obtained from the energy equation. The analysis developed here is for the case of a circular tube with fully developed flow, constant heat rate, and moderate Prandtl number. The Cess eddy diffusivity model used in Chapter II and the velocity profile obtained in that chapter are needed here. The analysis is based on the key assumption that the eddy diffusivities of heat and momentum are equal (Reynolds analogy). The temperature profile can also be predicted using the energy equation and Reynolds analogy. In the latter part of this chapter the calculation procedures will be outlined and the results will be compared and discussed with the heat transfer data of others for both solvent and drag reducing flows.

Integral Expressions for Heat Transfer Coefficient

The analysis begins with the defining equation for the heat transfer coefficient

$$\dot{q}_o'' = h\ (T_o - T_m) \tag{3.1}$$

From Fourier's Law of heat conduction the following must also apply at the wall surface

$$\dot{q}_o'' = + k\left(\frac{\overline{\partial T^*}}{\partial r}\right)_{r = r_o} \tag{3.2}$$

Equating the two equations and solving for the heat transfer coefficient yields

$$h = \frac{k}{T_o - T_m}\left(\frac{\overline{\partial T^*}}{\partial r}\right)_{r = r_o} \tag{3.3}$$

From Equation (3.3) it can be seen that only two expressions are needed in order to evaluate the heat transfer coefficient, that is: an expression for the difference in wall and mixed mean temperature $(T_m - T_o)$ and one for the slope of the temperature profile at the wall $(\overline{\partial T^*}/\partial r)_{r=r_o}$.

To obtain the expression for the temperature difference let us start with the defining equation for mixed mean temperature

$$T_m = \frac{2}{r_o^2\, U_m} \int_0^{r_o} \overline{U^*}\ \overline{T^*}\ r\ dr \tag{3.4}$$

With the aid of the defining equation for U_m, Equation (2.11), Equation (3.4) becomes

$$T_m - T_o = \frac{2}{r_o^2\, U_m} \int_0^{r_o} \overline{U^*}(\overline{T^*} - T_o) r\ dr \tag{3.5}$$

Non-dimensionalizing Equation (3.5) such that

$$\overline{U} = \frac{\overline{U^*}}{U_m}\ ,\ \overline{y} = \frac{y}{r_o}\ ,\ \overline{r} = \frac{r}{r_o} \tag{3.6}$$

where $y = r_o - r$. Then Equation (3.5) becomes

$$T_o - T_m = 2 \int_0^1 \overline{U}\ (\overline{T^*} - T_o)(1-\overline{y})d\overline{y} \qquad (3.7)$$

Since the values of $\overline{T^*}$ at every point in the flow are not known, an expression for $(\overline{T^*} - T_o)$ in terms of flow parameters that are usually known is desired. Start with the time-averaged differential energy equation for a circular tube in cylindrical coordinates.

$$\frac{1}{r}\frac{\partial}{\partial r}\left[r\rho c\left(\alpha \frac{\partial \overline{T^*}}{\partial r} - \overline{ut}\right)\right] = \overline{U^*}\rho c \frac{\partial \overline{T^*}}{\partial x} \qquad (3.8)$$

where $\alpha = k/\rho c$ is the thermal diffusivity of the fluid. The coordinate system is shown in Figure 1.

In writing Equation (3.8), the following assumptions were made:

a) The velocity profile is fully developed.

b) Axial conduction is negligible.

c) The flow is steady and axisymmetric.

d) The fluid properties are constant.

In Equation (3.8) the velocity and temperature perturbations are

$$\begin{aligned} U &= \overline{U^*} + u \\ T &= \overline{T^*} + t \end{aligned} \qquad (3.9)$$

In order to proceed further, an expression should be defined to replace the non-linear term $\overline{ut}$ in Equation (3.8). Consequently, the eddy diffusivity of heat is defined as

$$\varepsilon_H = \frac{-\overline{ut}}{\frac{\partial \overline{T^*}}{\partial r}} \qquad (3.10)$$

Replacing the non-linear term in Equation (3.8) by Equation (3.10), Equation (3.8) becomes

$$\frac{1}{r}\frac{\partial}{\partial r}\left[r(\alpha+\varepsilon_H)\frac{\partial \overline{T^*}}{\partial r}\right] = \overline{U^*}\frac{\partial \overline{T^*}}{\partial x} \tag{3.11}$$

Consider the case of constant heat rate in the axial direction. If the temperature profile is fully established, then the rate of change of temperature with length must be the same at every point. Therefore,

$$\frac{\partial \overline{T^*}}{\partial x} = \frac{dT_m}{dx} = \text{Constant} \tag{3.12}$$

With the assumption of constant heat rate per unit of tube length, Equation (3.11) becomes

$$\frac{1}{r}\frac{\partial}{\partial r}\left[r(\alpha+\varepsilon_H)\frac{\partial \overline{T^*}}{\partial r}\right] = \overline{U^*}\frac{dT_m}{dx} \tag{3.13}$$

Before attempting to integrate Equation (3.13), let us shift the independent variable as follows

$$y = r_o - r \tag{3.14}$$

Then Equation (3.13) becomes

$$\frac{1}{r_o-y}\frac{\partial}{\partial y}\left[(r_o-y)(\alpha+\varepsilon_H)\frac{\partial \overline{T^*}}{\partial y}\right] = \overline{U^*}\frac{dT_m}{dx} \tag{3.15}$$

Equation (3.15) may be integrated twice using the boundary conditions

$$\overline{T^*} = T_o \quad \text{at} \quad y = 0$$

and (3.16)

$$\frac{\partial \overline{T^*}}{\partial y} = 0 \quad \text{at} \quad y = r_o$$

The result of the integration is

$$\overline{T^*} - T_o = \frac{dT_m}{dx} \int_0^y \left[\frac{\int_{r_o}^{y_1} \overline{U^*}(r_o - y_2)dy_2}{(r_o - y_1)(\alpha + \varepsilon_H)} \right] dy_1 \qquad (3.17)$$

If the heat input is constant in the axial direction, then an energy balance dictates that

$$\frac{dT_m}{dx} = \frac{2\dot{q}_o''}{r_o U_m \rho c} \qquad (3.18)$$

Substituting Equation (3.18) in Equation (3.17) and then non-dimensionalizing such that

$$\overline{U} = \frac{\overline{U^*}}{U_m} , \quad E = \frac{\varepsilon_M}{\nu} = \frac{\varepsilon_H}{\nu} , \quad \overline{y} = \frac{y}{r_o} \qquad (3.19)$$

Equation (3.17) becomes

$$\overline{T^*} - T_o = \left(\frac{2r_o\dot{q}_o''}{\rho c \nu}\right) \int_0^{\overline{y}} \left[\frac{\int_1^{\overline{y}_1} \overline{U}(1-\overline{y}_2)\, d\overline{y}_2}{(E(\overline{y}_1) + \frac{1}{Pr})(1-\overline{y}_1)} \right] d\overline{y}_1 \qquad (3.20)$$

Here $Pr = \nu/\alpha$ is the fluid Prandtl number.

Note that in Equation (3.20) the key assumption is that the eddy diffusivities of heat and momentum are equal at any particular point in the flow. This is the essence of analogy proposed by Reynolds (15). Current knowledge of the relationship between the eddy diffusivity for heat and the eddy diffusivity for momentum is in a state of uncertainty. In view of this, it is believed that for the Prandtl number range of this study, $1 < Pr < 20$, the choice of $\varepsilon_H = \varepsilon_M$ is not

unreasonable. This assumption enables us to use the same eddy diffusivity model that was proposed in Chapter II.

Equation (3.20) is the expression for $(\overline{T^*} - T_o)$ that should be substituted in Equation (3.7) to give one of the two expressions for evaluating Equation (3.3) for the heat transfer coefficient. After substitution Equation (3.7) becomes

$$T_o - T_m = \frac{4r_o \dot{q}_o''}{\rho c \nu} \int_0^1 \left\{ \bar{U}(1-\bar{y}) \int_0^{\bar{y}} \left[\frac{\int_1^{\bar{y}_1} \bar{U}(1-\bar{y}_2)d\bar{y}_2}{(E(\bar{y}_1)+\frac{1}{Pr})(1-\bar{y}_1)} \right] d\bar{y}_1 \right\} d\bar{y} \tag{3.21}$$

In order to obtain the second expression in Equation (3.3), start with Equation (3.20). Differentiating this expression with respect to y yields

$$\frac{\partial \overline{T^*}}{\partial y} = \frac{2\dot{q}_o''}{\rho c \nu} \left[\frac{\int_1^{\bar{y}} \bar{U}(1-\bar{y}_1)d\bar{y}_1}{(E(\bar{y})+\frac{1}{Pr})(1-\bar{y})} \right] \tag{3.22}$$

Evaluating Equation (3.22) at the wall surface (y = 0) yields

$$\left(\frac{\partial \overline{T^*}}{\partial y}\right)_{y=0} = \left(\frac{2\dot{q}_o'' Pr}{\rho c \nu}\right) \int_1^0 \bar{U}(1-\bar{y})d\bar{y} \tag{3.23}$$

where it is assumed that E = 0 at the wall surface.

Transforming Equation (3.3) in the form of the new independent variable y and substituting Equations (3.21) and (3.23) into the transformed form of Equation (3.3) gives

$$h = \left(\frac{k}{2r_o}\right) \frac{Pr \int_1^0 (1-\bar{y})\bar{U}\, d\bar{y}}{\int_0^1 \bar{U}(1-\bar{y})\left\{ \int_0^{\bar{y}} \left[\frac{\int_1^{\bar{y}_1} \bar{U}(1-\bar{y}_2)d\bar{y}_2}{(E(\bar{y}_1)+\frac{1}{Pr})(1-\bar{y}_1)} \right] d\bar{y}_1 \right\} d\bar{y}} \qquad (3.24)$$

Equation (3.24) is the equation that is used for the heat transfer coefficient calculations. Note that only two new inputs, thermal conductivity (k) and Prandtl number (Pr) are introduced in this equation compared to the equation for the velocity profile, Equation (2.9). In using Equation (3.24) for heat transfer calculations it is assumed that the velocity profile and the distribution for eddy diffusivity as introduced in Chapter II are known.

Equation (3.24) is most often expressed in non-dimensional form as follows

$$Nu = \frac{Pr \int_1^0 (1-\bar{y})\bar{U}d\bar{y}}{\int_0^1 \bar{U}(1-\bar{y})\left\{ \int_0^{\bar{y}} \left[\frac{\int_1^{\bar{y}_1} \bar{U}(1-\bar{y}_2)d\bar{y}_2}{(E(\bar{y}_1)+\frac{1}{Pr})(1-\bar{y}_1)} \right] d\bar{y}_1 \right\} d\bar{y}} \qquad (3.25)$$

where $Nu = h(2r_o)/k$ is the Nusselt number.

This solution can be represented in a different way that allows a more convenient presentation of the results and comparison with the data in the literature. By dimensional reasoning,

$$Nu = St\ Re\ Pr \qquad (3.26)$$

where

$St = h/U_m \rho c$ is the Stanton number

$Re = U_m(2r_o)/\nu$ is the Reynolds number

$Pr = \mu c/k$ is the Prandtl number

Combining Equations (3.25) and (3.26) and solving for St yields

$$St = \frac{\int_1^0 \bar{U}(1-\bar{y})d\bar{y}}{Re \int_0^1 \bar{U}(1-\bar{y})\left\{ \int_0^{\bar{y}} \left[\frac{\int_1^{\bar{y}_1} \bar{U}(1-\bar{y}_2)d\bar{y}_2}{(E(\bar{y}_1)+\frac{1}{Pr})(1-\bar{y}_1)}\right] d\bar{y}_1 \right\} d\bar{y}} \qquad (3.27)$$

In this work the heat transfer data will be presented in terms of Stanton number or Nusselt number as a function of Reynolds number.

In the process of deriving an expression for the heat transfer coefficient, an equation was also obtained that can be used to predict the non-dimensional temperature profile. Substituting Equation (3.1) for the wall surface heat flux into Equation (3.20) yields

$$\overline{T^*} - T_o = (T_o - T_m)\left(\frac{2r_o h}{\rho c \nu}\right) \int_0^{\bar{y}} \left[\frac{\int_1^{\bar{y}_1} \bar{U}(1-\bar{y}_2)d\bar{y}_2}{(E(\bar{y}_1)+\frac{1}{Pr})(1-\bar{y}_1)}\right] d\bar{y} \qquad (3.28)$$

Then

$$\theta = -\,Re\ St \int_0^{\bar{y}} \left[\frac{\int_1^{\bar{y}_1} \bar{U}(1-\bar{y}_2)d\bar{y}_2}{(E(\bar{y}_1)+\frac{1}{Pr})(1-\bar{y}_1)}\right] d\bar{y} \qquad (3.29)$$

where $\theta = \overline{T^*} - T_o / T_m - T_o$ is the non-dimensional temperature.

Equation (3.29) predicts the non-dimensional temperature profile with no additional input parameters. In using Equation (3.29) for temperature profile prediction it is assumed that the heat transfer coefficient, velocity profile and eddy diffusivity distribution are known.

Calculation Procedures

The calculation procedure at this point is very straightforward and is a continuation of the procedure outlined in Chapter II for the velocity profile determination.

The inputs to the iterative computer scheme are again the values of R, F, A^+ and K plus the two new input parameters k and Pr.

Computation starts with the assumption that the distributions of the velocity profile and the eddy diffusivity are already stored in the computer program. The heat transfer coefficient and the temperature profile distribution are computed within the iterative computer program from Equations (3.24) and (3.29) respectively. The numerical integrations were performed using a 1/3 - Simpson's Rule with 400 equally spaced integrational increments. See Appendix C for the computer flow chart.

Results and Discussion

The suggested heat transfer prediction scheme was implemented for solvent flows to verify the computational procedure and to check the validity of the model. A comparison between the present prediction scheme and several analytical models and correlations as well as the experimental data of Debrule (14) was made at different Prandtl

and Reynolds numbers for Newtonian fluids. The theoretical models and correlations used for this comparison are listed in Table I, Appendix A.

The solvent heat transfer experiments of Debrule (14) in a 0.377 in. I.D. smooth pipe were conducted at three different Pr (Pr = 4.38, Pr = 6.16, Pr = 10.3). Only the solvent experimental data of Debrule were used for this comparison, because they covered a wide range of Reynolds and Prandtl numbers and Debrule reported enough information to start the calculations. The point by point comparison of the predicted Stanton numbers with the experimental data is shown in Figure 9. This figure demonstrates the dependence of the Stanton number on the Reynolds number of the flow at different Prandtl numbers. The agreement with the experimental data is considered to be very good.

The solvent models of von Karman (16) and Friend and Metzner (17) listed in Table I are the only ones considered here because they were modified to account for drag reduction by Poreh and Paz (4), and Wells (6) respectively. According to semiempirical model of von Karman (16) the flow is divided into three regions: a viscous sublayer, a buffer zone, and a turbulent core. By calculating heat flux it was found that according to von Karman's model

$$St = \frac{Nu}{Re\ Pr} = \frac{(f/8)}{1+5\sqrt{f/8}\ \{(Pr-1)+\ln[1+\frac{5}{6}(Pr-1)]\}} \qquad (3.30)$$

Modification of Equation (3.30) for drag reducing flows will be explained later.

The semiempirical model of Friend and Metzner (17) for heat transfer is

$$St = \frac{Nu}{Re\ Pr} = \frac{(f/8)}{\frac{\overline{U_1^*}}{U_\tau}(f/8)^{1/2}(Pr-1)F(Pr)+1.2} \qquad (3.31)$$

Equation (3.31) was basically developed from the assumption of complete similarity between the temperature and velocity profiles. Since at high Prandtl numbers there is a difference between the profiles, this difference is expressed as a function of Prandtl number only and is shown in the first term of the denominator. The value of the second term in the denominator has also been changed from 1 to 1.2 to agree with their correlation for purely viscous fluids. Friend and Metzer have found that for a large range of Prandtl number

$$F(Pr) = (Pr)^{-1/3} \qquad (3.32)$$

and $\overline{U_1^*}/U_\tau$ was found to be a constant equal to 11.8.

The Nusselt numbers predicted by the present model are compared with the solvent theoretical models of von Karman (16), and Friend and Metzner (17) in Figure 10. The predicted values shown in Figure 10 have been curve fitted. The experimental flow rate, pressure drop solvent data of Debrule (14) were used for these predictions. It seems from Figure 10 that the present model is closer to the experimental results than the other models; however, the differences in the values of Nusselt numbers predicted by the different models are not large.

Comparison of the present model with the more conventional correlations is made in Figure 11. The comparisons made are based upon

the three equations:

Sieder-Tate (18) equation:

$$Nu = 0.027\ Pr^{1/3}\ Re^{0.8} \tag{3.33}$$

Kays (19) equation:

$$\text{for } 1.0 < Pr < 20$$

$$Nu = 0.0155\ Pr^{0.5}\ Re^{0.83} \tag{3.34}$$

Dittus-Boelter (20) equation:

$$Nu = 0.023\ Pr^{0.4}\ Re^{0.8} \tag{3.35}$$

The experimental data of Debrule (14) were used in these predictions. From Figure 11 it seems that again the present model is as close to the experimental results as the other correlations. Among these five other mentioned prediction techniques, the von Karman model (16) and Kays' (19) equation are closest to the present model and to the experimental results.

Figure 12 shows the plot of the theoretical values of the Stanton number, calculated from the experimental values of the friction factor, Prandtl and Reynolds numbers using the present theoretical model compared to the experimental values of Stanton number. The data is for solvent flows. The correlation between the theoretical values is good and all the experimental data are predicted by the theoretical model within an error of $\pm$ 10 percent. This shows some indication about the reliability of the present model in predicting the heat transfer coefficients for solvent flows.

Very few experimental temperature profile measurements are available in the literature. The measurements of Smith, Gowen, and Wasmund (21) was the only one that had enough information to start the calculations.

Smith, Gowen, and Wasmund (21) measured heat transfer data at Pr = 6.2 and radial temperature profiles at Pr = 5.7 for the turbulent flow of water in a 2.058 in. I.D. smooth pipe. The predicted heat transfer coefficients show excellent agreement with the reported experimental data of Smith, et al. (21); this is shown in Figure 12.

Temperature profile for water flowing turbulently in a pipe shows a semilogarithmic relationship in the turbulent core that is similar to the universal velocity profile. The universal temperature profile takes the form

$$T^+ = A \ln y^+ + B$$

where (3.36)

$$T^+ = (T_o - \overline{T^*})\, U_\tau \rho c/\dot{q}_o''$$

The temperature measurements of Smith, et al. (21) were reported in the form of universal temperature profile. This form of non-dimensional temperature profile does not require knowledge of the heat transfer coefficient and the profile can be predicted if the velocity profile is known. Rearrangement of Equation (3.20) gives the desired equation for predicting the universal temperature profile. The desired equation is

$$T^+ = \left(\frac{2r_o U_\tau}{\nu}\right) \int_0^{\bar{y}} \left[\frac{\int_1^{\bar{y}_1} \bar{U}(1-\bar{y}_2)\, d\bar{y}_2}{\left(E(\bar{y}_1) + \frac{1}{Pr}\right)(1-\bar{y}_1)}\right] d\bar{y}_1 \qquad (3.37)$$

Figure 13 shows the universal temperature profile T^+ vs. log y^+. This figure compares the predicted temperature profiles with the experimental data of Smith, et al. (21) at three different Reynolds numbers. The predicted and experimental temperature profiles are in very good agreement.

The drag reduction prediction techniques deduced from the solvent theoretical models and correlations are listed in Table I, Appendix A. First these theoretical models and correlations will be discussed and then compared with the present model.

Poreh and Paz (4) extended von Karman's (16) semiemprical model so that it could be applied to drag reducing flows. The analysis of heat transfer in dilute polymer solutions presented by Poreh and Paz is similar to that of von Karman. The velocity profile consists of three different regions: a viscous sublayer, a buffer region and a turbulent zone. They generalized von Karman's model by changing the limits of the three regions so that the velocity profile in the turbulent zone would fit the measurements of Elata, et al. (5) in pipe flow of dilute polymer solutions. Poreh and Paz (4) assumed that in the cases of Newtonian as well as polymeric solutions

$$y_1^+/y_j^+ = 0.43 \tag{3.38}$$

where y_1^+ denotes the edge of the viscous sublayer and y_j^+ is the intersection of the shifted equation for the turbulent zone with the viscous sublayer equation.

They have proposed the following expression for the velocity profile in the buffer zone.

$$\ln(y_2^+/y_1^+) = \frac{1.32\ y_j^+ - 4.9}{y_j^+ - 5.8} \tag{3.39}$$

where y_2^+ is the edge of the buffer zone.

As shown by Equation (3.39), their velocity profile is dependent on one parameter, y_j^+, which is related to ΔU^+ and the polymer properties by the following expressions

$$y_j^+ - 2.5\ \ln\ y_j^+ = \Delta U^+ + 5.5 \tag{3.40}$$

and

$$\Delta U^+ = 2.5\ C\ \ln\ (\tau_w\ t_1/\mu) \tag{3.41}$$

where t_1 is a characteristic relaxation time of the polymer molecules, μ the viscosity of the solution, and C a concentration dependent parameter. Equation (3.41) is based on experiments of Elata, et al. (5).

Poreh and Paz (4) calculated heat transfer coefficients for flows of dilute polymeric solutions by the following expression

$$St = (f/8)^{1/2}/\{y_1^+(\ln[Pr-(Pr-1)\frac{y_1^+}{y_2^+}]+(Pr-1))+(8/f)^{1/2} + \frac{125}{16}(f/8)\} \tag{3.42}$$

Equation (3.42) shows that Stanton or Nusselt numbers are functions of Pr, Re, y_1^+, y_2^+, and f. Compared to the present model, the model of Poreh and Paz requires two additional inputs, y_1^+ and y_2^+. To evaluate y_1^+ and y_2^+, information about the properties of the polymer solution and the polymer are required.

Wells (6) has derived an equation for predicting heat transfer rates in drag reducing solutions by modifying Friend and Metzner's (17)

semiempirical relation for Newtonian fluids. An implicit assumption in the derivation is that the reduction of onset points for the heat transfer and friction are the same. It was mentioned earlier that for purely viscous fluids the ratio $\overline{U_1^*}/U_\tau$ in Equation (3.31) is a constant, but for drag reducing fluids the dimensionless velocity has been found (3) to vary with shear stress such that

$$\frac{\overline{U_1^*}}{U_\tau} = 5.77 \log \frac{\overline{U_1^*}}{U_\tau} + 5.5 + \beta \log \frac{U_\tau}{U_\tau^*} \qquad (U_\tau \geq U_\tau^*) \quad (3.43)$$

where β is the drag reduction parameter, and U_τ^* the critical shear stress above which drag reduction occurs. β and U_τ^* can be obtained from the following friction factor correlation given by Wells (6)

$$F^{-1/2} = C_1 \log Re\, F^{1/2} - C_2 \qquad (U_\tau \geq U_\tau^*) \quad (3.44)$$

where

$$C_1 = 4 + \frac{\beta}{2^{1/2}} \left(\frac{n}{2-n}\right)$$

$$C_2 = 0.394 + \frac{\beta}{2^{1/2}} \log \left[\frac{U_\tau^* D^{\frac{n}{2-n}} 2^{\frac{n}{2(2-n)}}}{(a/\rho)^{1/2-n}}\right]$$

Equation (3.44) is written in slightly different form than that suggested by Meyer (3) to account for shear thinning fluids. a and n are the parameters of power law purely viscous properties.

Thus Equation (3.31) is modified by taking into account the change in the wall layer thickness. Therefore the heat transfer can be found from the following equation

$$Nu = \frac{(f/8)\, Re\, Pr}{1.02(\overline{U_1^*}/U_\tau)(f/8)^{1/2}(Pr-1)(Pr)^{-1/3}+1.2} \quad (3.45)$$

Wells equation shows that Stanton or Nusselt numbers are functions of Pr, Re, f and $\overline{U_1^*}/U_\tau$. Keeping in mind that in order to calculate the thickness of the near-wall region ($\overline{U_1^*}/U_\tau$), the values of the coefficient (a) and the exponent (n) of power law viscosity should be known. These are not requirements for the present model.

Since drag reducing polymeric additives increase the thickness of the near-wall region, models of Poreh and Paz (4), and Wells (6) require calculations for the thickness of the wall layer or a way to account for this thickening. As it was pointed out earlier, Poreh and Paz have changed the limits of the three regions of the flow such that their velocity profile would fit the measurements of Elata, et al. (5) in pipe flow of dilute polymer. Wells accounts for this thickening of the near-wall region by using Meyer's (3) equation and calculates the thickness from Equations (3.43) and (3.44). The suggested model of this study accounts for the thickening of the wall layer in a very logical fashion and does not require fitting the velocity profile to experimental measurements or the use of some correlation to calculate the thickness. The thickening of the near-wall region is accounted for in the iterative procedure that calculates A^+, the constant that characterizes the thickness of the wall layer. This procedure was explained in Chapter II.

The last prediction technique to be discussed in this section is the correlation of Smith, et al. (10). They measured the effects of drag reducing polymeric additives on heat transfer phenomenon in cases of maximum drag reduction. Smith, et al. found that heat transfer reduction obtained by polymer solutions was limited by the following best-fit asymptote

$$(St)(Pr)^{0.6} = (f/8) \qquad (3.46)$$

Equation (3.46) shows that the heat transfer during maximum drag reduction conditions obeys a Dittus-Boelter type correlation. They claim that this correlation also appears to be applicable to the polymer-dependent region if the wall-bulk temperature difference is small and if the solution is not highly shear-thinning. The correlation of Smith, et al. (10) does not give an insight to the mechanism by which drag reduction occurs and is only applicable to drag reducing solutions. In addition, velocity profile, eddy diffusivity distribution, and temperature profile cannot be predicted by this correlation.

The general scope of available experimental heat transfer data in drag reducing fluids that reported enough information to start the calculations are shown in Table II, Appendix A. There are a total of seven experiments wherein polymer solution was used. The general characteristics of the polymer solution used are also outlined. Most of the experimental results were reported in form of a graph and there is some error involved in replotting these experimental results. In this work the experimental data are denoted by closed symbols, the open symbols are used to show the predicted values by the present model, and the half open symbols show the predictions made by the prediction techniques of the others.

Gupta, Metzner, and Hartnett (22) have presented heat transfer and friction data for 0.745 in. I.D. pipe flow. The solution employed was of ET-597, a water soluble partially hydrolized polyacrylamide of

high molecular weight at concentrations of 100, 500, 4500 ppm. The lower concentration data exhibited no significant drag reduction and the higher concentration data were limited to early stages of transition. Only the 500 ppm data will be evaluated here. Although the Prandtl numbers ranged from 10.87 to 11.38, a single Prandtl number of 11.1 was used in the predictions.

The Stanton numbers predicted by the present model are compared to the predictions given by the techniques of Poreh and Paz (4), Wells (6), Smith, et al. (10), and the experimental data of Gupta, et al. in Figure 14. The differences in the values of Stanton numbers predicted by the different techniques are not large. It seems from Figure 14 that the present model and the correlation of Smith, et al. predict the experimental results equally well. The models of Wells and Poreh and Paz are not as close to the experimental data.

Debrule (14) has reported friction and heat transfer data for Polyox solutions in a 0.377 in. I.D. smooth pipe at Pr numbers 4.38, 6.16, and 10.3. Debrule's measurements were conducted in the constant heat flux mode. In his excellent experimental study careful attention has been paid to minimize mechanical and thermal degradation and effect of entrance section in the experiments. To my knowledge, it is the only study that controlled all the experimental conditions.

Comparison of the predicted values of Stanton numbers with the experimental data of Debrule for 10 ppm WSR-301 Polyox solution at three different Prandtl numbers are shown in Figure 15. The agreement with the experimental results is considered to be very good. The solvent data are also shown on the same figure to demonstrate the amount of reduction in heat transfer $[(St_{water}-St_{Poly.})/St_{water}]$. For

example from Figure 15 at Re = $7x10^4$ and Pr = 4.38 the heat transfer is reduced by about 77.6 percent and this is a considerable amount of reduction in the heat transfer due simply to the addition of polymer.

McNally (23) has obtained heat transfer and friction data for solutions of 2, 10, and 20 ppm WSR-301 Polyox in water. The measurements were made in a 0.78 in. I.D. smooth pipe. The heat transfer and pressure drop data were obtained at two different temperatures, and the friction factors corresponding to the heat transfer data were not reported. The Reynolds, Prandtl and Stanton numbers corresponding to heat transfer data were reported at film temperature of $149.5^{o}F$ and friction factors were reported at temperature of $73.3^{o}F$. In order to be able to predict McNally's data, the reported friction factors were used along with the reported normalized heat transfer data. McNally normalized his heat transfer data by making the reasonable assumption that heat transfer and friction onset points should be nearly the same under isothermal conditions. He made the correction by dividing the film Reynolds number by 2.76 and multiplying the j-factor by 1.22.

$$(Re)_{corr.} = (Re)_f/C_M$$

$$j_{corr.} = j(C_M)^{0.2} = f/8 \qquad (3.47)$$

where $C_M = 2.76$ is the McNally correction factor. The correction made the onset points coincide and yet did not alter the correlation of the pre-onset data.

The predicted Stanton numbers are compared with the experimental data of McNally in Figure 16. The agreement is good. For comparison the predictions made by the correlation of Smith, et al. (10) are

also shown on the same figure. The 2 ppm data is predicted by both prediction techniques equally well. Smith, et al. predict the 10 ppm data slightly better, but the present model predicts the 20 ppm data far better than the correlation of Smith, et al.

Monti (24) reported experimental data on friction and heat transfer coefficients for polyacrylamide ET-597 in a concentration range of 250-2000 ppm together with all the information on elastoviscous properties of the solution (such as the shear stress-shear strain rate dependence and the apparent viscosity-temperature dependence). All the experimental data were taken in a smooth wall straight circular pipe of 0.423 in. I.D. in fully developed turbulent flow conditions.

Figure 17 shows the experimental data of Monti compared with the predicted values of Nusselt number as a function of Reynolds number for solutions of 250, 500, 750 and 1000 ppm ET-597 in water. The Reynolds numbers used in Figure 17 are based on the viscosity of water as presented by Monti. The agreement between the predicted values and the experimental results is quite good.

After applying the present model to the experimental data of Howard (25), Pruitt, et al. (26), and Keuroughlian (27), it was noticed that the present model did not predict some of the experimental data very well. The problem was investigated and it was found that the friction factors corresponding to those particular data points all fall on or above the "maximum drag reduction asymptote" as given by Virk (28).

A three layer model describing the velocity profile in drag reducing fluids has been proposed by Virk. He suggested that drag reducing polymers create a new intermediate layer between the viscous

sublayer and the turbulent core, which he named the elastic sublayer. According to Virk, the velocities in this region can be described by a universal law:

$$U^+ = 11.7 \ln y^+ - 17.0 \qquad (3.48)$$

In the extreme case, when the elastic sublayer becomes large, and the extent of the turbulent core region is negligible, the friction coefficient is obtained by the integration of Equation (3.48) and can be described by a universal law:

$$(F)^{-1/2} = 19.0 \log (Re\ F^{1/2}) - 32.4 \qquad (3.49)$$

Equation (3.49) was termed by Virk the maximum drag reduction asymptote.

For the friction factor data points that fell on or above the maximum drag reduction asymptote, the value of K, the von Karman constant, was changed from a value of 0.4 to 1/11.7; since, according to Virk (28) for the case of maximum drag reduction, the fully turbulent logarithmic region does not exist and the value of K should correspond to the slope of the elastic sublayer region. This change in K improved the predicted values. In addition this change renders the previous interpretation of A^+ invalid. Since the elastic sublayer extends all the way to the center line, A^+ cannot characterize the thickness of the wall layer for these flows. In fact, A^+ was as low as the value of A^+ for solvent flows.

A second method was tried to overcome the discrepancy in the predicted values. In this method the Reichardt's (11) expression for the eddy diffusivity in the center portion of the pipe was left out of the Cess model and only Van Driest's (8) wall region eddy

diffusivity expression was used. This method did not improve the predicted values at all.

The non-dimensional velocity profiles in wall layer coordinates for the two maximum drag reduction methods are shown in Figure 18. The velocity profiles are for 10 ppm W301 data of Keuroughlian (27) at Re = 15.62×10^3. For comparison, the velocity profile with value of K = 0.4 and the elastic sublayer equation suggested by Virk (28) are also shown. The velocity profile with value of K = 1/11.7 agrees reasonably well with Virk's equation and this is a strong indication that the value of K = 1/11.7 should be used for the case of maximum drag reduction. Consequently in predicting the experimental data of Howard (25), Pruitt, et al. (26) and Keuroughlian (27) K was set equal to 1/11.7 for flows where the friction factor was on the maximum drag reduction asymptote.

Howard (25) conducted an experimental investigation to determine the effects of small concentration of aged Polyox WSR-301 and fresh Polyhall M-295 on the friction factor and convection heat transfer properties of water flowing in a 1/2 in. pipe. Howard reported experimental heat transfer and friction data for aged Polyox WSR-301 and fresh Polyhall M-295 in a range of 5-500 ppm.

Among Howard's experimental data only the 50 ppm data of fresh Polyhall M-295 and 12.5 ppm aged Polyox WSR-301 were chosen for predictions because these data showed less scatter in the reported friction factor data than most of Howard's results. As shown in Figure 19, four of Howard's experimental friction factors were on or above the Virk's maximum drag reduction asymptote. The value of K was set at 1/11.7 for these points. In Figure 20, the predicted values of

Stanton numbers are compared with the experimental data of Howard (25) for 50 ppm Polyhall M-295. The predictions with the value of K = 0.4 for the four data points are also shown by an arrow to illustrate the improvement of the predicted values when K was changed. For comparison purposes the predictions made by the correlation of Smith, et al. (10) are also shown. The agreement between the present model and the experimental data is good, and, as shown in Figure 20, the predictions made by the suggested model of this study is closer to the experimental results than the correlation of Smith, et al. Also shown on Figure 20, the experimental results of aged Polyox WSR-301 are predicted by the present model and the correlation of Smith, et al. Both models underpredict the experimental data by the same amount, and the predicted values are considerably lower than the experimental values. This underprediction could be due to either the unrealibility of the reported experimental results or the aging process which resulted in scission of the Polyox molecules and thus reduced its effectiveness.

Pruitt, Whitsitt and Crawford (26) reported both heat transfer and friction factor data for Separan AP-30. The data were obtained in a smooth pipe of 0.50 in I.D. The data for 10 and 100 ppm solutions of AP-30 were compared with the predicted values of present model and the predictions made by Smith, et al. (10), Wells (6), and Poreh and Paz (4). This comparison is shown in Figure 21. The 10 ppm data is predicted equally well by the four techniques and the agreement with experimental results is good. The 100 ppm data is predicted equally well by the present model and the model of Poreh and Paz. The Wells model is not as close to the experimental results and the Smith, et al. correlation is high. The poor prediction of the Smith, et al.

correlation could be the consequence of the 100 ppm data being highly shear-thinning, and, as discussed by Smith, et al., their correlation does not work well for highly shear-thinning solutions. The friction factors for two of the 100 ppm data points were on the maximum drag reduction asymptote as shown in Figure 19; these points were calculated with the present model with K = 0.4 and K = 1/11.7. Both predictions are shown on Figure 21.

Keuroughlian (27) reported heat transfer and friction factor data for 0.117 in. I.D. pipe flow. The heat transfer data reported were the average values for the test section and for constant heat flux mode. The solutions used were polyethylene oxide (Polyox) and distilled water.

The data for 10 ppm N3000 and 10 ppm W301 solutions of Polyox are compared with the predicted values of Stanton numbers given by the present model and the prediction techniques of Wells (6) and Smith, et al. (10). This is shown in Figure 22. The 10 ppm N3000 data are predicted slightly better by the correlation of Smith et al. than by the present model. The Wells model is not as close to the experimental results; however, the differences in the values of Stanton numbers predicted by the different techniques are not large. In the case of 10 ppm W301 experimental data, these differences are much larger, and the correlation of Smith, et al. is close to the experimental data. The present model and the Wells model are equally far from the experimental results. As shown in Figure 19, the experimental friction factors for the four data points used were on or above the maximum drag reduction asymptote, therefore these points were also predicted with K = 1/11.7. Both predictions are shown in Figure 22. The reason for the discrepancy in the predicted values of this model as compared to the experimental data

is not known. The present model has predicted Debrule's (14) 10 ppm Polyox experimental data quite well, which basically uses the same type of polymer, concentration and temperature range as those used by Keuroughlian (27) in his experiments which are in a higher range of Reynolds number. The underprediction cannot be contributed to the low range of Reynolds numbers, or the type of polymer used, because in previous comparisons this was proven, not to be the case. The only explanation could be that the data of Keuroughlian is on the maximum drag reduction asymptote and the present model appears not to be as good for the case of maximum drag reduction. The experimental data of Keuroughlian was the only set of experimental data which the present model did not predict satisfactorily. The good prediction of Smith, et al.'s correlation can be explained as the consequence of the fact that their equation is based on the best-fit asymptote of the heat transfer data of Keuroughlian (27) for the maximum drag reduction case. The present model should be checked with more experimental data for the case of maximum drag reduction to determine whether the inability of the model to predict this particular case is general or not.

Figure 23 compares the theoretical values of Stanton numbers calculated from the measured values of the friction factor, Prandtl and Reynolds number using the present theoretical model with the experimental values. The correlation between the theoretical and experimental values, except for the measurements with 10 ppm W301 of Keuroughlian (27) which were not included, is reasonable and almost all of the polymer experimental data are predicted by the theory within an error of $\pm$ 20 percent. This shows that the present model is reasonably good at predicting heat transfer coefficients in drag reducing flows.

As demonstrated throughout this chapter, the suggested model of this study in most cases predicts the available experimental heat transfer data reasonably well, as compared to the existing theoretical models and correlations for solvent and drag reducing flows. Due to lack of information on different fluid properties and the complexibility of some of the theoretical models, further comparison between the models was not possible. Therefore, no general conclusions can be drawn as to the reliability of the existing models. Clearly the present model proposes an alternative method for predicting heat transfer reduction in drag reducing flows. The great advantage of this model over the other theoretical models is the efficient method of obtaining A^+, the constant that characterizes the thickness of the wall layer, in contrast to models of Wells (6), Poreh and Paz (4), and Howard (7), which basically match a mathematical expression to the measured velocity profile to account for the thickening of the near-wall region. In the present model A^+ is determined directly from the information about the general flow parameters. The damping factor A^+, is of great interest, as the turbulent eddies are damped by the drag reducing polymer the near-wall region thickens. As the near-wall region thickens, less momentum is transferred near the tube wall, this results in drag reduction. The mechanism of drag reduction might be a result of this damping action.

The sensitivity of the present model was checked against the variation in the Prandtl number and friction factor measurements. These two parameters were chosen because they have a direct effect on the heat transfer predictions. A probable error of $\pm$ 10 percent was considered for the reported values of Pr and f. Three different sets of

experimental data were used to demonstrate these variations. The variation in these parameters was considered independently. Figures 24 and 25 show the variation in Pr and f respectively for the 10 ppm Polyox data of Debrule (14) at Pr = 4.38, Gupta's (22) 500 ET-597 data, and 20 ppm Polyox data of McNally (23). The predicted values with the variations in Pr and f have been curve fitted. As shown in Figure 24 the present model is not very sensitive to the variation of Pr, and the difference between the two limits of prediction is not large. Figure 25 suggests that the present model is more sensitive to the variation in pressure drop measurements and there is a large difference between the two limits of prediction.

CHAPTER IV

SUMMARY, CONCLUSIONS, AND RECOMMENDATIONS

Summary and Conclusions

The accomplishments of this investigation may be summarized as follows:

1. For turbulent drag reducing flows in pipes, Reischman's (2) scheme was extended to predict mean velocity profile using the proposed eddy diffusivity model of Cess (1). The Cess model for turbulent transport of momentum can also be utilized in the prediction of turbulent diffusivities for polymer pipe flows. The model is simple and straightforward and requires only information about the general flow parameters.

2. The validity of the prediction scheme has been demonstrated in Chapter II for solvent and drag reducing flows and showed good agreement with the velocity profile experimental results.

3. The Cess eddy diffusivity model shows that in the drag reducing flows the turbulent transport of momentum is lower than that of a comparable solvent flow. This reduction in eddy diffusivity implies reduction in turbulent mixing and consequently reduced heat transfer coefficients.

4. For heat transfer predictions in drag reducing pipe flows a theoretical model was developed. The model is for fully developed

velocity and temperature profiles, constant heat rate per unit of tube length, and moderate Prandtl number. The model is simple and straightforward and requires information on pressure drop, flow rate, thermal conductivity, and Prandtl number.

5. The suggested model of this study for drag reducing fluids was checked against three prediction techniques and experimental results of seven investigators. For most cases the model showed good agreement with the experimental results and prediction techniques. The maximum drag reduction data was not predicted well by the present model, and this might be a possible limitation of the model. More data are required for flows with large drag reduction to conclusively demonstrate the validity of the present model for flows at maximum drag reduction.

6. Temperature profiles were also predicted from a knowledge of mean velocity profile and eddy diffusivity distribution. The agreement with experimental results was good.

Recommendations

Based on observations made during this study, the following recommendations are made:

1. The present model should be checked with more experimental data for the case of maximum drag reduction to determine whether the inability of the model to predict this particular case is general or not.

2. Extend the internal flow prediction schemes to a fully developed two dimensional boundary layer.

An attempt was made to extend the prediction schemes outlined in Chapters II and III to an external fully developed boundary layer flow for the case of a flat plate with zero pressure gradient. A fundamental approach to the solution of the boundary layer equations for turbulent flows is to regard the turbulent boundary layer as a composite layer made up of inner and outer regions. For the inner region the Cess diffusivity model is no longer valid and only Van Driest's wall region eddy diffusivity should be used; and for the outer region a constant diffusivity modified by an intermittancy factor is used. The inner and outer regions are established from the continuity of eddy diffusivity expressions. At present the problem is how to determine value of A^+, the constant that characterizes the thickness of the wall layer. The value of A^+ can no longer be determined by the normalization condition as outlined in Chapter II; since the mean $(\overline{U^*})$ and the mass average (U_m) velocities do not match at the center of the pipe, there is no way to terminate the iteration procedure for determination of A^+. Once the value of A^+ is determined the boundary layer momentum and energy equations could be solved by an efficient and reliable finite difference method such as that of Cebeci and Smith (29).

BIBLIOGRAPHY

(1) Cess, R. D. "A Survey of the Literature in Heat Transfer in Turbulent Tube Flow." Westinghouse Research Report 8-0529-R24. Philadelphia: Westinghouse Corp., 1958.

(2) Reischman, M. M. "Laser Anemometer Measurements in Drag Reducing Flows." (Ph.D. Thesis, Oklahoma State University, 1973.)

(3) Meyer, W. A. "A Correlation of the Frictional Characteristics for Turbulent Flow of Dilute Viscoelastic Non-Newtonian Fluids in Pipes." AIChE J., Vol. 12, NO. 3(May, 1966), pp. 522-525.

(4) Poreh, M., and U. Paz. "Turbulent Heat Transfer to Dilute Polymer Solutions." Int. J. of Heat Mass Transfer, Vol. 11, NO. 5(1968), pp. 805-812.

(5) Elata, C., J. Lehrer, and A. Kahanovitz. "Turbulent Shear Flow of Polymer Solutions." Isr. J. of Tech., Vol. 4, NO. 1 (1966), pp. 87-95.

(6) Wells, C. S. "Turbulent Heat Transfer in Drag Reducing Fluids." AIChE J., Vol. 14, NO. 3(May 1968), pp. 406-410.

(7) Howard, R. G. "An Alternative Method for Predicting the Behavior of Drag Reducing Agents." Report No. 3554. Anapolis, Maryland: Naval Ship Research and Development Center, 1971.

(8) Van Driest, E. R. "On Turbulent Flow Near a Wall." J. Aeron Sci., Vol. 23(1956), p. 1007.

(9) Virk, P. S., E. W. Merrill, H. S. Mickley, K. A. Smith, and E. L. Mollo-Christensen. "The Toms Phenomenon: Turbulent Pipe Flow of Dilute Polymer Solutions." J. Fluid Mech., Vol. 30, part 2(1967), pp. 305-328.

(10) Smith, K. A., G. H. Keuroughlian, P. S. Virk, and E. W. Merril. "Heat Transfer to Drag Reducing Polymer Solutions." AIChE J., Vol. 15, NO. 2(March, 1969), pp. 294-297.

(11) Reichardt, H. "Vollständige Darstellung der turbulenten Geschwindigkeitsverteilung in glatten Leitungen." ZAMM, Vol. 31(1951), p. 208.

(12) Tiederman, W. G., and W. C. Reynolds. "Stability of Turbulent Poiseuille Flow with Application to the Malkus Theory of Turbulence." Report NO. FM-2. Stanford, Calif.: Stanford University, Thermosciences Div., Dept. of Mechanical Engineering, 1965.

(13) Nikuradse, J. "Gesetzmässigkeiten der turbulenten Strömung in glatten Rohren." VDI-Forschungsheft, Vol. 356(1932).

(14) Debrule, P. M. "Friction and Heat Transfer Coefficient in Smooth and Rough Pipes with Dilute Non-Newtonian Fluids in Pipes." (Ph.D. Thesis, California Institute of Technology, 1972.)

(15) Reynolds, O. Scientific Papers of Osborn Reynolds. Vol. II Cambridge, London: University Press, 1901.

(16) von Karman, T. "The Analogy Between Fluid Friction and Heat Transfer." Trans ASME, Vol. 61(1939), p. 705.

(17) Friend, W. L., and A. B. Metzner. "Turbulent Heat Transfer Inside Tubes and the Analogy Among Heat Mass and Momentum Transfer." AIChE J., Vol. 4, NO. 4(Dec., 1958), pp. 393-402.

(18) Sieder, E. N., and C. E. Tate. "Heat Transfer and Pressure Drop of Liquids in Tubes." Ind. Eng. Chem., Vol. 28(1936), p. 1429.

(19) Kays, W. M. Convective Heat and Mass Transfer. 1st ed. New York: McGraw-Hill, 1966.

(20) Dittus, F. W., and L. M. K. Boelter. University of California at Berkeley. Publs. Eng., Vol. 2(1930), p. 443.

(21) Smith, J. W., R. A. Gowen, and B. Wasmund. "Eddy Diffusivities and Temperature Profiles for Turbulent Heat Transfer to Water in Pipes." AIChE Symp. Ser., Vol. 63, NO. 77(1967), pp. 92-101.

(22) Gupta, M. K., A. B. Metzner, and J. P. Hartnett. "Turbulent Heat Transfer Characteristics of Viscoelastic Fluids." Int. J. of Heat Mass Transfer, Vol. 10(1967), pp. 1211-1224.

(23) McNally, W. A. "Transport in Dilute Polymer Solutions." (Ph.D. Thesis, University of Rhode Island, 1968.)

(24) Monti, R. "Heat Transfer in Drag Reducing Solutions." Progress in Heat Transfer. Vol. 5. Oxford: Permanon Press, 1972, pp. 239-261.

(25) Howard, R. G. "Characterization of Heat and Momentum Transfer for Polyox WSR-301 and Polyhall M-295 Solutions." Report No. 7-551. Washington, D. C.: Naval Ship Research and Development Center, 1971.

(26) Pruitt, G. T., N. F. Whitsitt, and H. R. Crawford. "Turbulent Heat Transfer to Viscoelastic Fluids." Nat. Aeronaut. Space Admin. Contract NO. NAS 7-369. Dallas, Texas: The Western Co. Res. Div., 1966.

(27) Keuroughlian, G. H. "Heat Transfer to Dilute Polymer Solutions." (M.S. Thesis, Massachusetts Institute of Technology, 1967.)

(28) Virk, P. S. "An Elastic Sublayer Model for Drag Reduction by Dilute Polymer Solutions of Linear Macromolecules." J. Fluid Mech., Part 3(1971), pp. 417-440.

(29) Cebeci, T., and A. M. O. Smith. Analysis of Turbulent Boundary Layers. Vol. 15 New York: Academic Press, 1974.

APPENDIX A

TABLES

This appendix contains the tables referred to in the text of this thesis.

TABLE I

SUMMARY OF THEORETICAL MODELS AND CORRELATIONS USED FOR COMPARISON

Solvent	Drag Reduction
von Karman (16)	Poreh and Paz (4)
Friends and Metzner (17)	Wells (6)
Dittus-Boelter (20)	Smith, et al. (10)
Sieder-Tate (18)	--
Kays (19)	--

TABLE II

SUMMARY OF EXPERIMENTAL DATA USED FOR COMPARISON

Investigator	Polymer Characteristics		Reynolds Number Range	Prandtl Number Range
	Name	Concentration (ppm)		
Debrule (14)	Polyox WSR-301	10	$1x10^4$-$2.5x10^5$	4.38,6.16, 10.3
Gupta, Metzner and Hartnett (22)	Polyacrylamide ET-597	500	$1.5x10^4$-$5.5x10^4$	11.1
McNally (23)	Polyox WSR-301	2,10,20	$2.5x10^4$-$8.5x10^4$	7.1
Monti (24)	Polyacrylamide ET-597	250,500 750,1000	$1x10^4$-$1x10^5$	7.75
Howard (25)	Aged Polyox WSR-301 and Polyhall M-295	12.5 and 50	$2.5x10^4$-$2.5x10^5$	7.3
Keuroughlian (27)	Polyox N3000 and W301	10 and 10	$6x10^3$-$2.5x10^4$	6.14-6.36
Pruitt, Whitsitt and Crawford (26)	Separan AP-30	10,100	$5.5x10^3$-$7.5x10^4$	6.94-15.89

APPENDIX B

This appendix contains the Figures and Illustrations referred to in the text of this thesis.

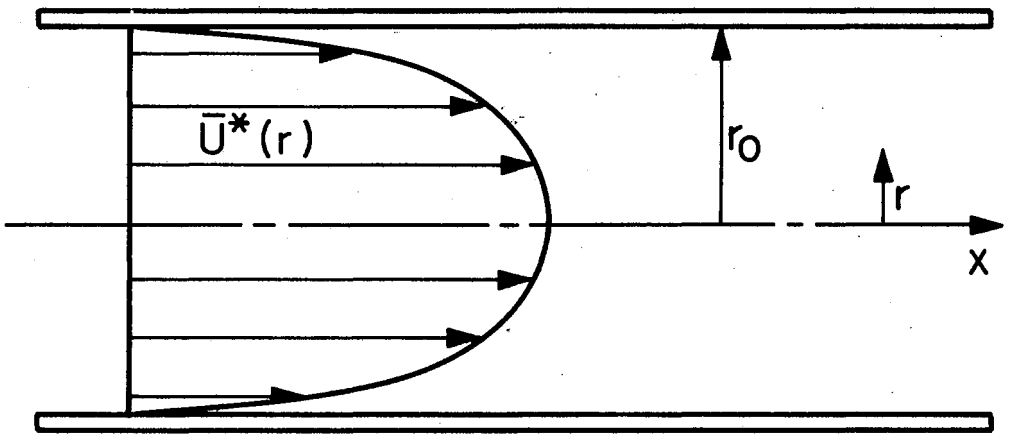

Figure 1. Diagram of the Coordinate System

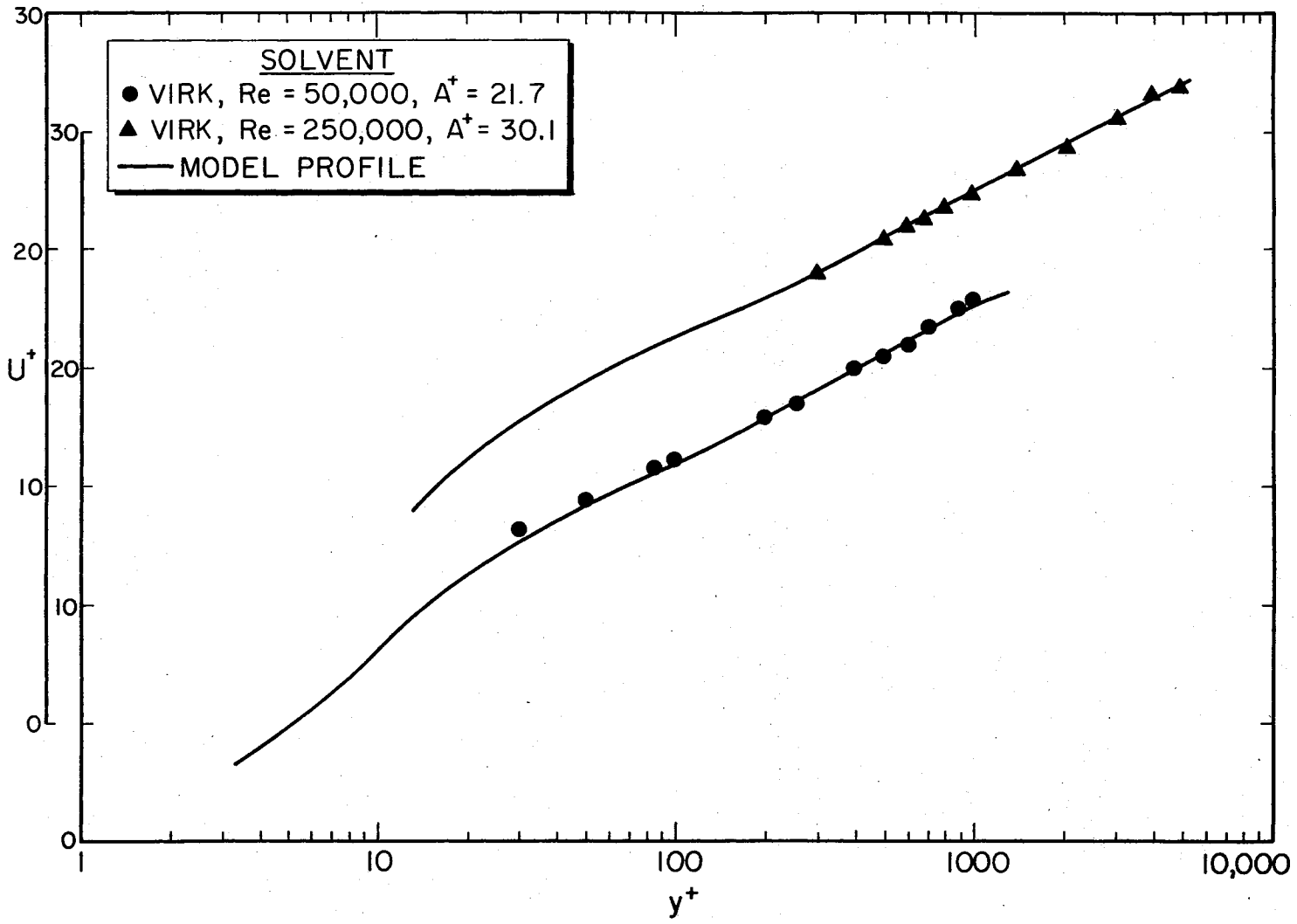

Figure 2. Comparison of Experimental and Predicted Velocity Profiles for Solvent Flows

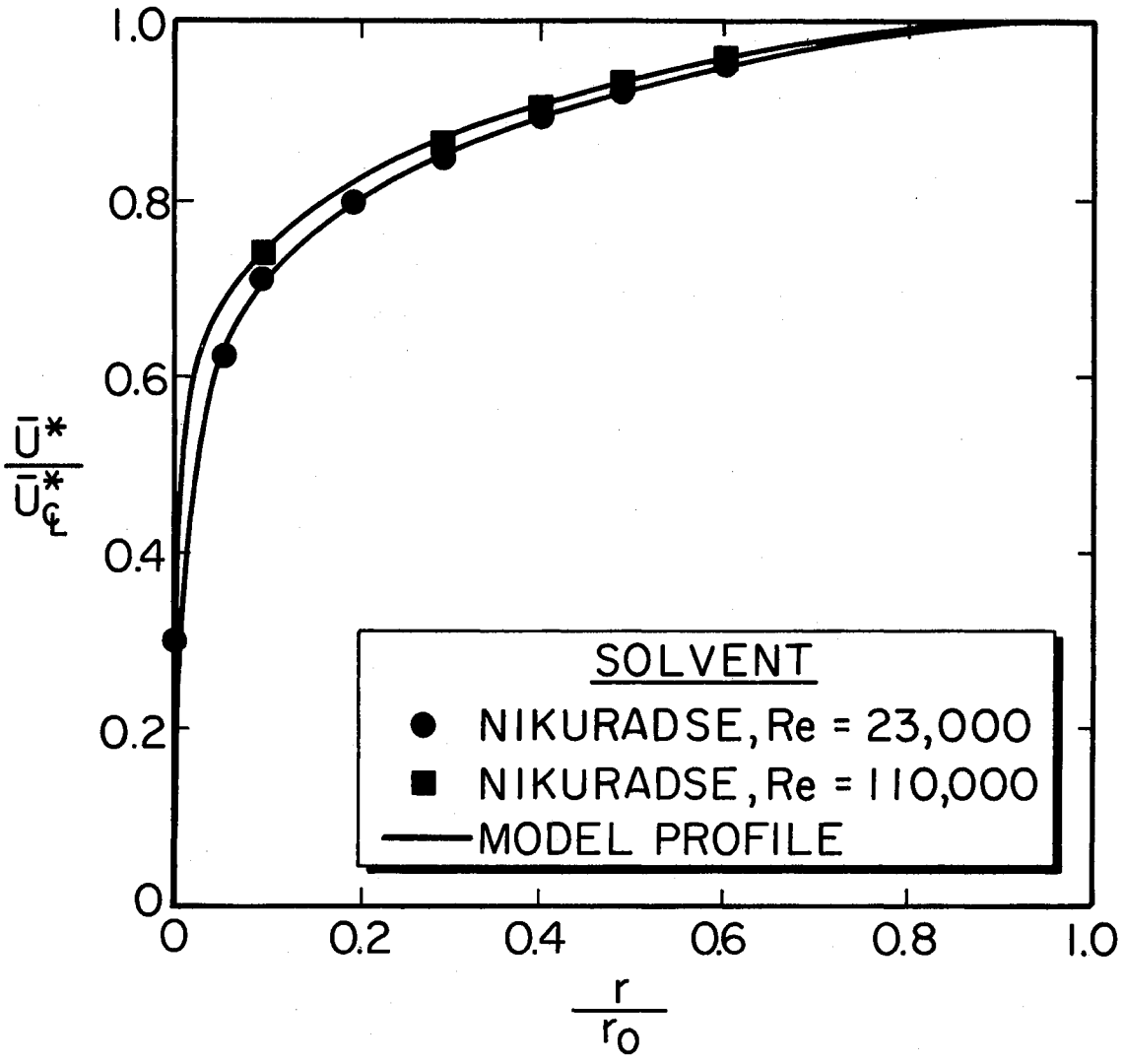

Figure 3. Comparison of Predicted and Experimental Dimensionless Velocity Profiles

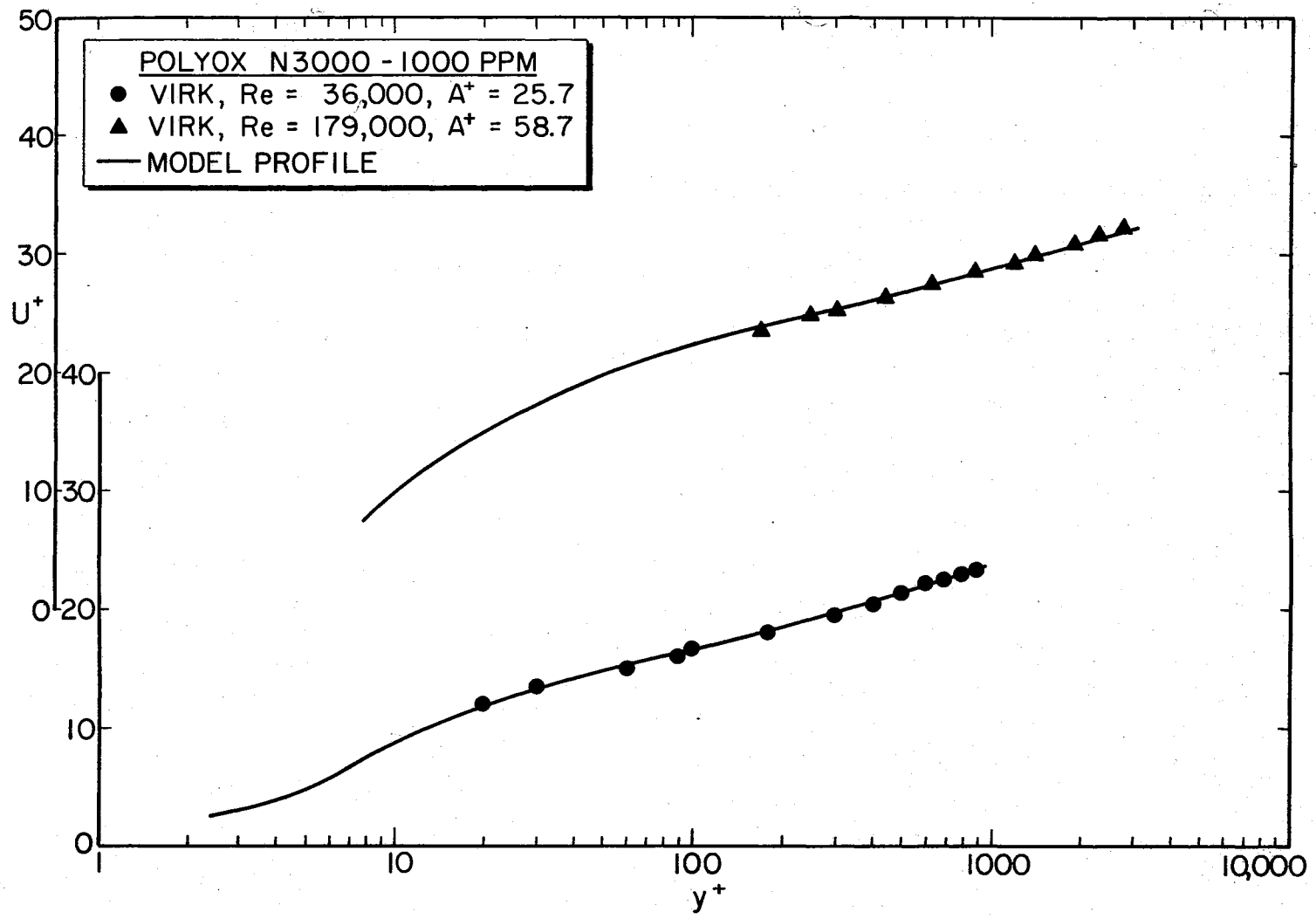

Figure 4. Comparison of Experimental and Predicted Velocity Profiles for Polyox-N3000

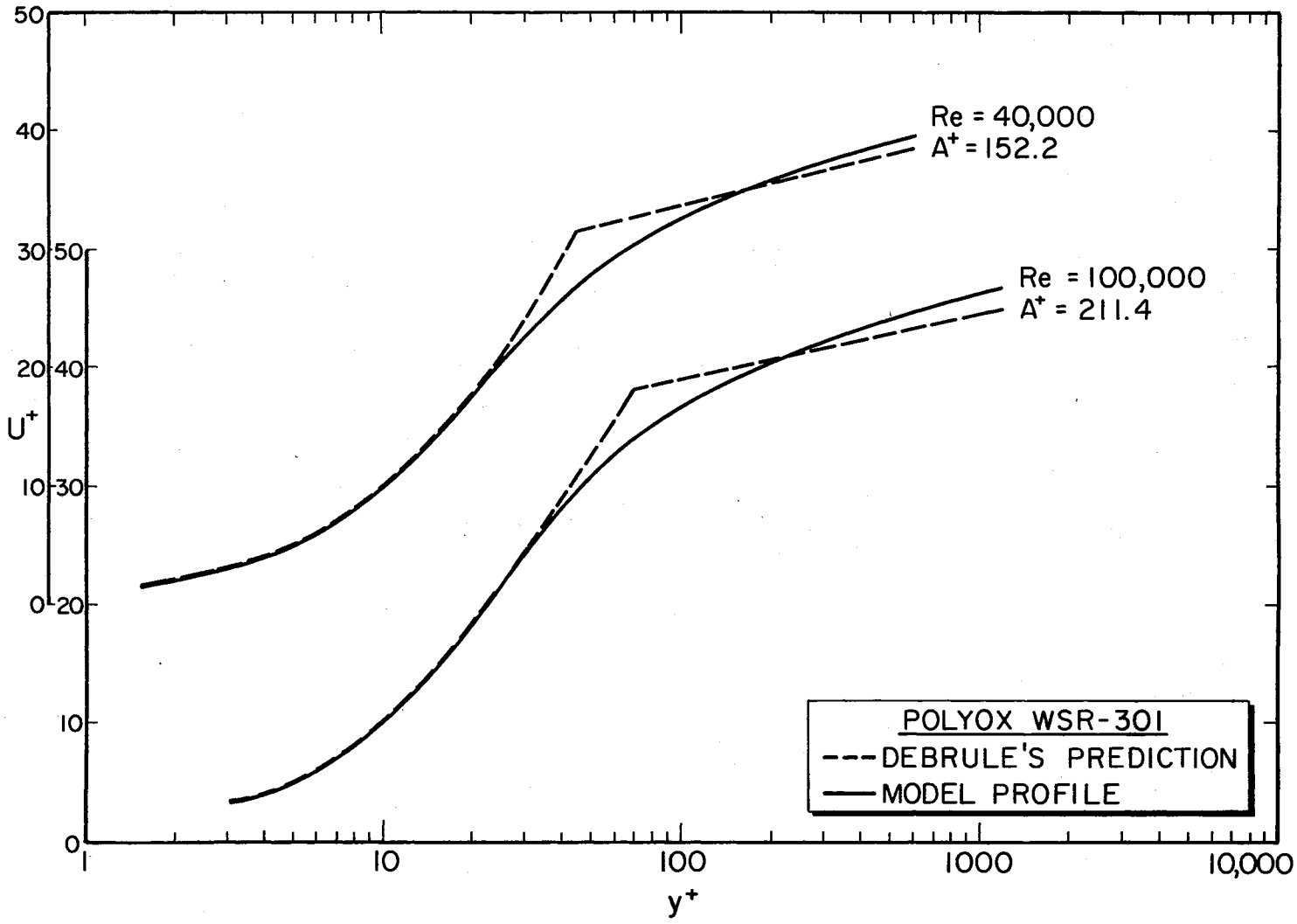

Figure 5. Comparison of Present Model with Predictions of Debrule for Polyox WSR-301 (Data from Debrule (14))

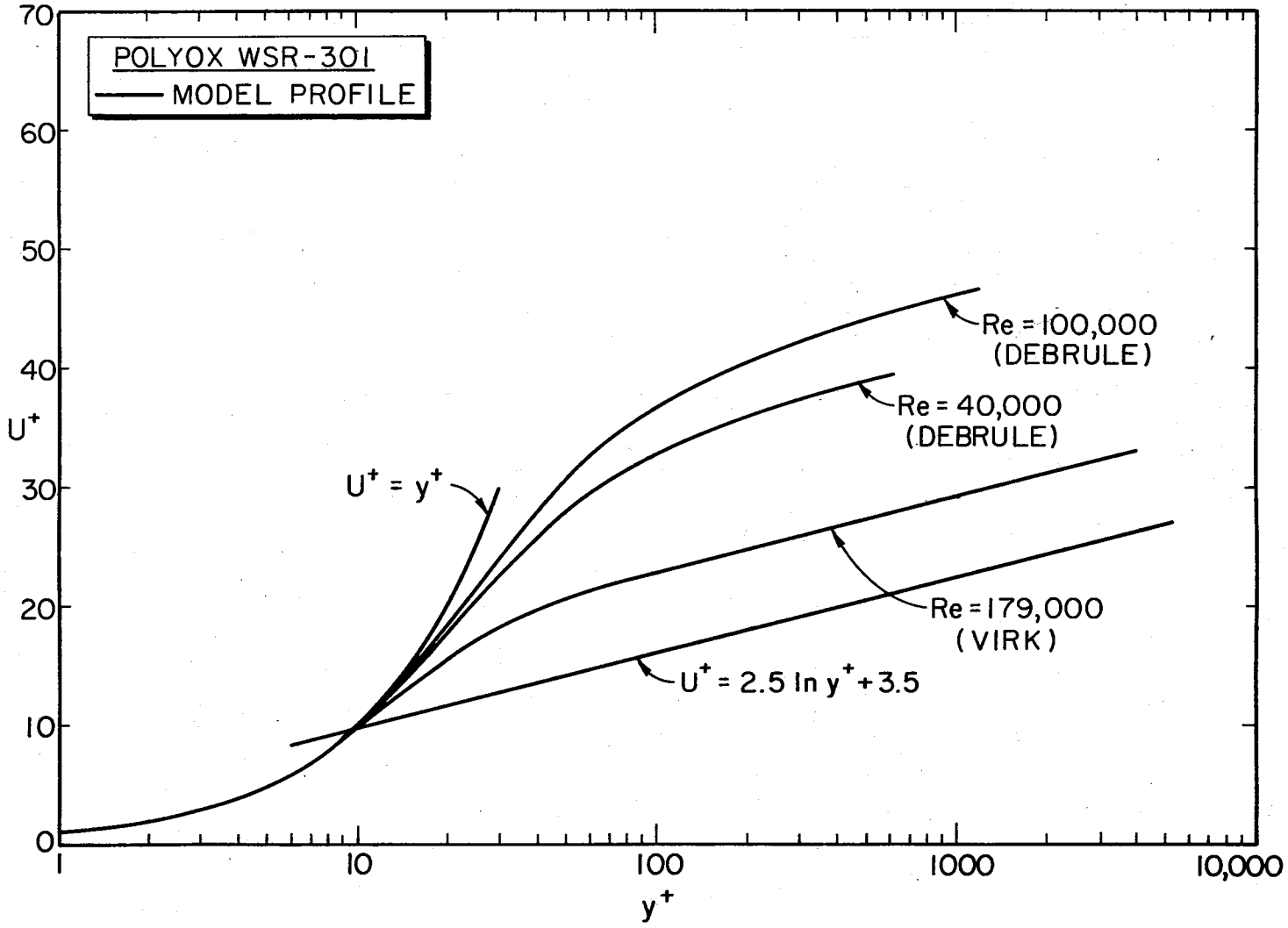

Figure 6. Predicted Mean Velocity Profiles for Solvent and Drag Reducing Flows

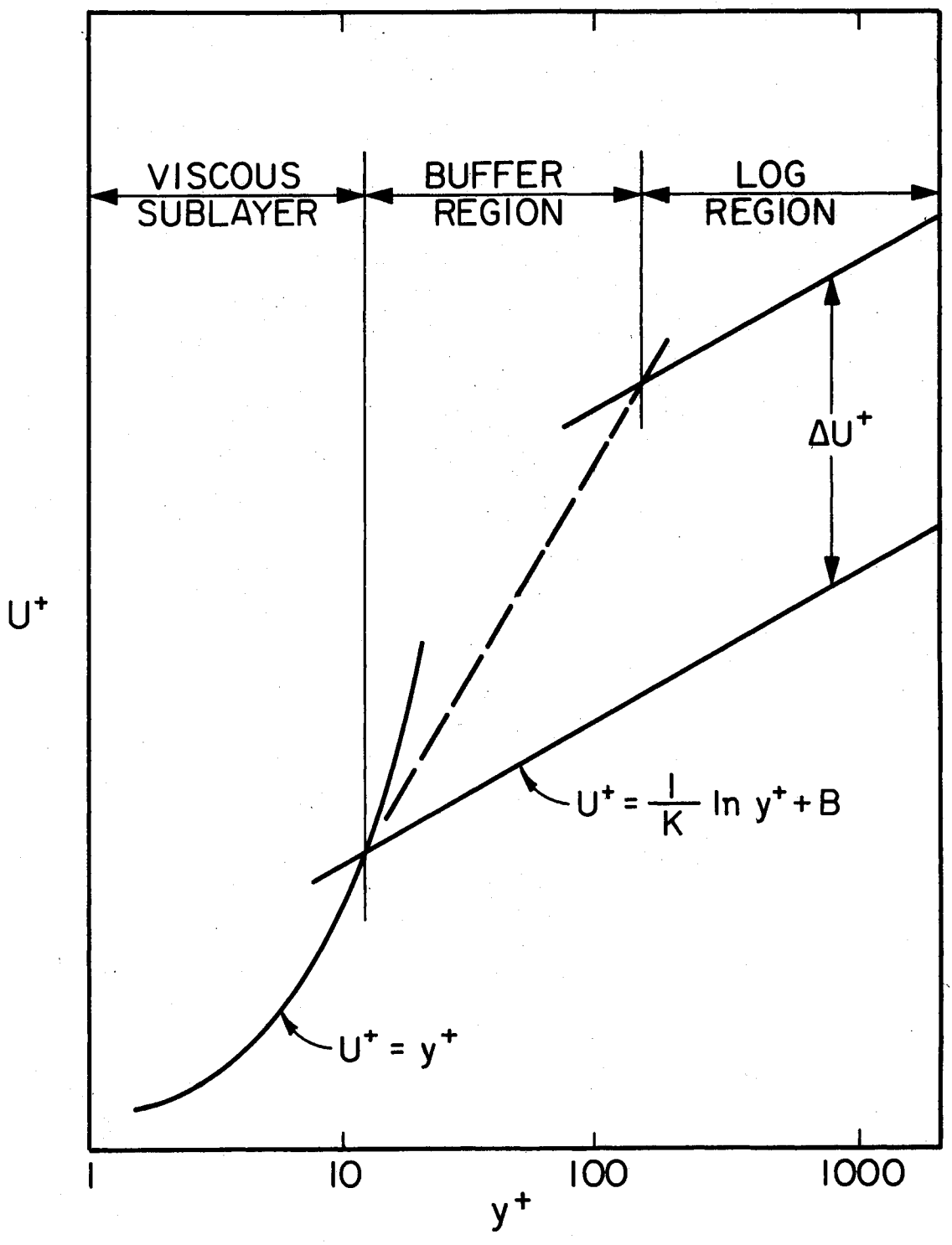

Figure 7. Generalized Non-Dimensional Velocity Profile

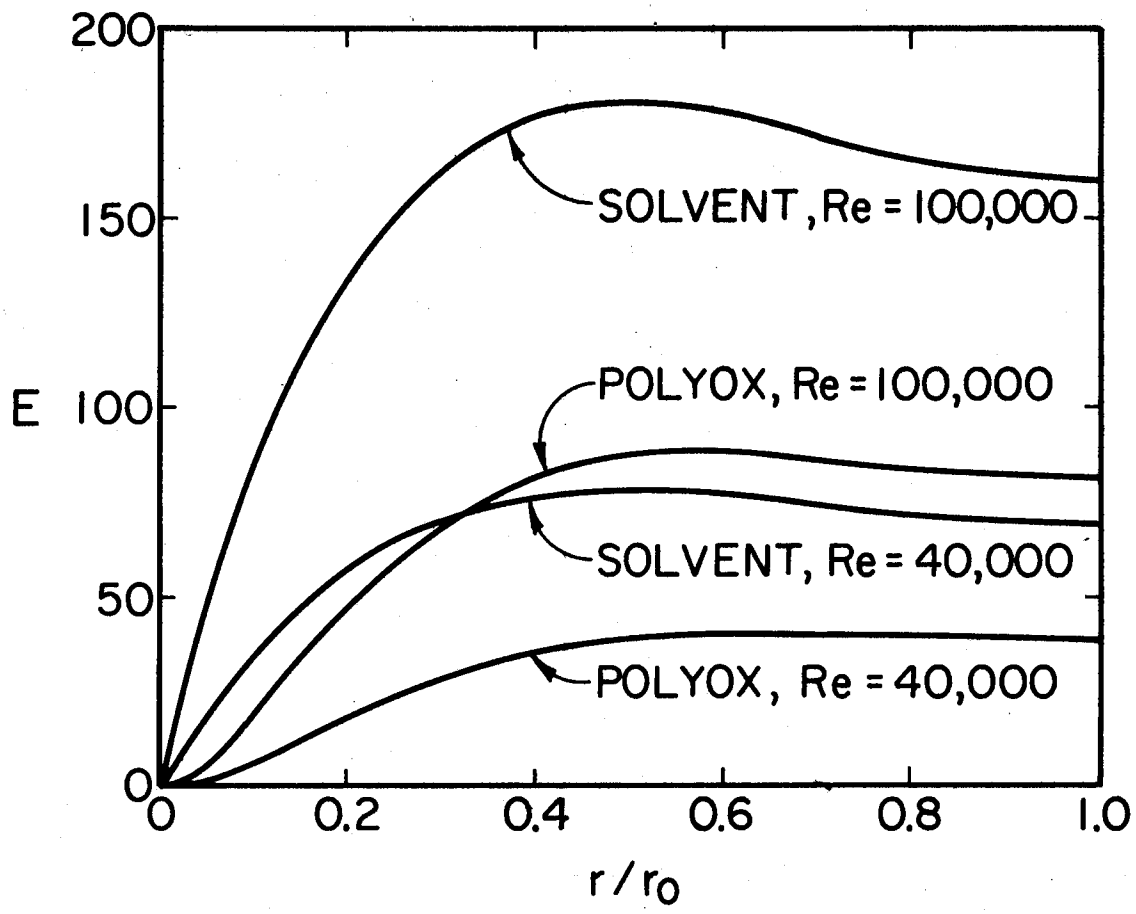

Figure 8. Comparison of Eddy Diffusivities for Solvent and Drag Reducing Flows

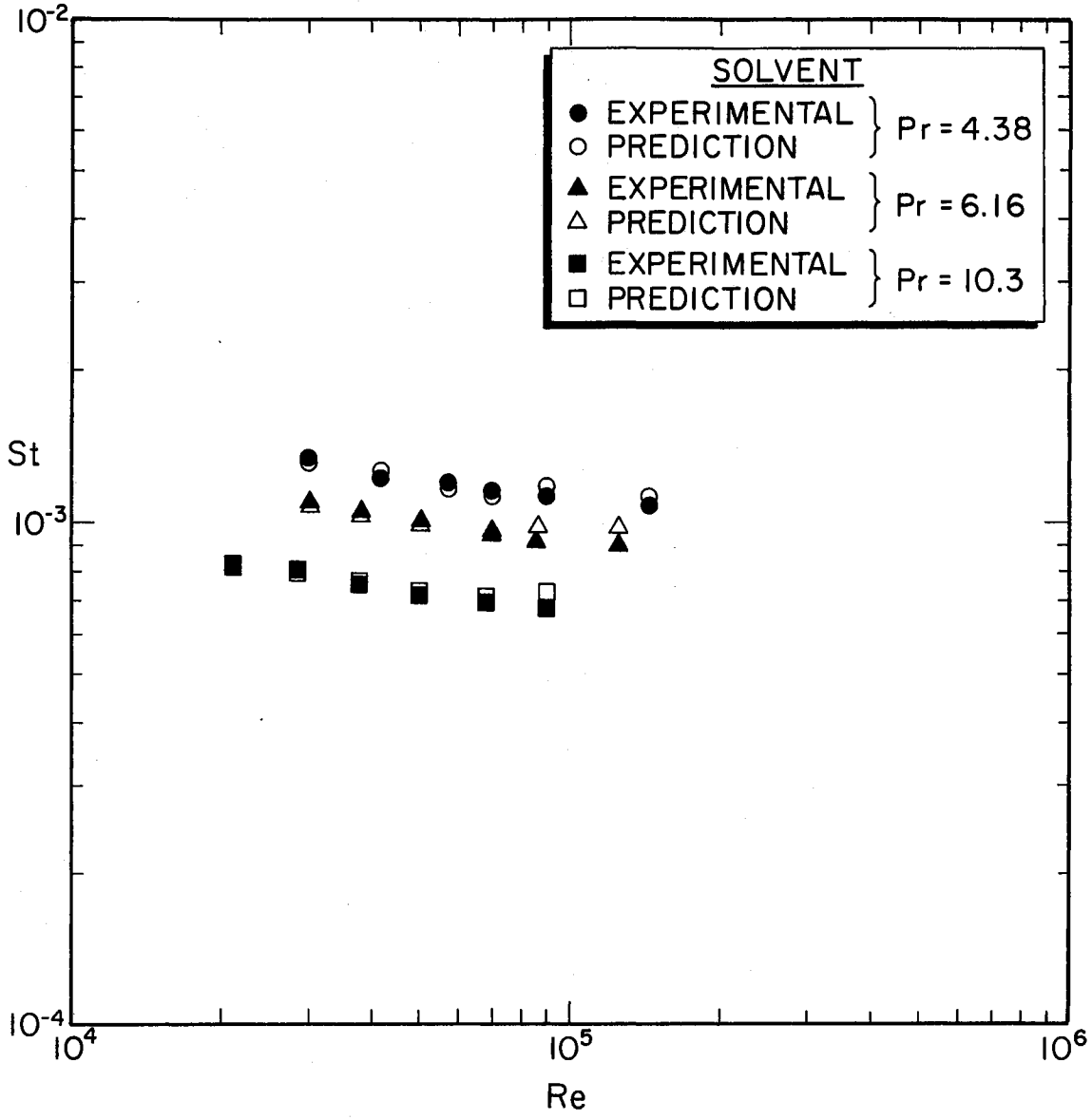

Figure 9. Comparison of Predicted Values of Stanton Number with Experimental Data of Debrule (14)

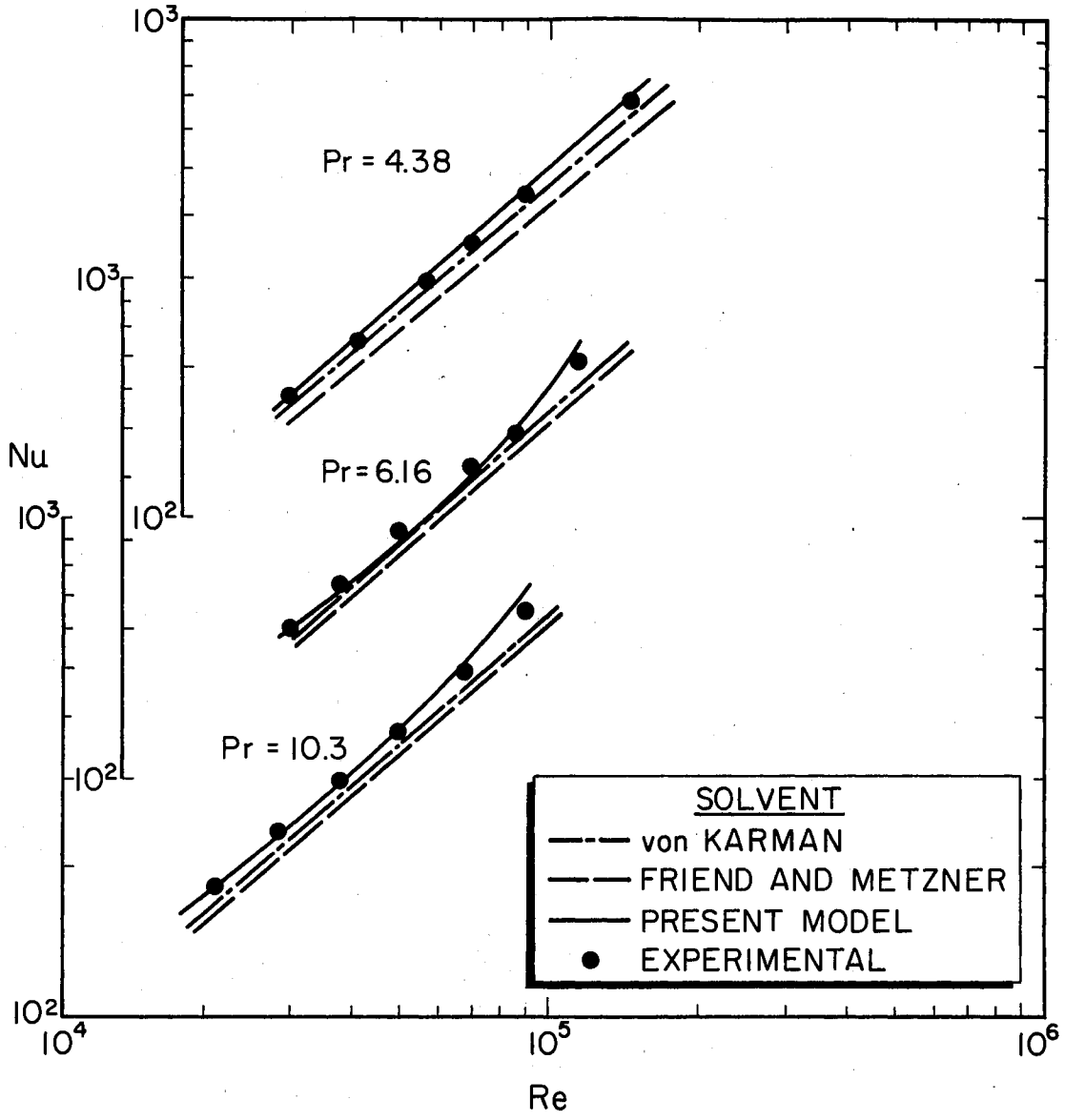

Figure 10. Comparison of Present Model with Different Theoretical Models (Data from Debrule (14))

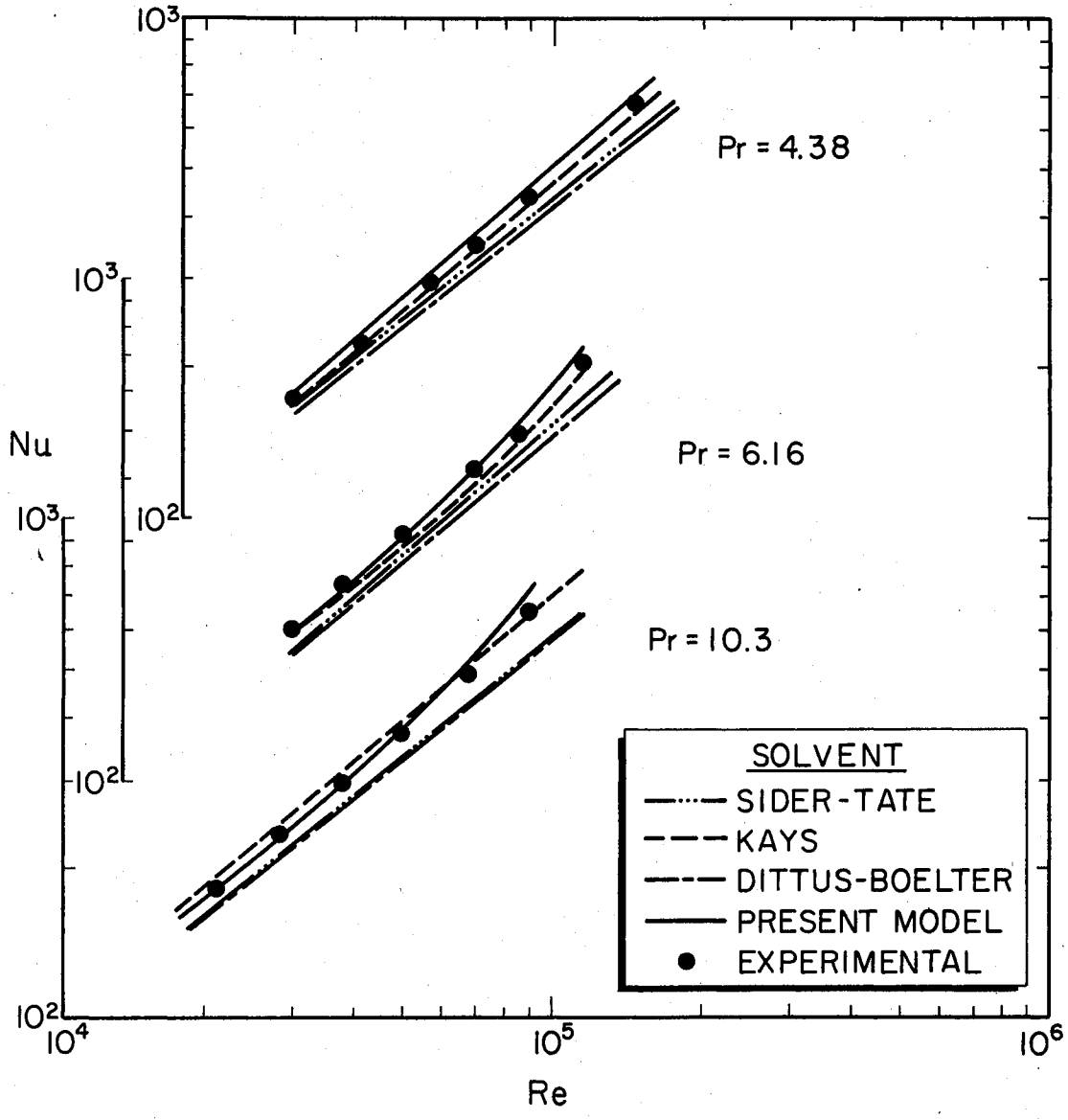

Figure 11. Comparison of Present Model with Different Correlations (Data from Debrule (14))

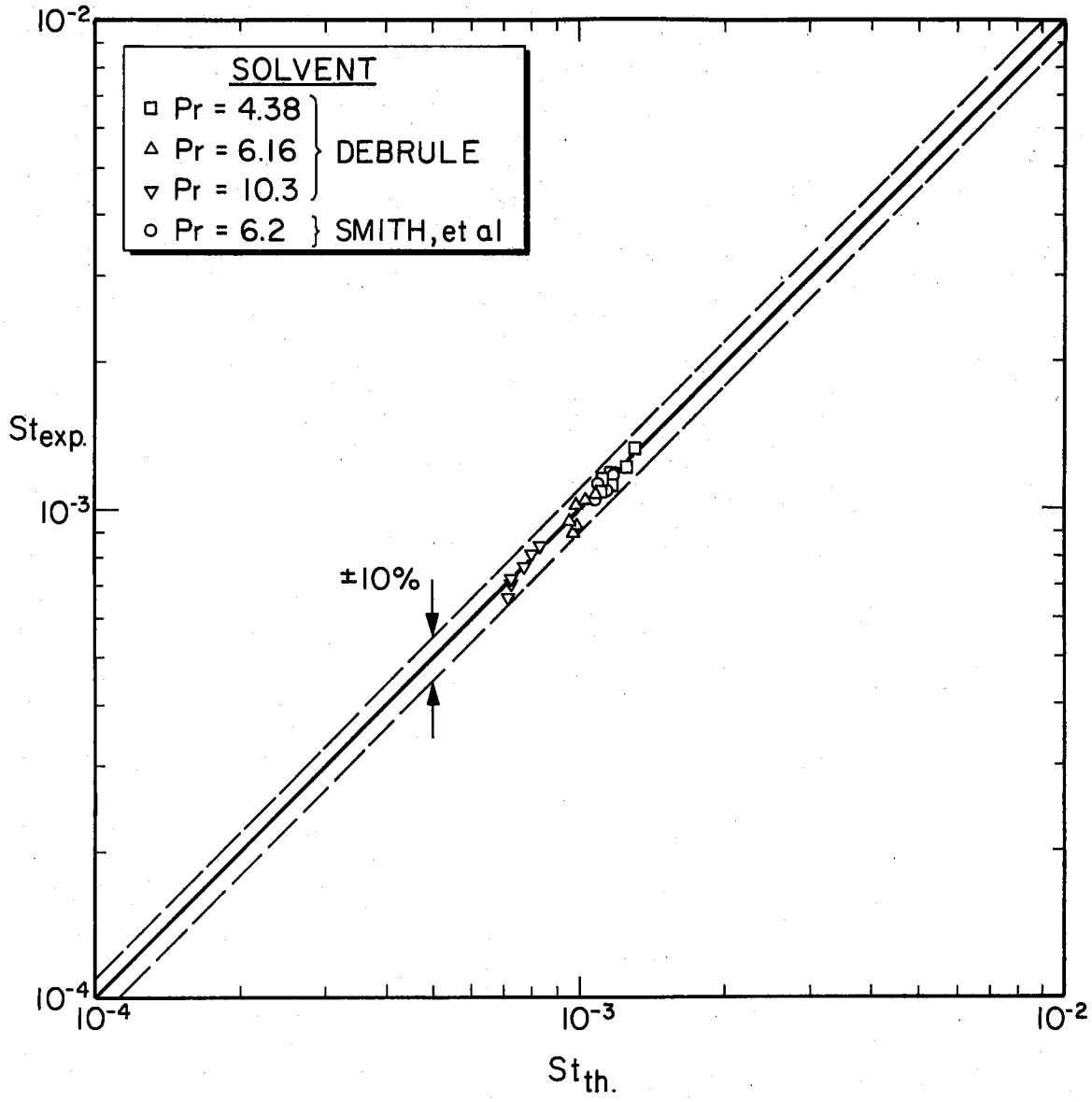

Figure 12. Comparison of the Predicted Stanton Number Using the Present Model with Measurements

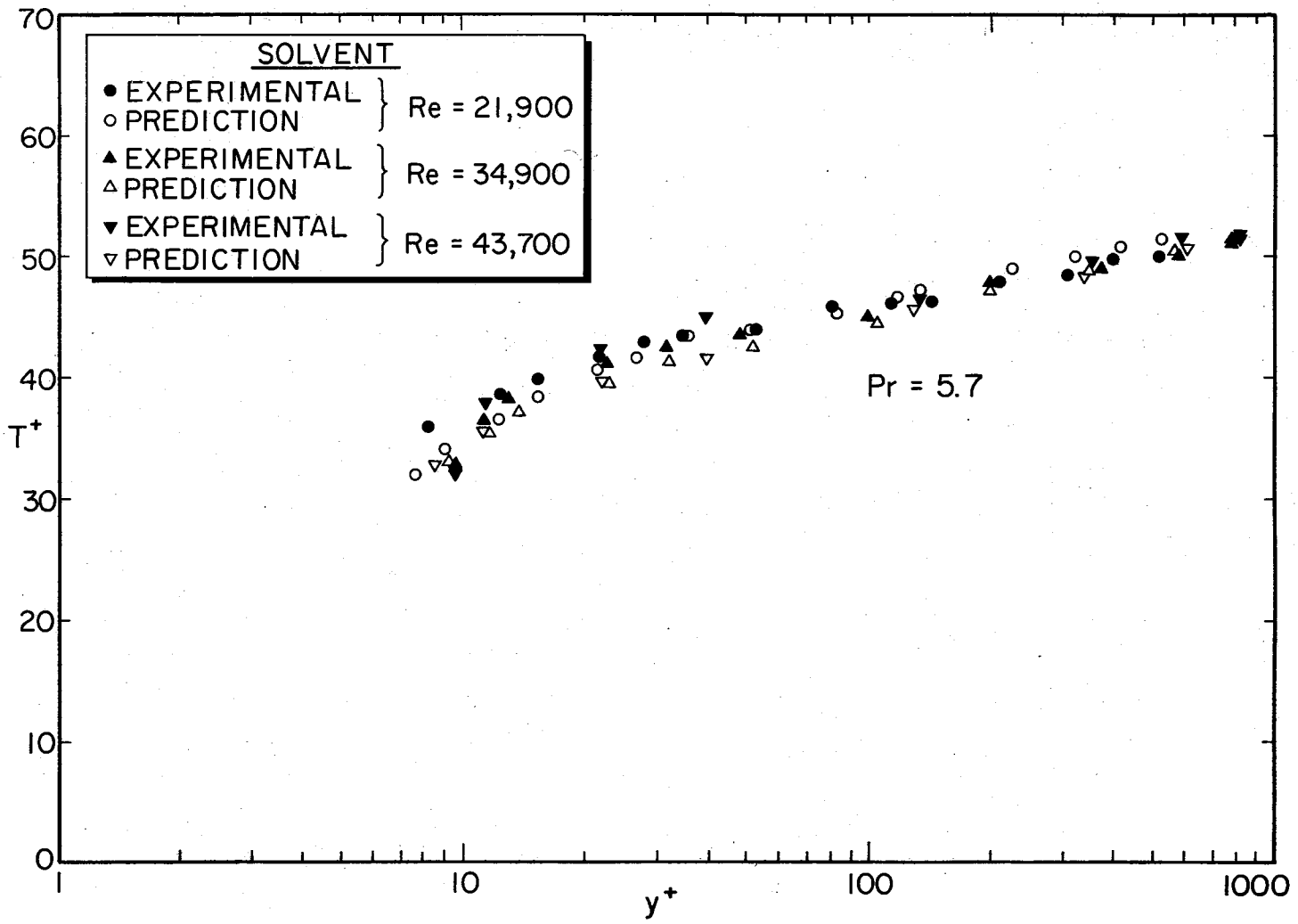

Figure 13. Universal Temperature Profiles

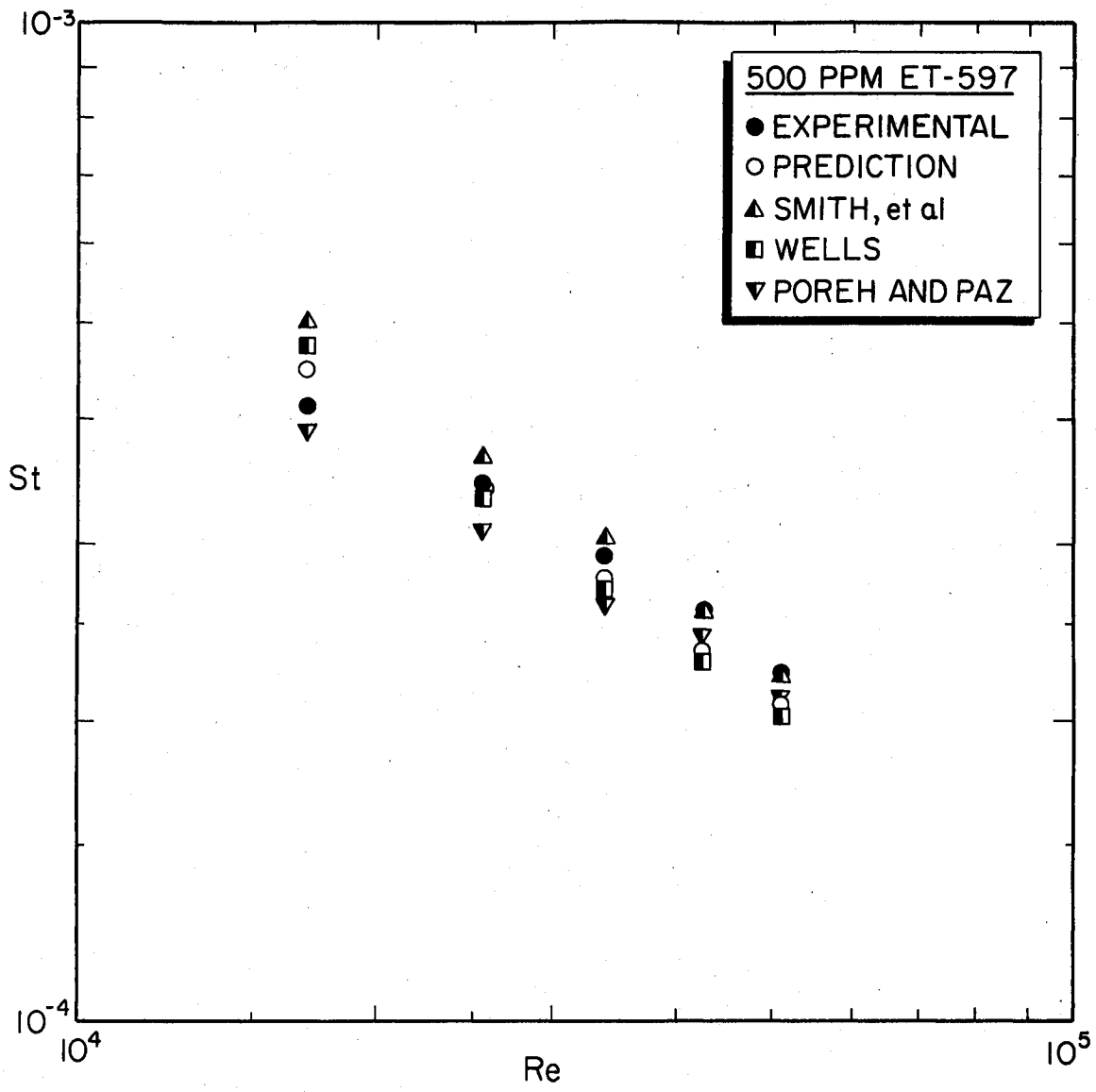

Figure 14. Comparison of Predicted Values of Stanton Number with Experimental Data of Gupta, et al. (22)

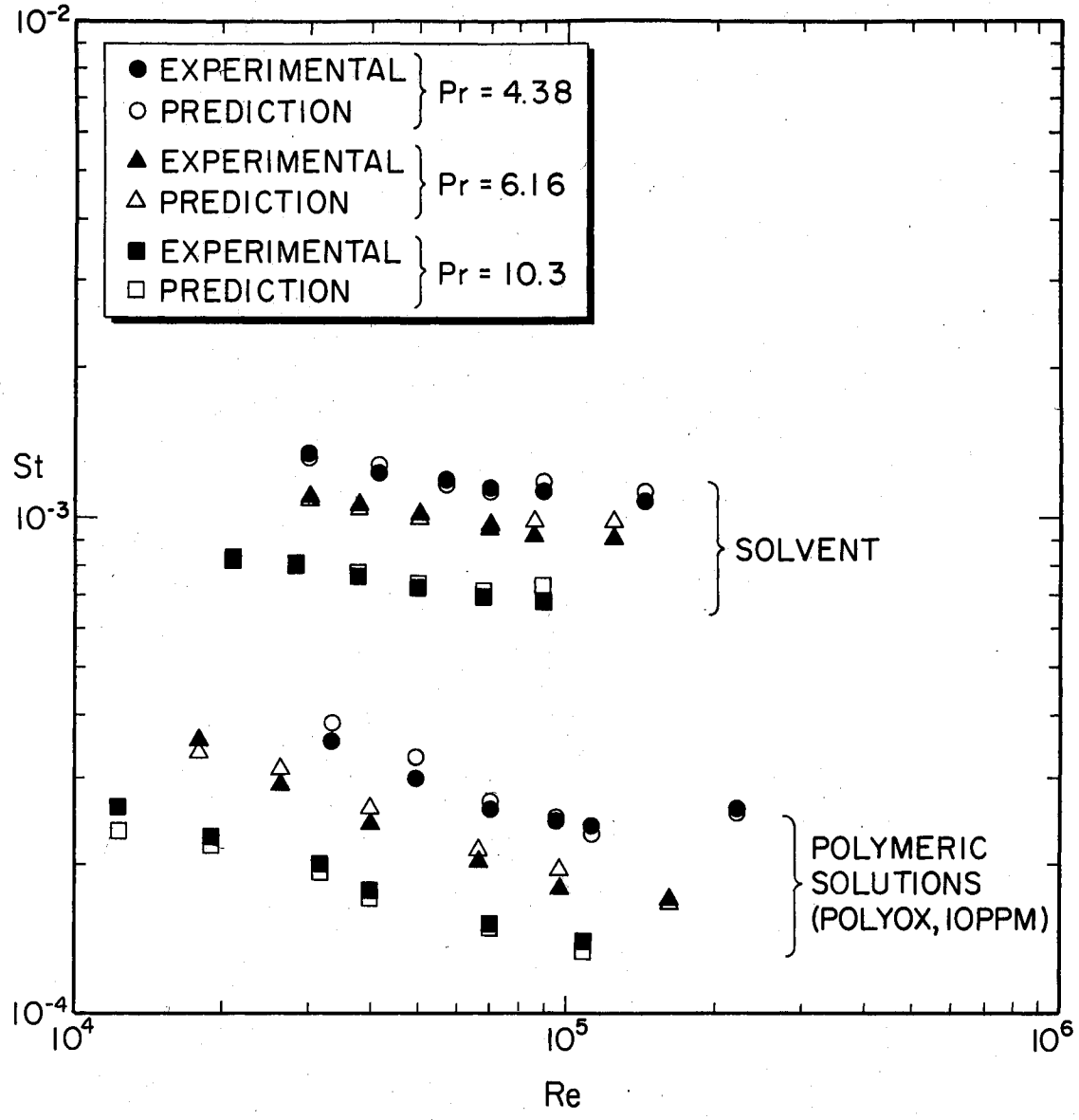

Figure 15. Comparison of Predicted Values of Stanton Number with Experimental Data of Debrule (14)

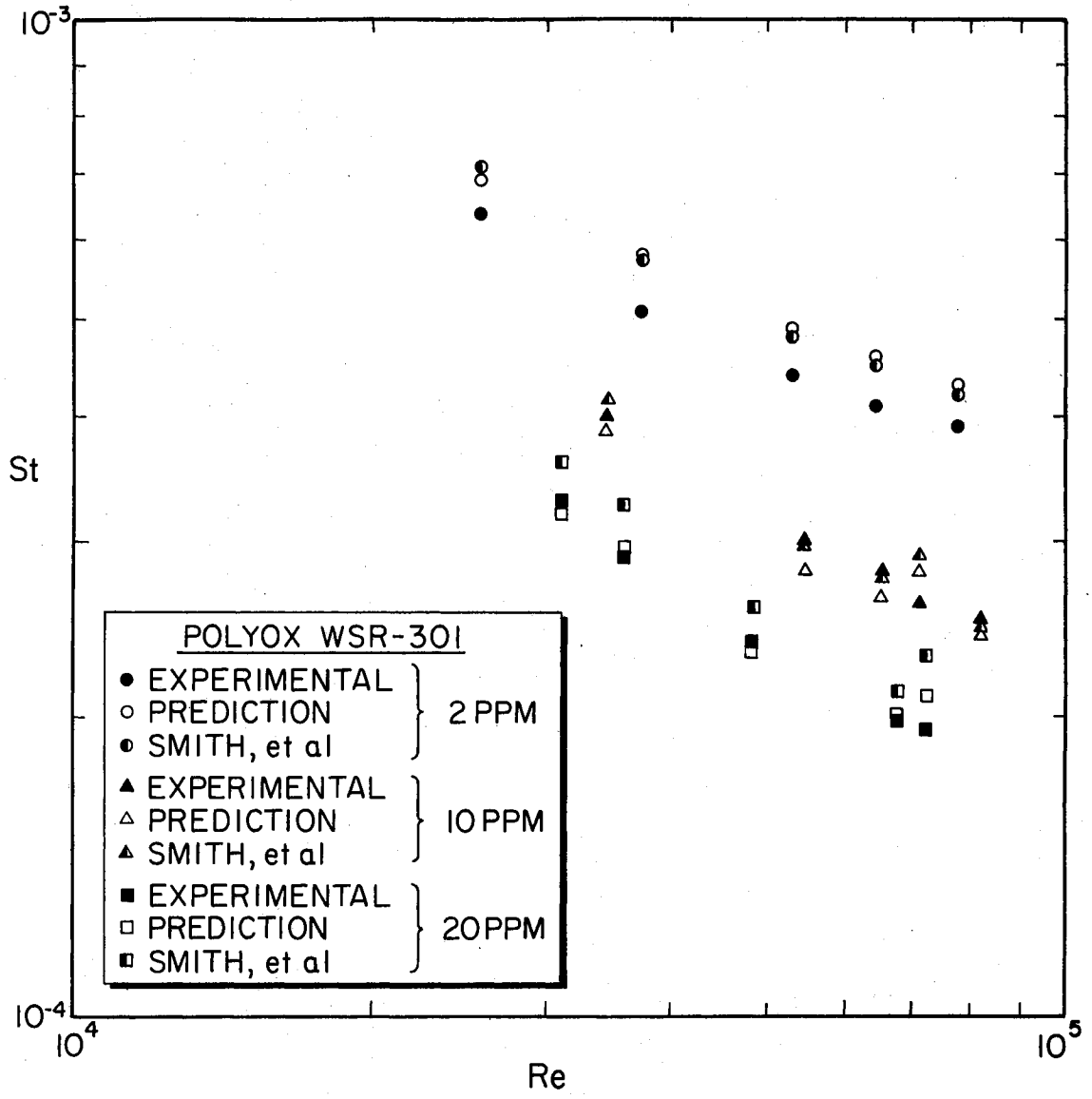

Figure 16. Comparison of Predicted Values of Stanton Number with Experimental Data of McNally (23)

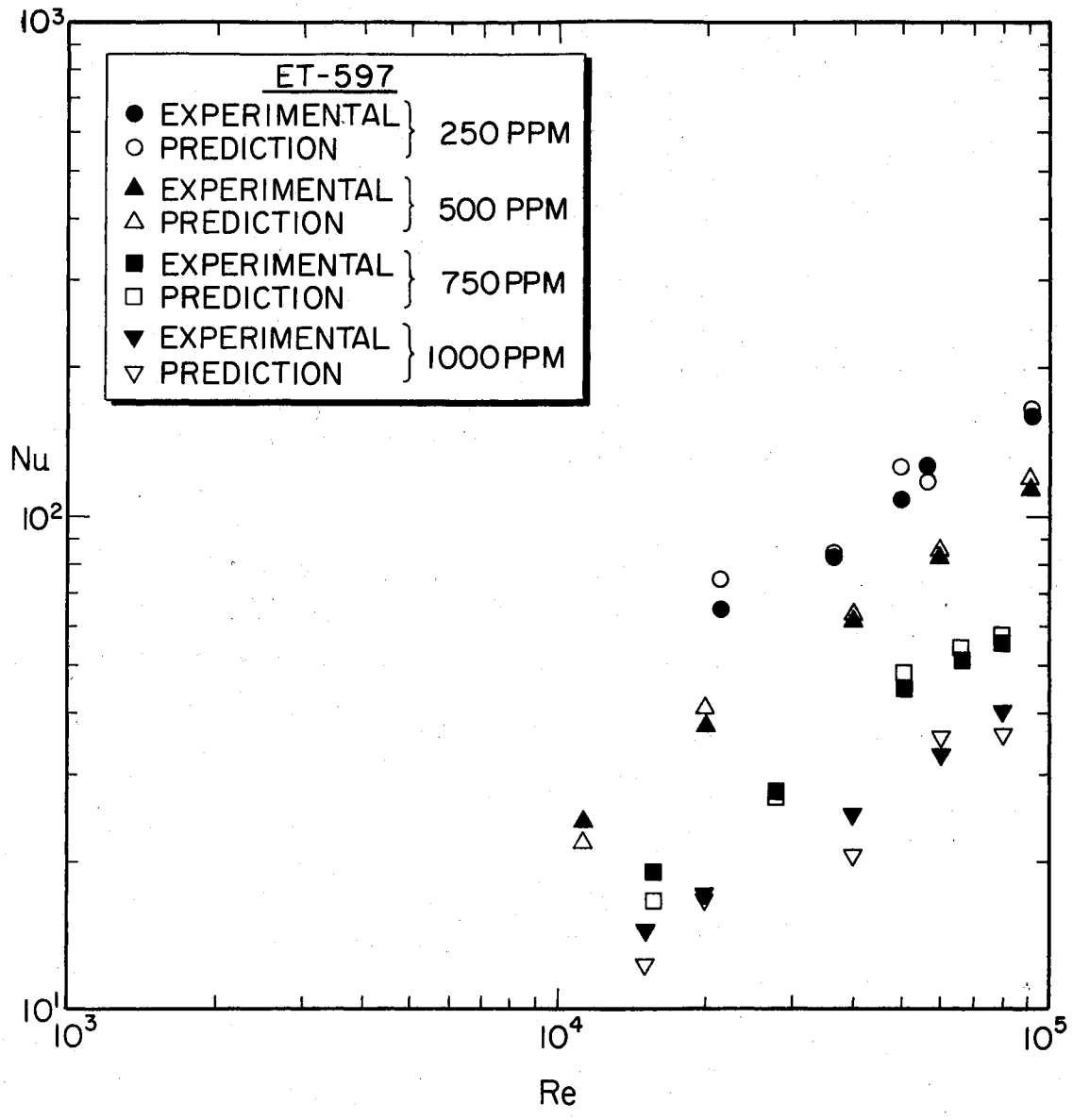

Figure 17. Comparison of Predicted Values of Stanton Number with Experimental Data of Monti (24)

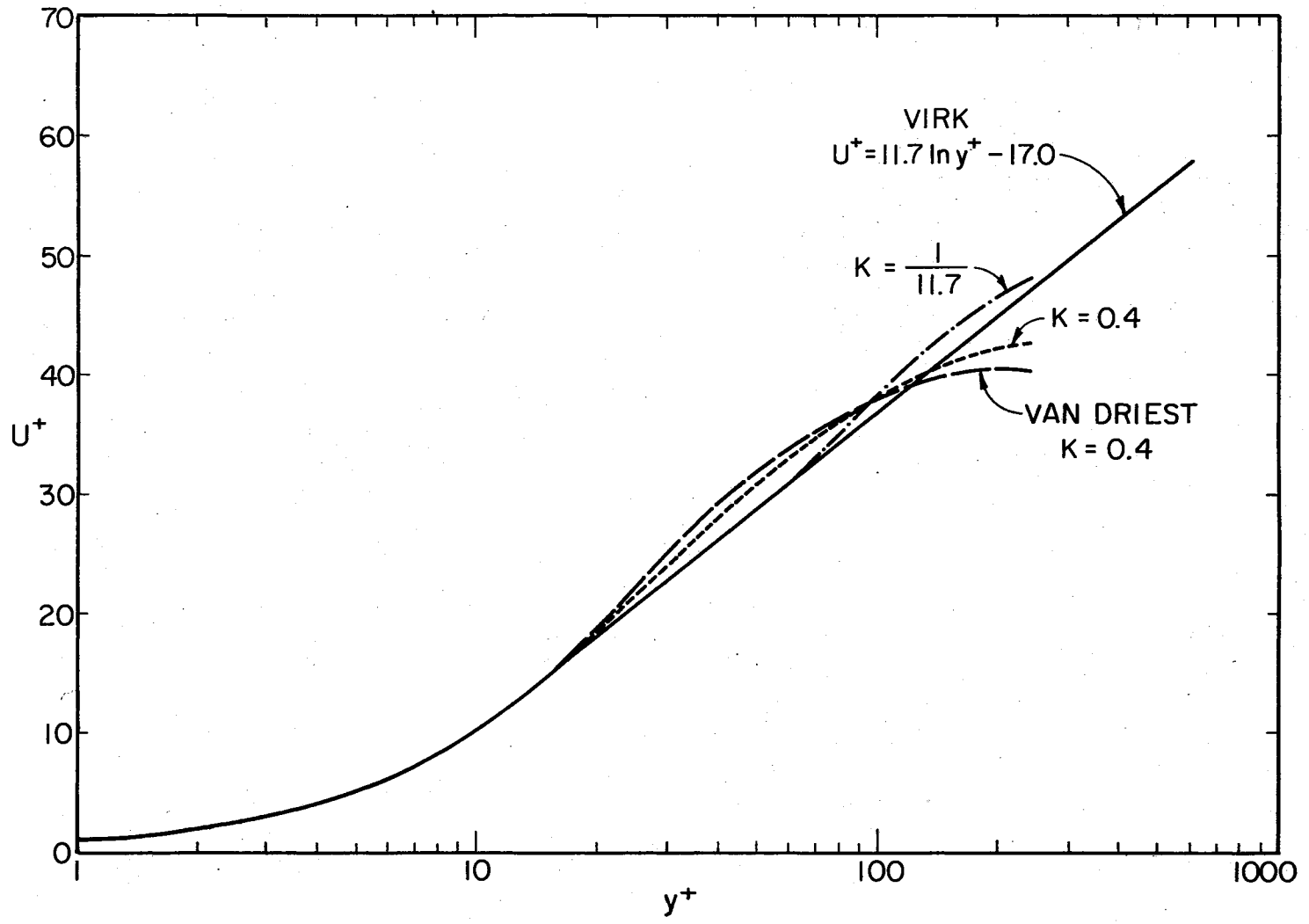

Figure 18. Non-Dimensional Velocity Profile for Maximum Drag Reduction

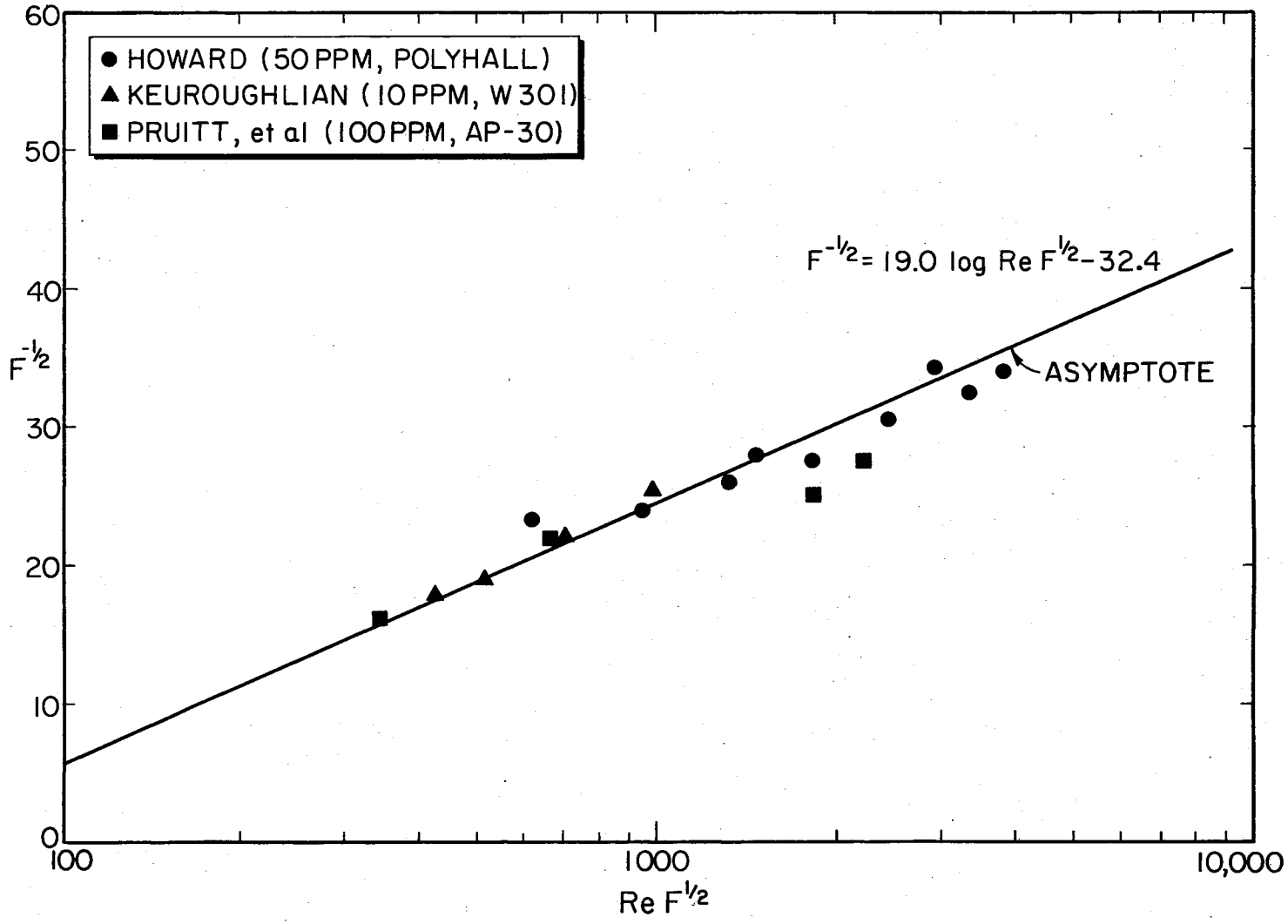

Figure 19. The Maximum Drag Reduction Asymptote

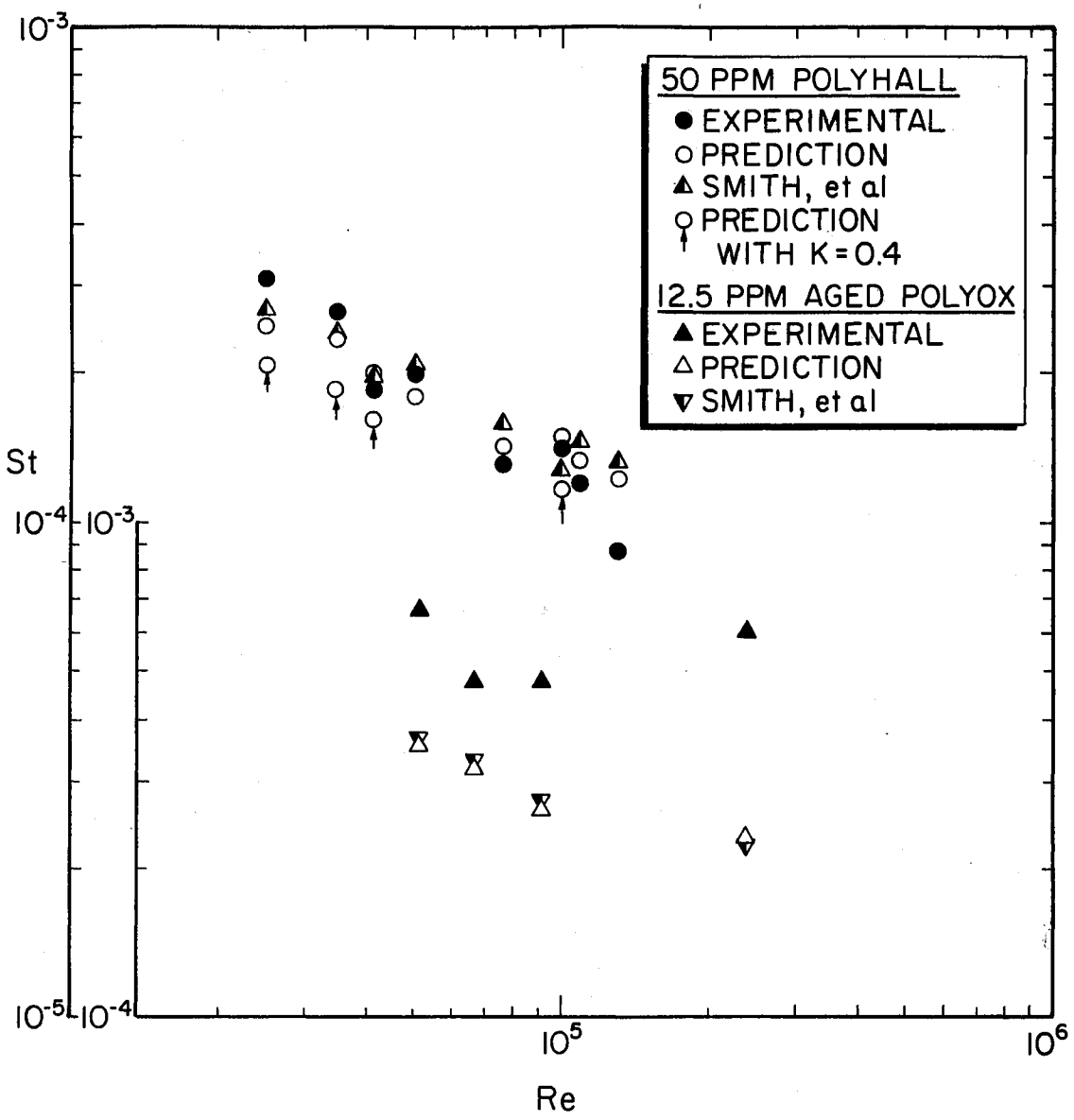

Figure 20. Comparison of Predicted Values of Stanton Number with Experimental Data of Howard (25)

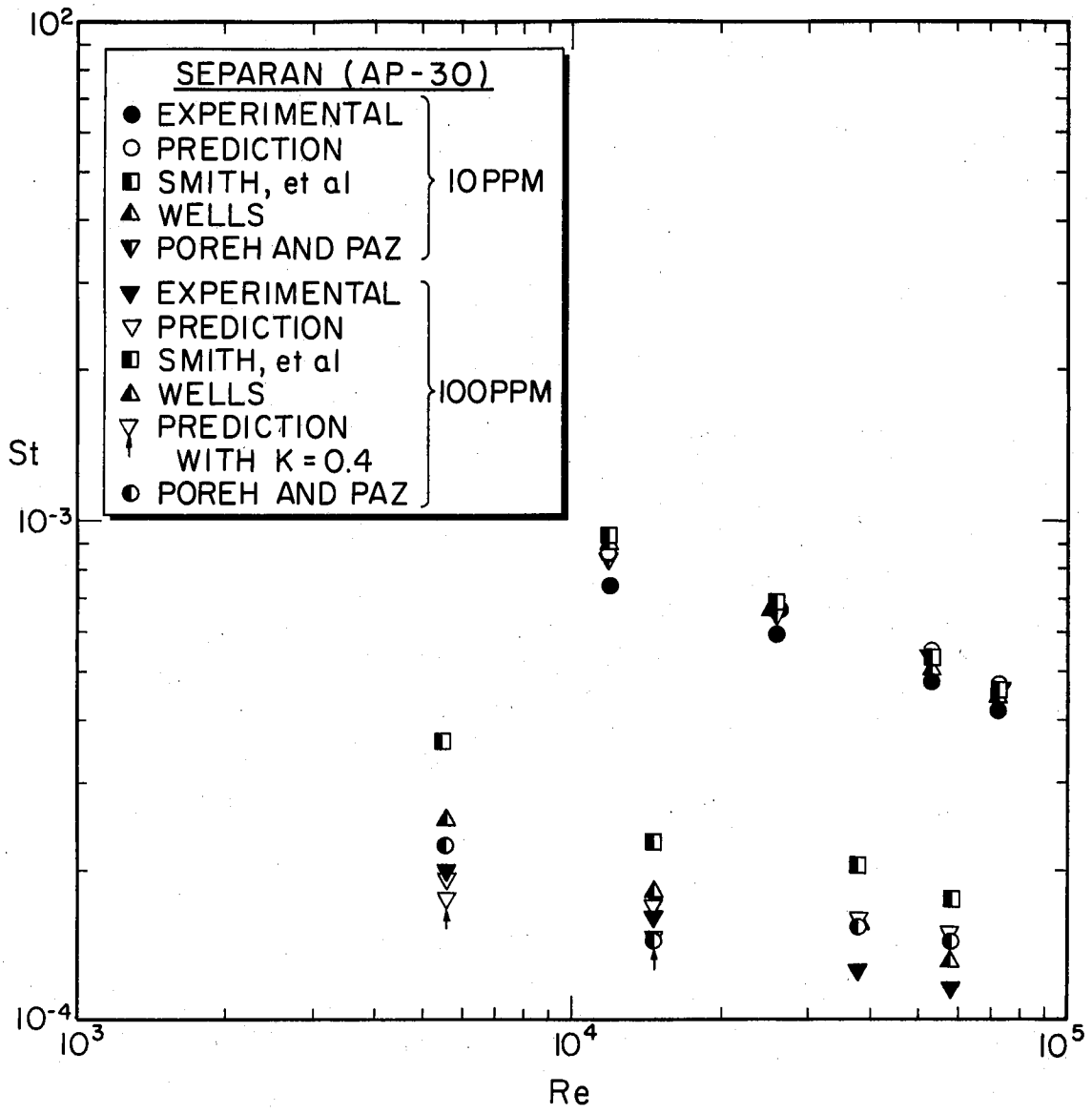

Figure 21. Comparison of Predicted Values of Stanton Number with Experimental Data of Pruitt, et al. (26)

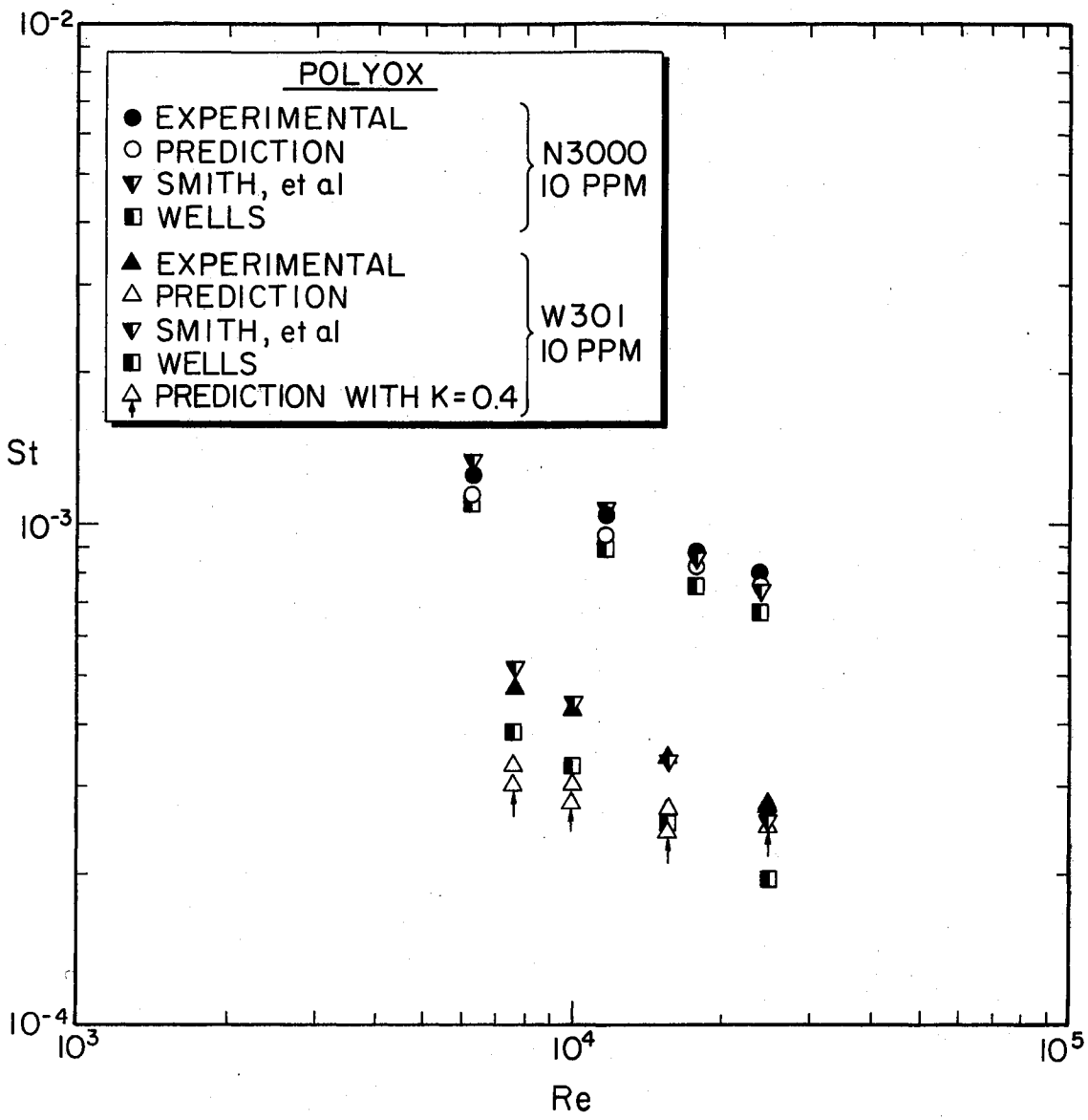

Figure 22. Comparison of Predicted Values of Stanton Number with Experimental Data of Keuroughlian (27)

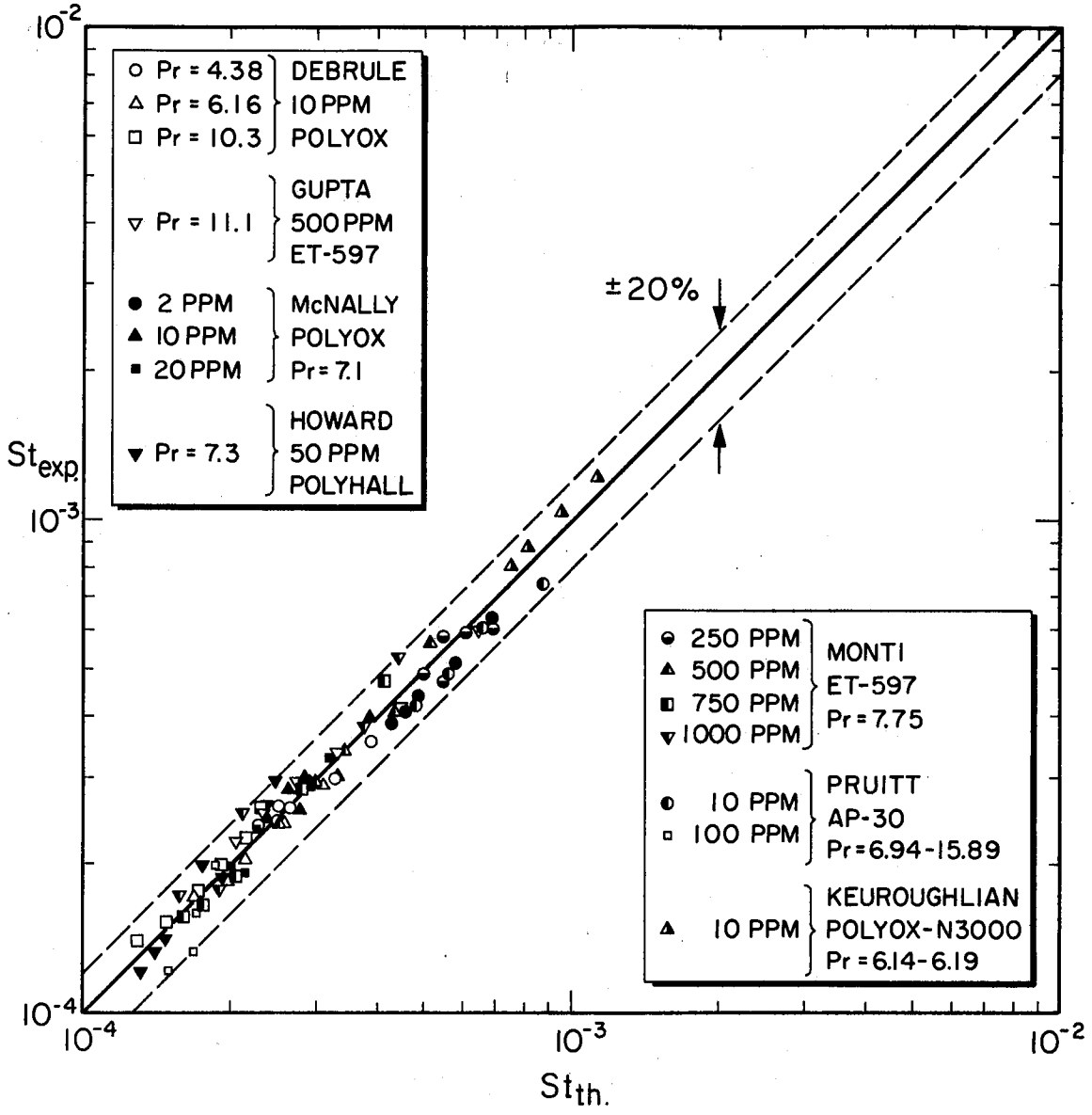

Figure 23. Comparison of the Predicted Stanton Number Using the Present Model with Measurements

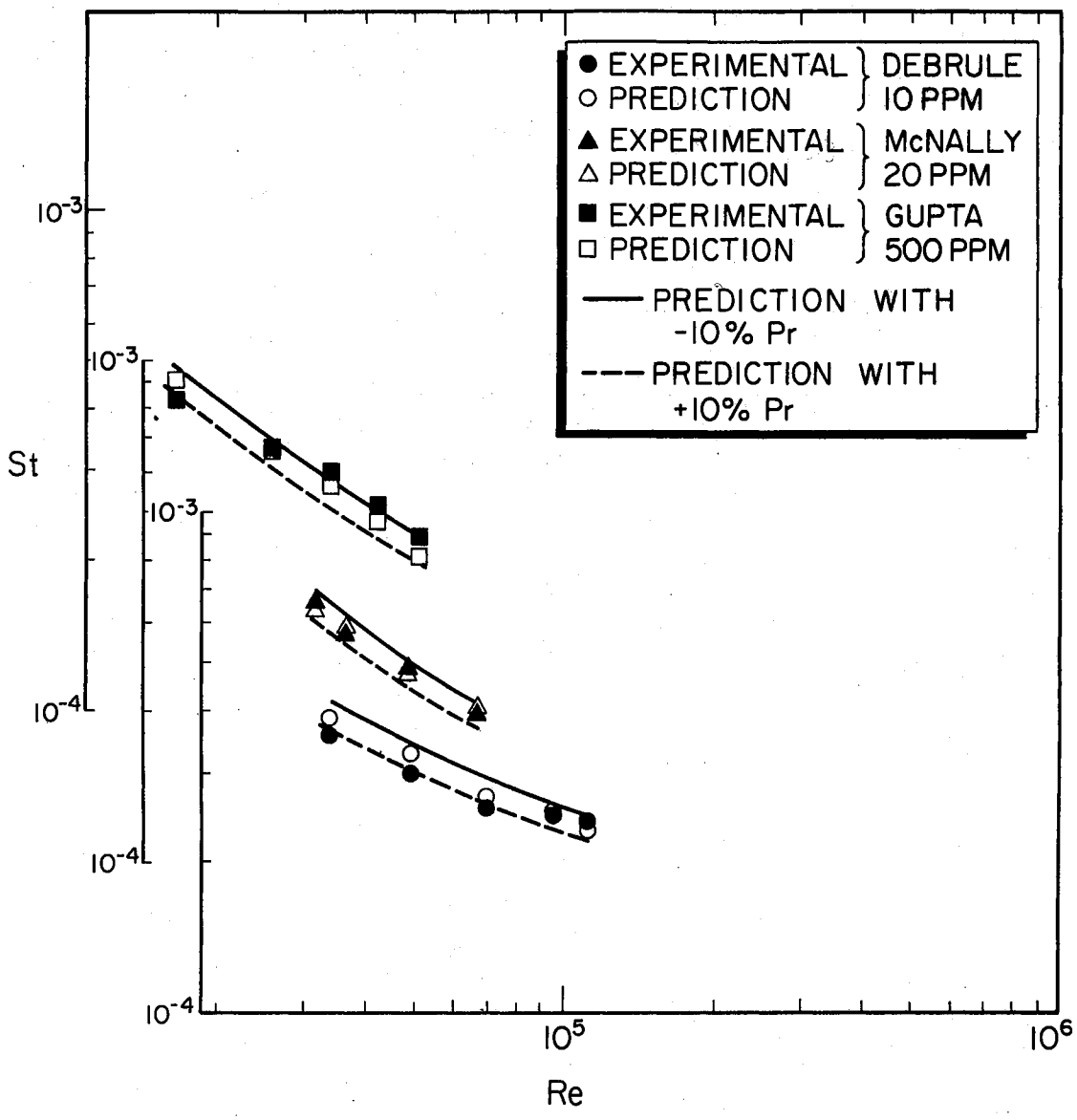

Figure 24. Sensitivity of the Present Model with Respect to $\pm$ 10% Variation in Prandtl Number (Pr)

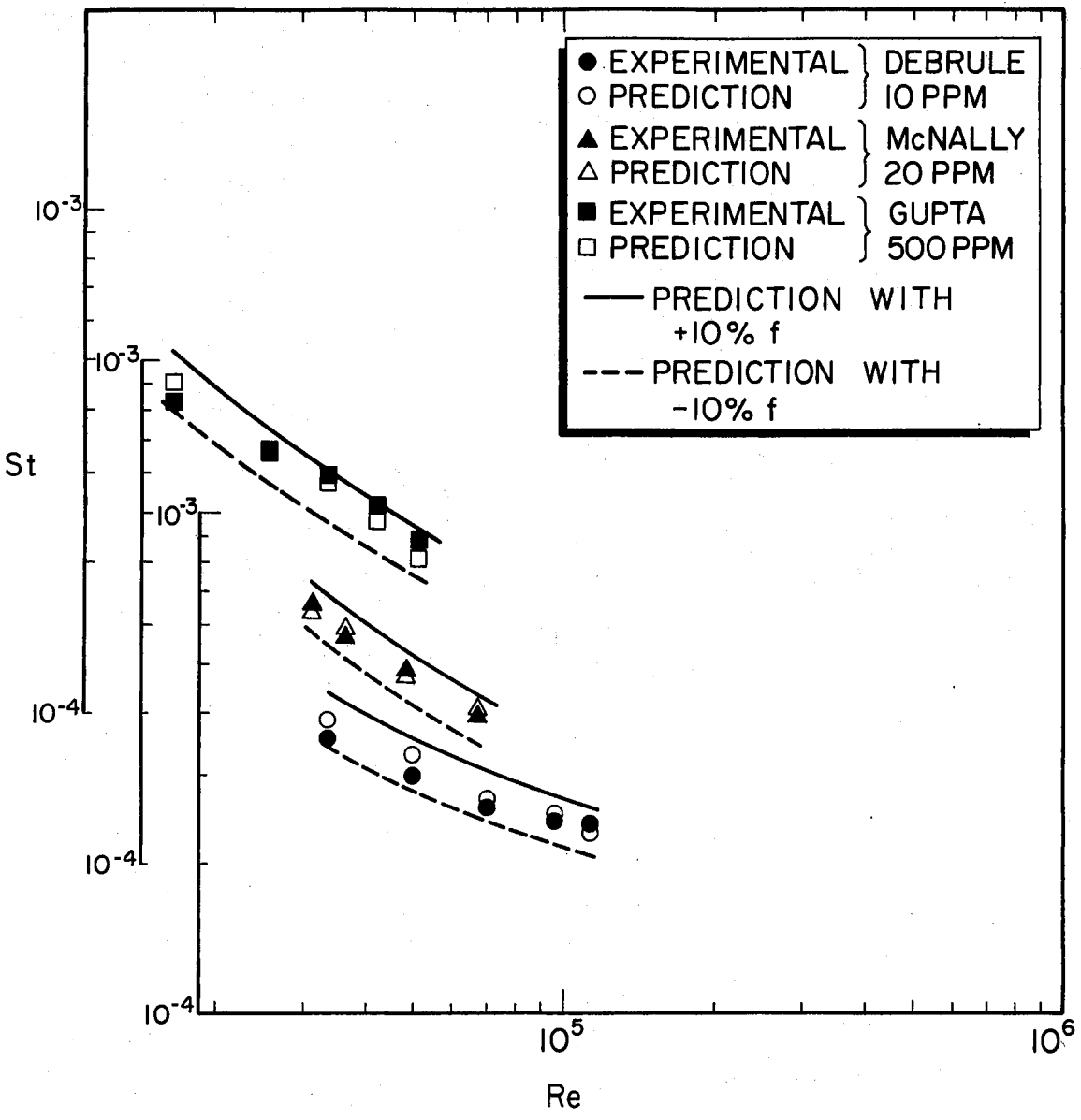

Figure 25. Sensitivity of the Present Model with Respect to $\pm$ 10% Variation in Friction Factor (f)

APPENDIX C

FLOW CHARTS

This appendix contains the computer flow charts referred to in the text of this thesis.

VELOCITY PROFILE

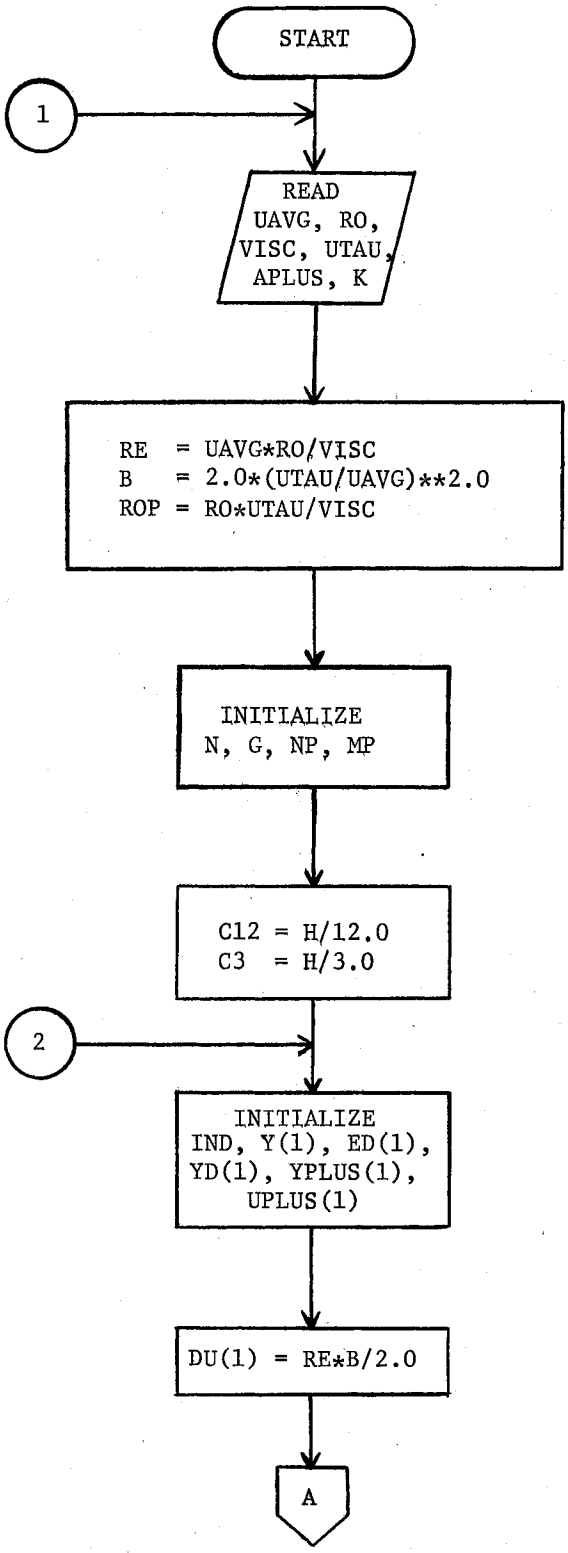

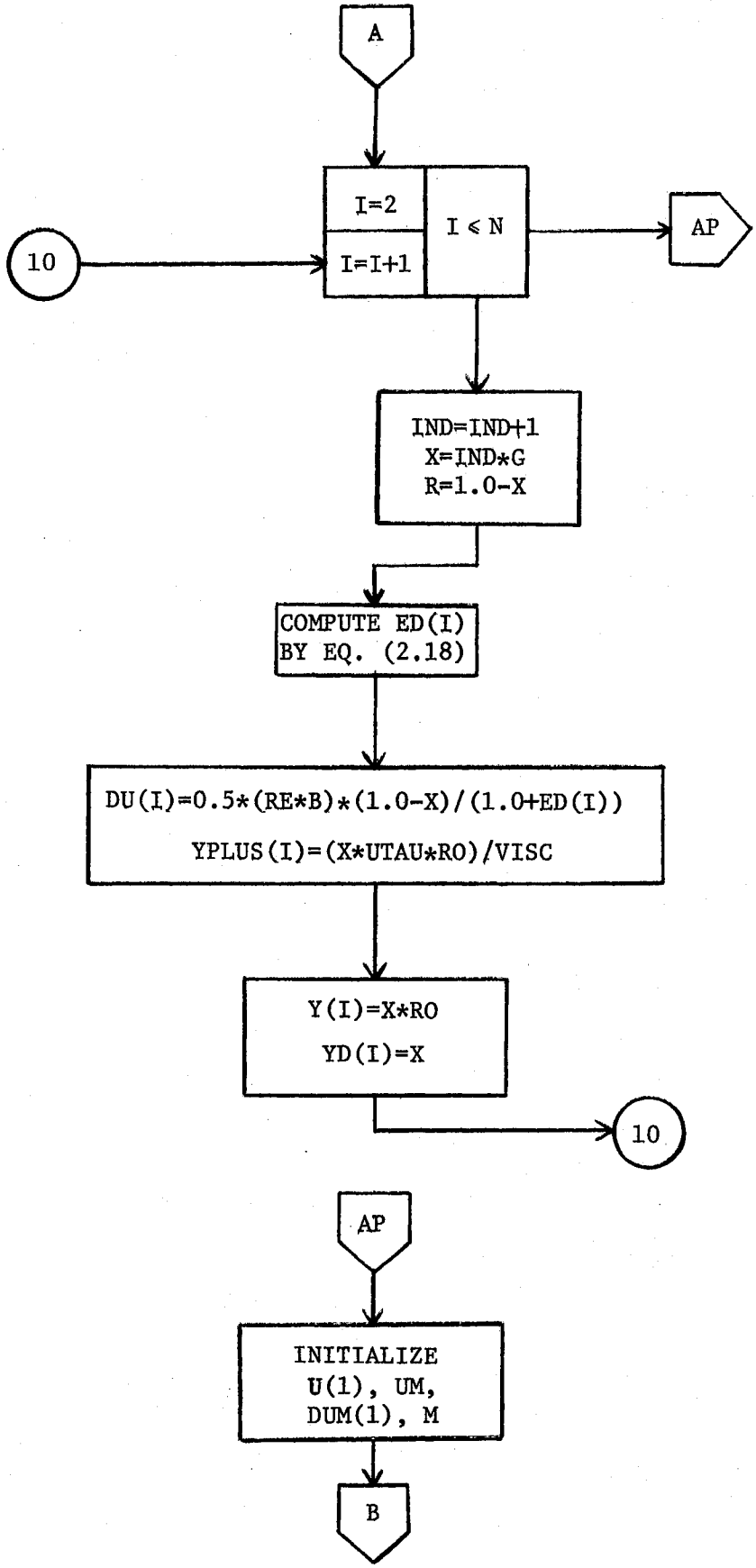
A
I=2
I=I+1
I ⩽ N
AP
10
IND=IND+1
X=IND*G
R=1.0-X
COMPUTE ED(I)
BY EQ. (2.18)
DU(I)=0.5*(RE*B)*(1.0-X)/(1.0+ED(I))
YPLUS(I)=(X*UTAU*RO)/VISC
Y(I)=X*RO
YD(I)=X
10
AP
INITIALIZE
U(1), UM,
DUM(1), M
B

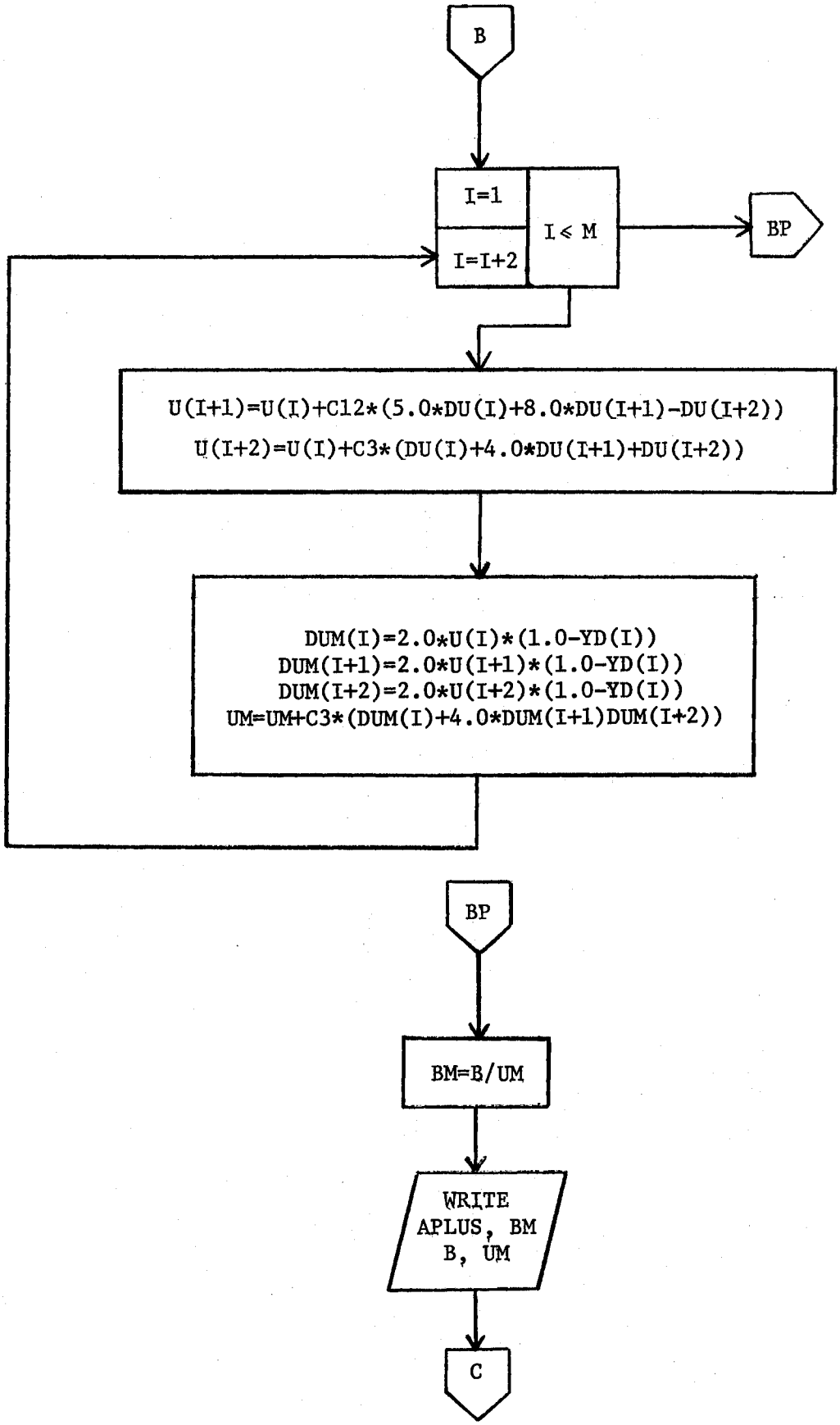
B
I=1
I=I+2
I ≤ M
BP
U(I+1)=U(I)+C12*(5.0*DU(I)+8.0*DU(I+1)-DU(I+2))
U(I+2)=U(I)+C3*(DU(I)+4.0*DU(I+1)+DU(I+2))
DUM(I)=2.0*U(I)*(1.0-YD(I))
DUM(I+1)=2.0*U(I+1)*(1.0-YD(I))
DUM(I+2)=2.0*U(I+2)*(1.0-YD(I))
UM=UM+C3*(DUM(I)+4.0*DUM(I+1)DUM(I+2))
BP
BM=B/UM
WRITE
APLUS, BM
B, UM
C

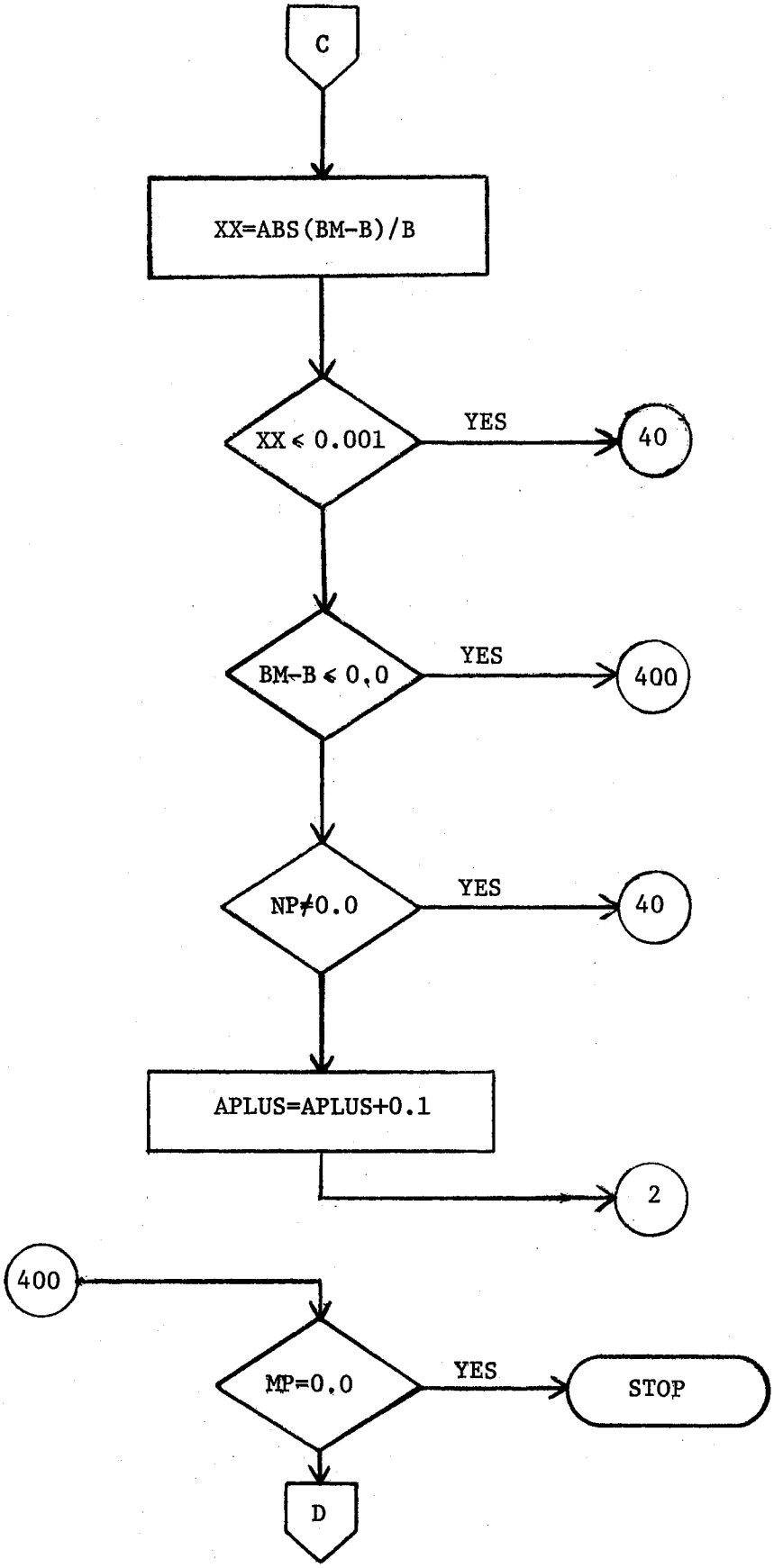
C
XX=ABS(BM-B)/B
XX ≤ 0.001
YES
40
BM-B ≤ 0.0
YES
400
NP≠0.0
YES
40
APLUS=APLUS+0.1
2
400
MP=0.0
YES
STOP
D

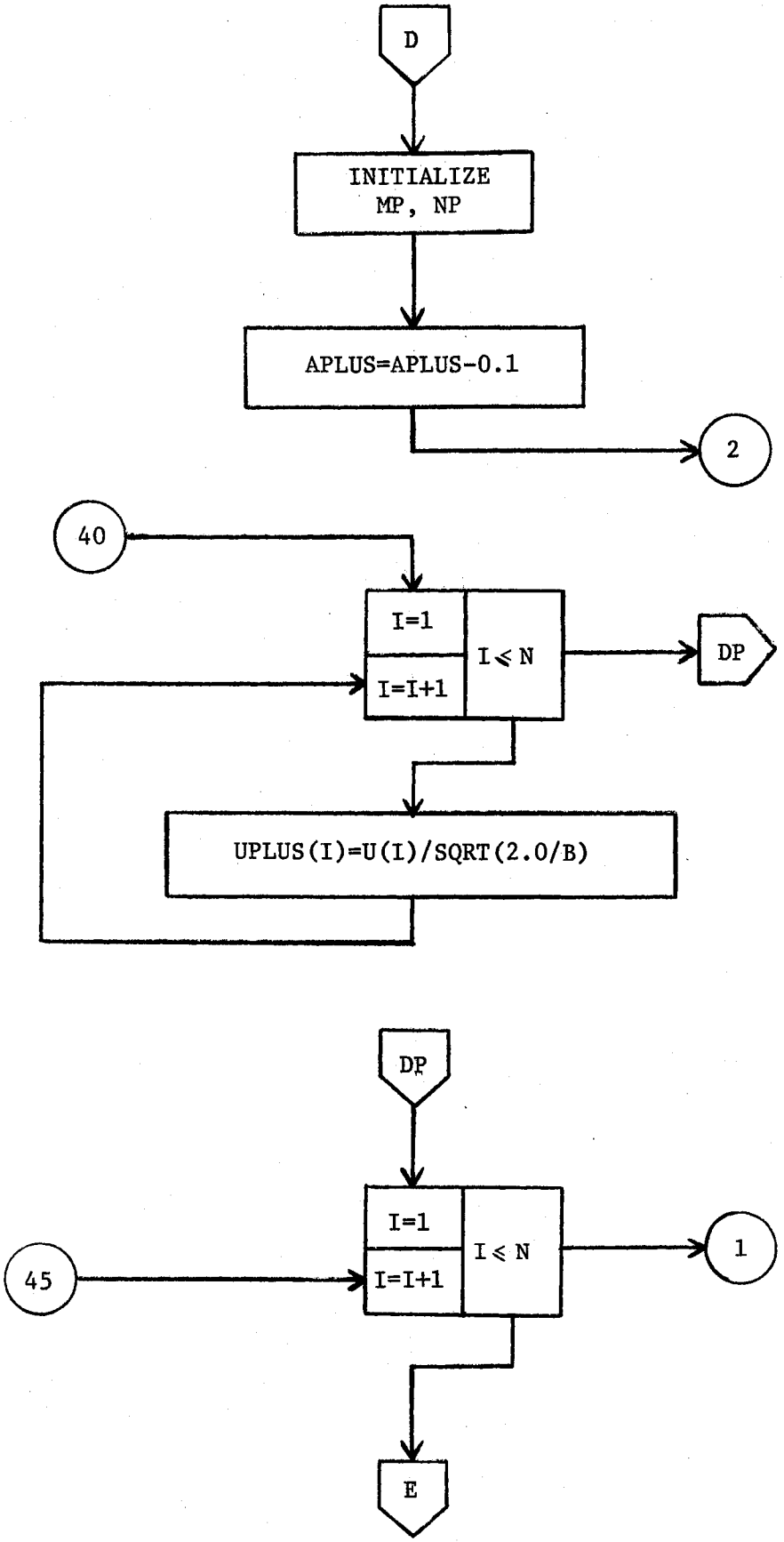
D
INITIALIZE
MP, NP
APLUS=APLUS-0.1
2
40
I=1
I=I+1
I ⩽ N
DP
UPLUS(I)=U(I)/SQRT(2.0/B)
DP
I=1
I=I+1
I ⩽ N
45
1
E

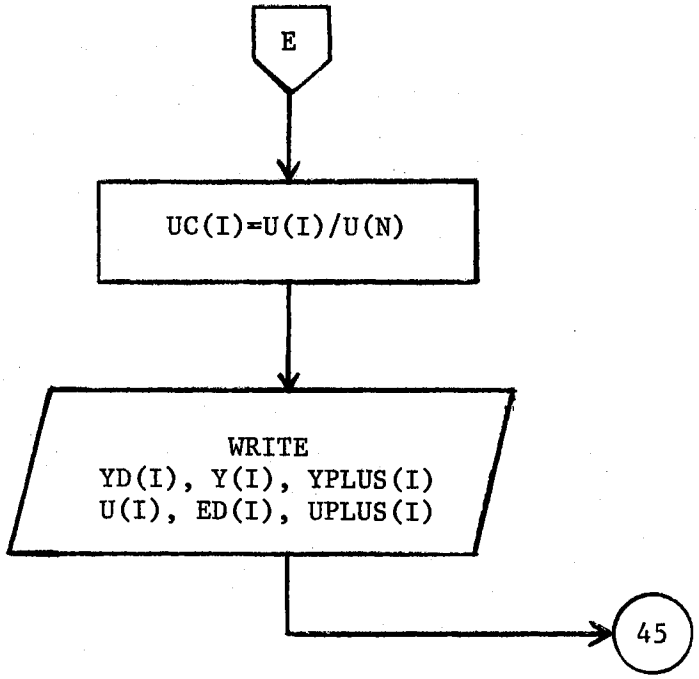
E
UC(I)=U(I)/U(N)
WRITE
YD(I), Y(I), YPLUS(I)
U(I), ED(I), UPLUS(I)
45

HEAT TRANSFER AND TEMPERATURE PROFILE

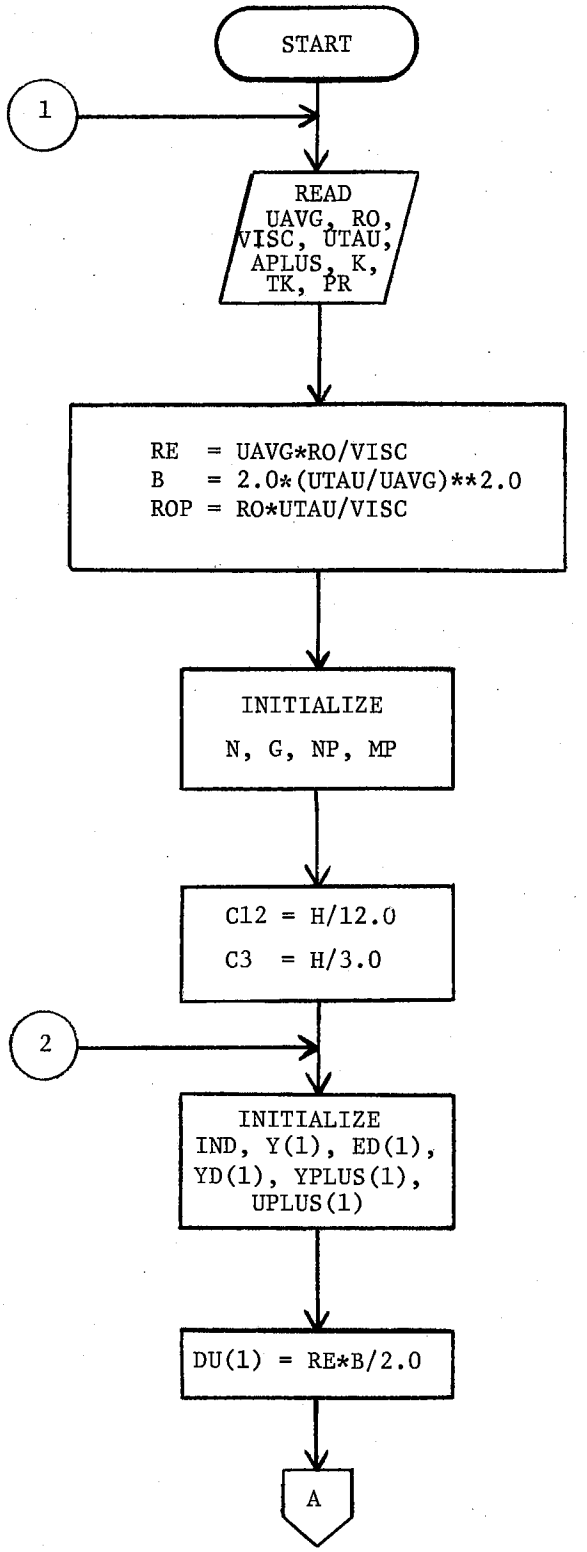

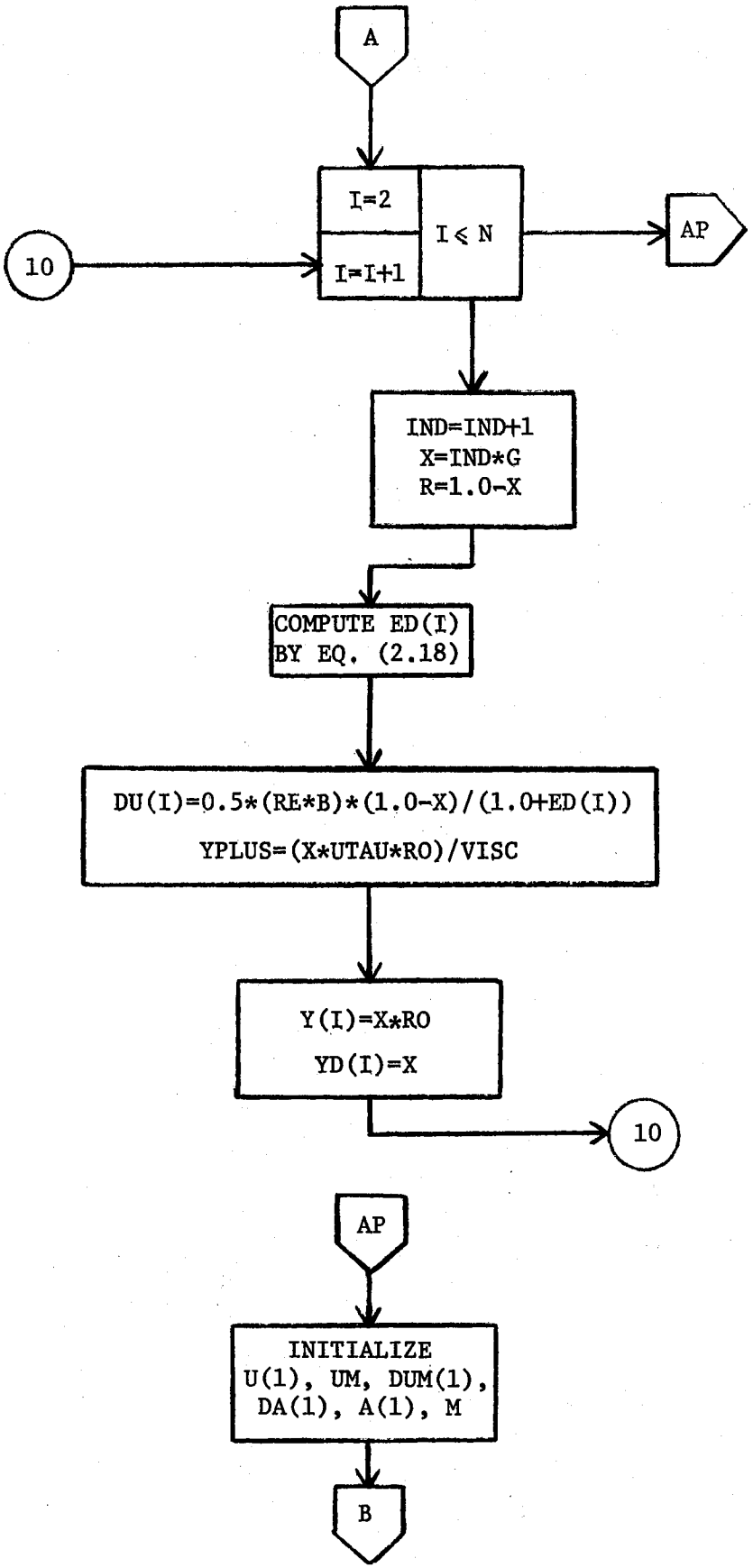
A
I=2
I=I+1
I ⩽ N
AP
10
IND=IND+1
X=IND*G
R=1.0-X
COMPUTE ED(I)
BY EQ. (2.18)
DU(I)=0.5*(RE*B)*(1.0-X)/(1.0+ED(I))
YPLUS=(X*UTAU*RO)/VISC
Y(I)=X*RO
YD(I)=X
10
AP
INITIALIZE
U(1), UM, DUM(1),
DA(1), A(1), M
B

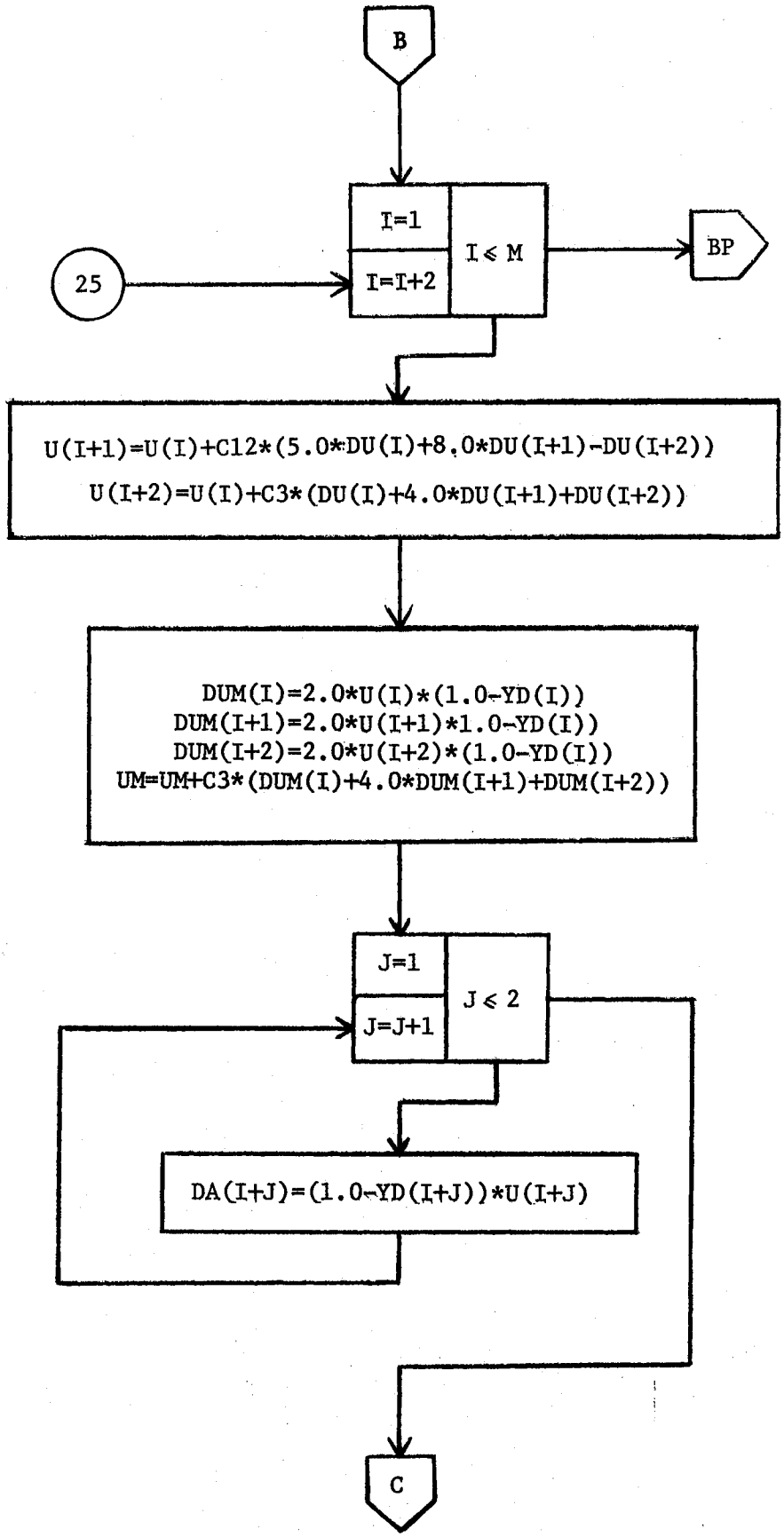
B
I=1
I=I+2
I ⩽ M
BP
25
U(I+1)=U(I)+C12*(5.0*DU(I)+8.0*DU(I+1)-DU(I+2))
U(I+2)=U(I)+C3*(DU(I)+4.0*DU(I+1)+DU(I+2))
DUM(I)=2.0*U(I)*(1.0-YD(I))
DUM(I+1)=2.0*U(I+1)*1.0-YD(I))
DUM(I+2)=2.0*U(I+2)*(1.0-YD(I))
UM=UM+C3*(DUM(I)+4.0*DUM(I+1)+DUM(I+2))
J=1
J=J+1
J ⩽ 2
DA(I+J)=(1.0-YD(I+J))*U(I+J)
C

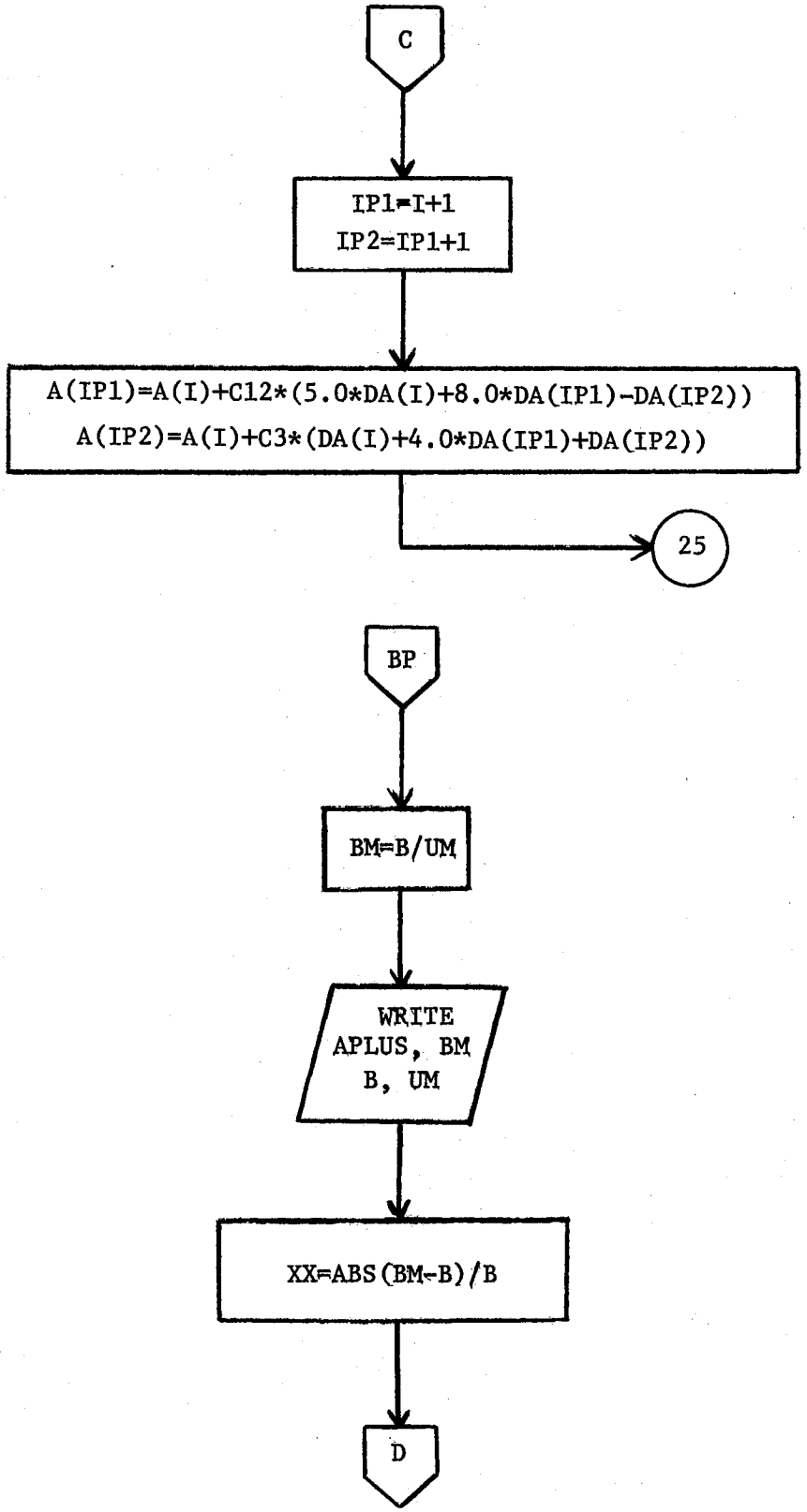
C
IP1=I+1
IP2=IP1+1
A(IP1)=A(I)+C12*(5.0*DA(I)+8.0*DA(IP1)-DA(IP2))
A(IP2)=A(I)+C3*(DA(I)+4.0*DA(IP1)+DA(IP2))
25
BP
BM=B/UM
WRITE
APLUS, BM
B, UM
XX=ABS(BM-B)/B
D

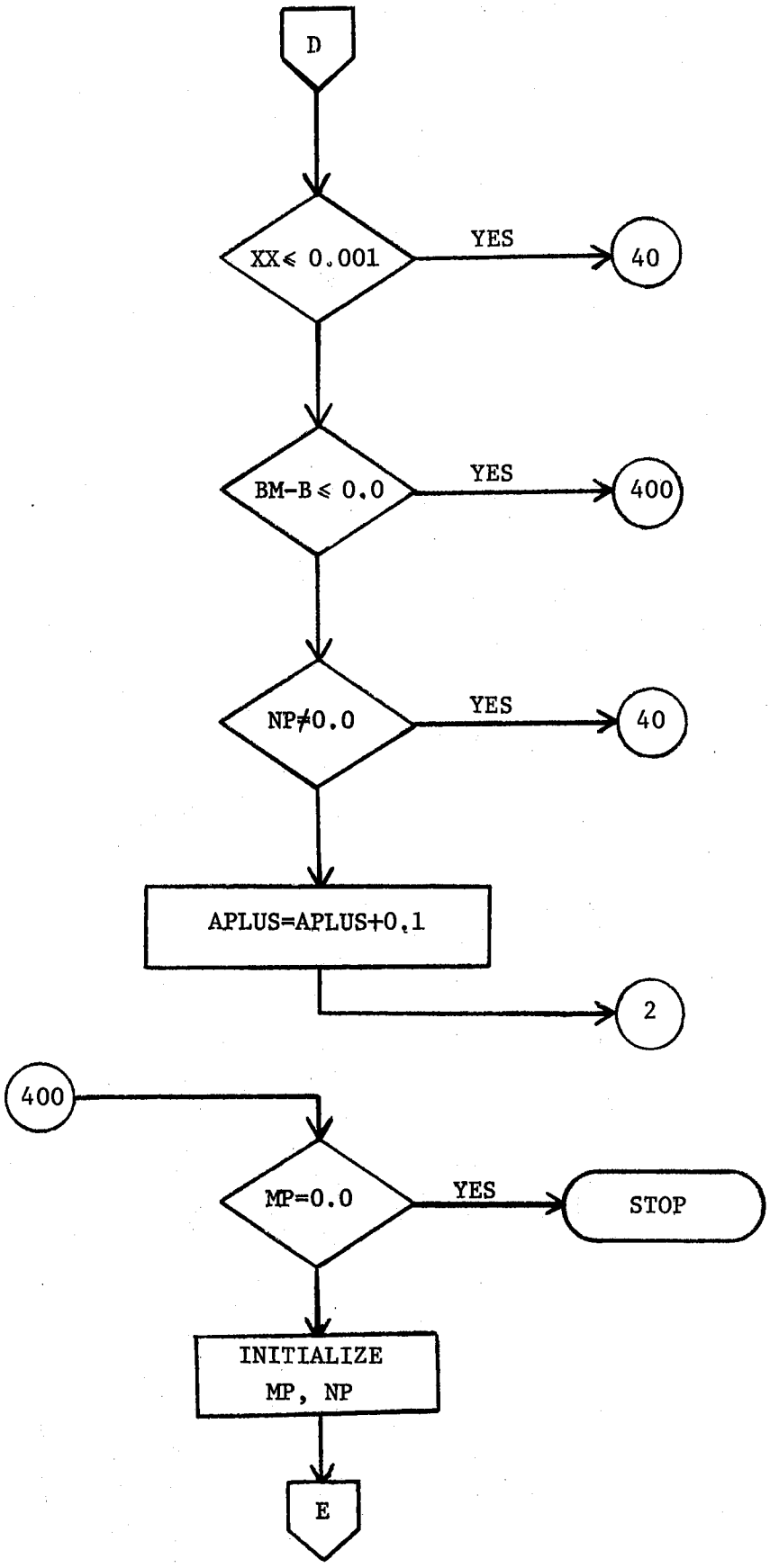
D
XX≤ 0.001
YES
40
BM-B≤ 0.0
YES
400
NP≠0.0
YES
40
APLUS=APLUS+0.1
2
400
MP=0.0
YES
STOP
INITIALIZE
MP, NP
E

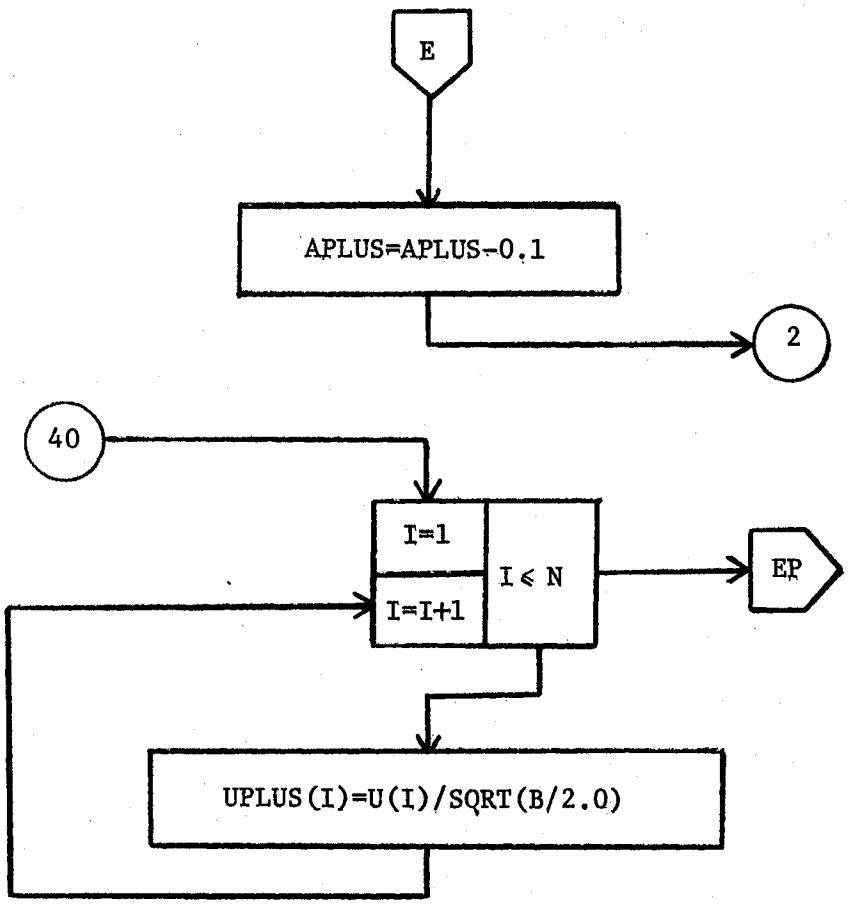
E
APLUS=APLUS-0.1
2
40
I=1
I=I+1
I ⩽ N
EP
UPLUS(I)=U(I)/SQRT(B/2.0)

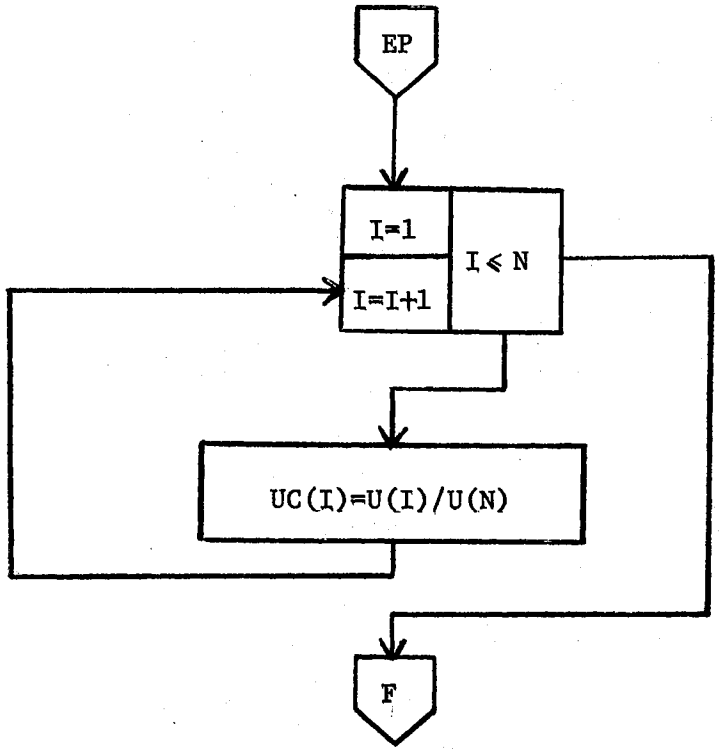
EP
I=1
I=I+1
I ⩽ N
UC(I)=U(I)/U(N)
F

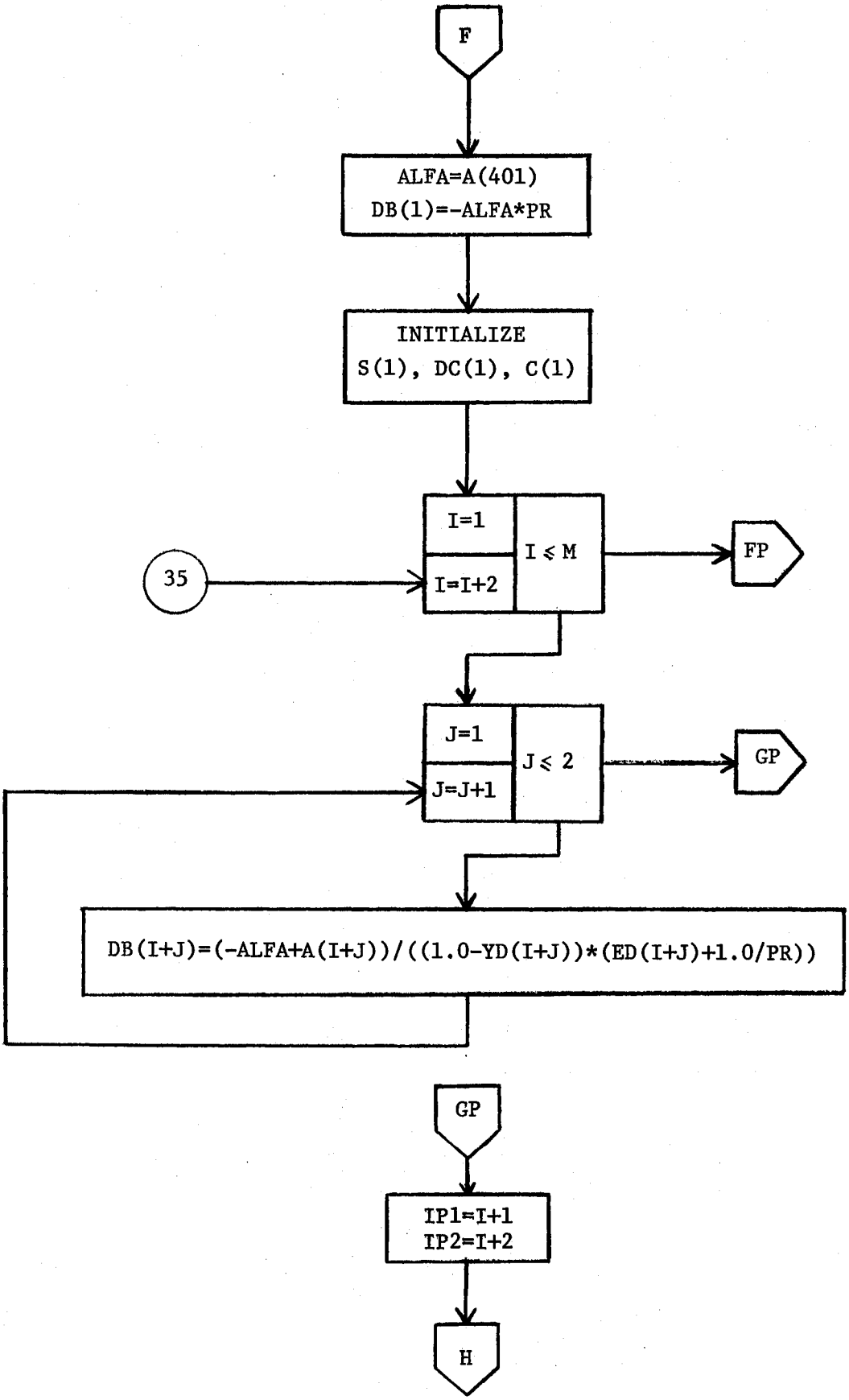
F
ALFA=A(401)
DB(1)=-ALFA*PR
INITIALIZE
S(1), DC(1), C(1)
I=1
I=I+2
I ⩽ M
35
FP
J=1
J=J+1
J ⩽ 2
GP
DB(I+J)=(-ALFA+A(I+J))/((1.0-YD(I+J))*(ED(I+J)+1.0/PR))
GP
IP1=I+1
IP2=I+2
H

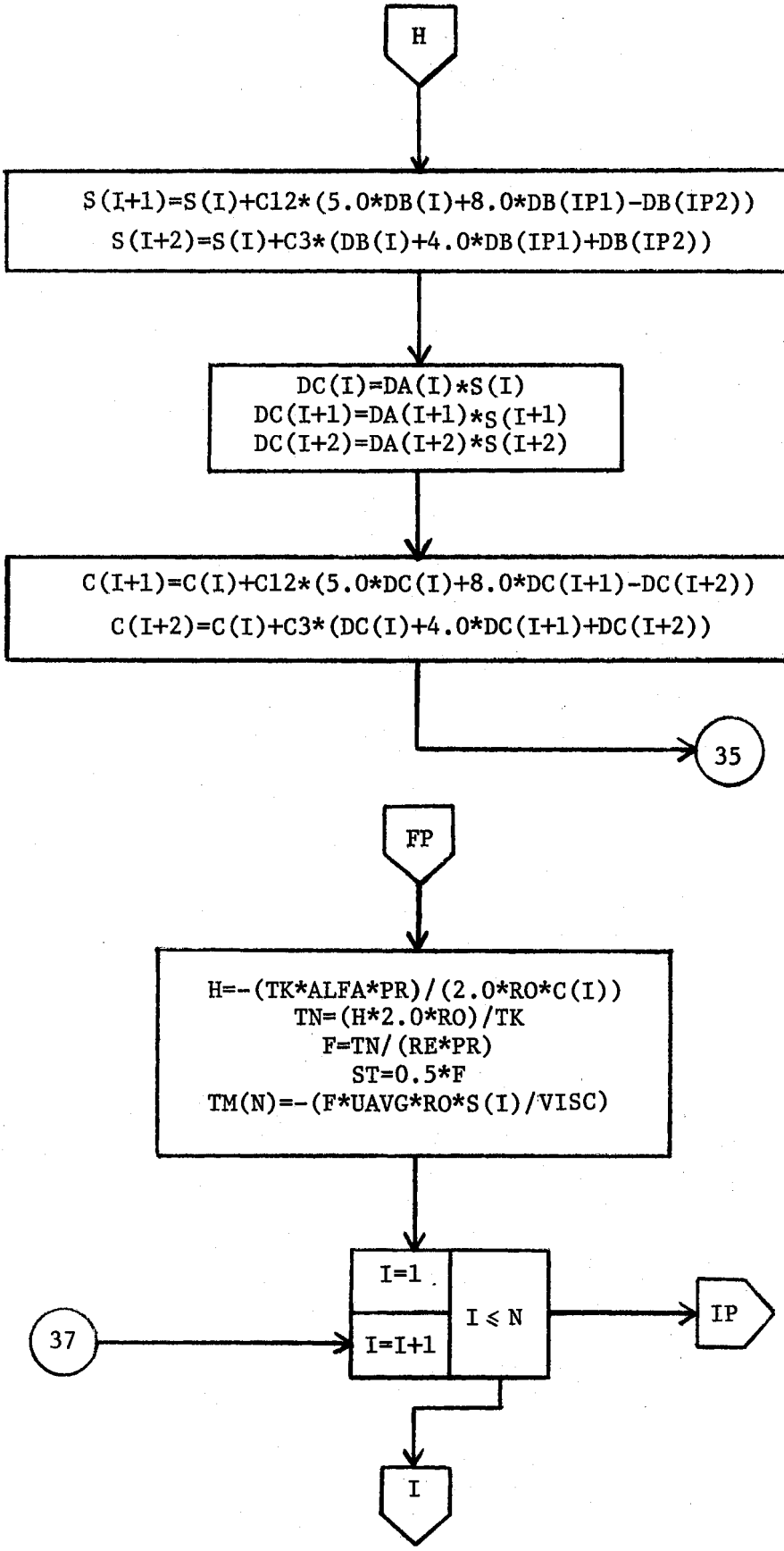
H
S(I+1)=S(I)+C12*(5.0*DB(I)+8.0*DB(IP1)-DB(IP2))
S(I+2)=S(I)+C3*(DB(I)+4.0*DB(IP1)+DB(IP2))
DC(I)=DA(I)*S(I)
DC(I+1)=DA(I+1)*S(I+1)
DC(I+2)=DA(I+2)*S(I+2)
C(I+1)=C(I)+C12*(5.0*DC(I)+8.0*DC(I+1)-DC(I+2))
C(I+2)=C(I)+C3*(DC(I)+4.0*DC(I+1)+DC(I+2))
35
FP
H=-(TK*ALFA*PR)/(2.0*RO*C(I))
TN=(H*2.0*RO)/TK
F=TN/(RE*PR)
ST=0.5*F
TM(N)=-(F*UAVG*RO*S(I)/VISC)
I=1
I=I+1
I ⩽ N
37
IP
I

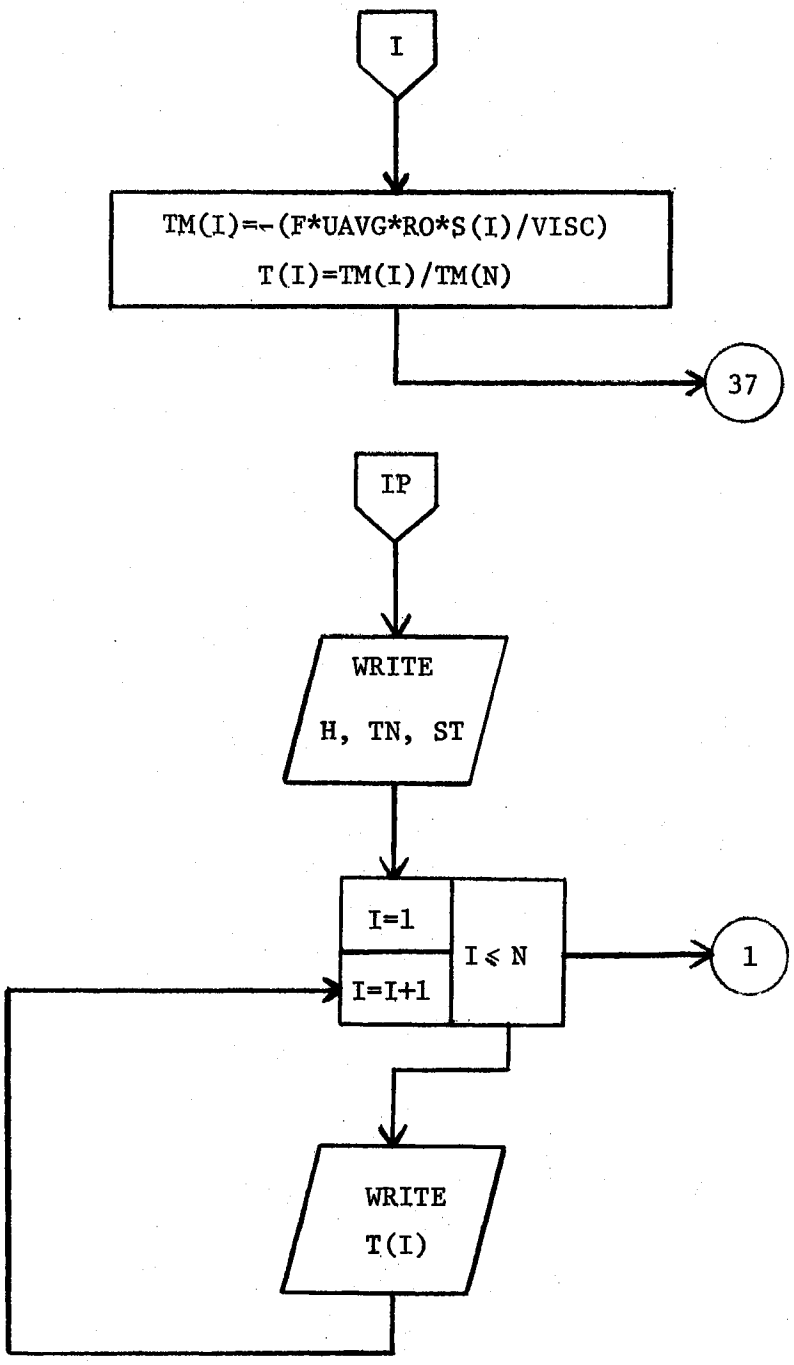
I
TM(I)=-(F*UAVG*RO*S(I)/VISC)
T(I)=TM(I)/TM(N)
37
IP
WRITE
H, TN, ST
I=1
I=I+1
I ⩽ N
1
WRITE
T(I)

NOMENCLATURE FOR COMPUTER FLOW CHARTS

APLUS	- A^+, constant that characterizes thickness of wall layer
ALFA	- numerater of Equation (3.24) after integration
A	- defined by $\int_0^{y_1} DA \, d\bar{y}_2$
B	- non-dimensional pressure drop (experimental value)
BM	- non-dimensional pressure drop from normalization conditions (calculated value)
C12, C3	- constants of Simpson's Rule
C	- denominator of Equation (3.24) after integration
DU	- integrand of Equation (2.9)
DUM	- integrand of Equation (2.12)
DA, DB, DC	- integrands of intergral expressions in Equation (3.24)
ED	- E, non-dimensional eddy diffusivity
G	- integrational increment, G = 0.0025
H	- heat transfer coefficient, Btu/(hr-ft^2-^{o}F)
K	- von Karman constant
M	- constant, M = N-2
N	- total number of increments, N = 401

PR - Prandtl number

RO - radius of pipe, ft.

RE - Reynolds number based on pipe radius

ROP - non-dimensional pipe radius

R - non-dimensional radial coordinate

ST - Stanton number

S - integral of second integration in denominator of Equation (3.24)

TN - Nusselt number

TK - thermal conductivity, Btu/(hr-ft-^{o}F)

TM - non-dimensional temperature

T - normalized temperature

UTAU - shear velocity, ft/sec

UAVG - mass average velocity, ft/sec

UPLUS - U^{+}, non-dimensional velocity

UM - non-dimensional velocity from normalization condition, after iteration UM = 1.0

UC - normalized velocity

VISC - kinematic viscosity, ft^{2}/sec

X - non-dimensional direction normal to wall

Y - coordinate direction normal to wall

YD - non-dimensional direction normal to wall

YPLUS - non-dimensional distance normal to wall

VITA

Afshin Jahanshahi Ghajar

Candidate for the Degree of

Master of Science

Thesis: PREDICTION OF HEAT TRANSFER COEFFICIENTS IN DRAG REDUCING TURBULENT PIPE FLOWS

Major Field: Mechanical Engineering

Biographical:

Personal Data: Born in Tehran, Iran, June 10, 1951, the son of Parvin and Iraj Jahanshahi Ghajar.

Education: Graduated from Hadaf High School, Tehran, Iran, May, 1969; received the Bachelor of Science degree in Mechanical Engineering from Oklahoma State University, May, 1974; completed the requirements for the Master of Science degree at Oklahoma State University, December, 1975.

Professional Experience: Graduate Teaching Assistant, School of Mechanical and Aerospace Engineering, Oklahoma State University, 1974-75.